



COPYRIGHT AND USE OF THIS THESIS

This thesis must be used in accordance with the provisions of the Copyright Act 1968.

Reproduction of material protected by copyright may be an infringement of copyright and copyright owners may be entitled to take legal action against persons who infringe their copyright.

Section 51 (2) of the Copyright Act permits an authorized officer of a university library or archives to provide a copy (by communication or otherwise) of an unpublished thesis kept in the library or archives, to a person who satisfies the authorized officer that he or she requires the reproduction for the purposes of research or study.

The Copyright Act grants the creator of a work a number of moral rights, specifically the right of attribution, the right against false attribution and the right of integrity.

You may infringe the author's moral rights if you:

- fail to acknowledge the author of this thesis if you quote sections from the work
- attribute this thesis to another author
- subject this thesis to derogatory treatment which may prejudice the author's reputation

For further information contact the University's Copyright Service.

sydney.edu.au/copyright

Geometric phase and periodic orbits of the equal-mass, planar three-body problem with vanishing angular momentum

Danya Rose

A thesis submitted in fulfilment of
the requirements for the degree of
Doctor of Philosophy

School of Mathematics and Statistics
University of Sydney



February 2016

Statement of originality

This is to certify that to the best of my knowledge, the content of this thesis is my own work. This thesis has not been submitted for any degree or other purposes.

I certify that the intellectual content of this thesis is the product of my own work and that all the assistance received in preparing this thesis and sources have been acknowledged.

D.Rose

Danya Rose

Acknowledgements

Writing any large body of work is necessarily a collaborative effort. This thesis would not have been written without the involvement and help of many people, to each of whom I am deeply indebted.

First and foremost, this project would have been nothing if not for the help and supervision of Holger Dullin. It is hard to express the fullness my gratitude to him.

Thanks also to Georg Gottwald and Samuel Mueller for being ears when needed, and also to the administrative staff, whose roles are often in the background of a Ph.D. and are in many ways to make their important jobs seem unnecessary.

Family, friends and colleagues form a supporting cast during the Ph.D. process. Thanks to my parents, Kathy and Jim, for showing interest in my work even when my explanations were cryptic beyond compare, and the same to my siblings Eric, James and Marissa. I will have more time for you now.

To my office-mates over the years, thanks for all the coffee (lots of coffee), the sharing of experience and advice, the distractions (sometimes needed, sometimes... not), occasionally reading something I threw your way and giving me the chance to read your work, and the friendships. To name some of the guilty, my appreciation goes out to Duncan Sutherland, John Maclean, Jakub Tomczyk, Jack Moon, Matthew Chan, Yinan Zhang, and others too numerous to name.

For being there outside the academic world (though some of you were in it on your own paths at the time), I have to mention Gerry O'Connor and Paddy Neumann, Ben Sinclair and Ramon Molesworth. You have been friends since ever we met, and I have missed you while my head has been buried in this work.

Last, and far—astronomically far—from least, to Mia. For everything.

Abstract

Geometric phase can explain the rotation of a dynamical system independent of angular momentum. The canonical example of such is a cat (a non-rigid body with an inbuilt control system), falling from an inverted position, being able to re-orient itself with negligible total angular momentum so as to land on its feet. The system of three bodies moving under mutual gravitation is similarly non-rigid, capable of changing size and shape under the dynamics of that force.

Using coordinates that reduce by translations and rotations and simultaneously regularise all binary collisions, which separate shape dynamics from rotational dynamics, we show how certain discrete symmetries (including both reversing and non-reversing symmetries of the equations of motion) can force the geometric phase of motion periodic to vanish.

This result is illustrated with periodic orbits discovered in a numerical survey, many of which are heretofore unknown, and the findings of this survey are discussed in detail, including stability, geometric phase, and classification of orbits.

A note on technology

This thesis was prepared primarily as an electronic document for electronic submission. As such, while it is suitable for printing, its figures were prepared using the **Asymptote** vector programming language with some level of user interactivity in mind. One of the options available when integrating **Asymptote** with L^AT_EX is to include 3D graphics as “pop-out” documents. When using a suitable PDF reader, such as Adobe® Reader, with Java® enabled, double-clicking on any of the figures will open it as a new window or tab. The 3D figures can then be rotated and zoomed, while 2D figures are simply enlarged.

It may be necessary to adjust the settings/preferences in Adobe® Reader for the 3D content to appear. The following is valid for Adobe® Acrobat Reader DC. To ensure 3D is correctly enabled, open the preferences window (by going to the menu: Edit→Preferences...), navigate to the tab entitled “3D & Multimedia” and ensure that the checkbox labelled “Enable playing of 3D content” is checked. Hardware rendering (DirectX or OpenGL), where available, is preferred, but all settings other than the one above must be chosen by the user according to what works best on the system used to read and interact with this document (the default is expected to work, however).

Appendix F, due to its size, is presented as a separate document. Some links within this document, which have the form “ $t0(1,1)$ ”, if clicked upon, will open the appropriate page of the appendix if the file “rose_db_appendix.pdf” is in the same directory as this document. Unfortunately, the 3D content of Appendix F may take a long time to load, depending somewhat upon the specifications of the user’s computer system, during which time the PDF reader may not respond to user commands. Rest assured, however, that the software has not crashed or frozen - unless, by some ill fortune, it has. In such cases, the author must sadly fall back on the traditional defence in IT: “It works for *me!*”

The author hopes that this functionality is nevertheless of some benefit to the reader.

Common symbols and terms

(j, k, l) : Cyclic permutations of $(1, 2, 3)$.

Σ, Π : Sum and product without index are obtained by replacing (j, k, l) in the summand or factor by all cyclic permutations of $(1, 2, 3)$ and adding or multiplying the resulting terms to obtain the result.

$\tilde{t} \in \mathbb{R}$: Physical time.

$m_j \in \mathbb{R}^+$: Mass of body j .

$m \in \mathbb{R}^+$: Sum of masses, $m = m_1 + m_2 + m_3$.

$M \in \mathbb{R}^+$: Product of masses, $M = m_1 m_2 m_3$.

$\mu_j \in \mathbb{R}^+$: Reduced mass: $\frac{1}{\mu_j} = \frac{1}{m_k} + \frac{1}{m_l}$.

$X_j \in \mathbb{C}$: Position of body j relative to the centre of mass. All three $X_1 X_2 X_3$ form a (possibly degenerate) triangle.

Orientation: The direction in which the indices of the vertices of $X_1 X_2 X_3$ are ordered in the plane: increasing counter-clockwise = *positive orientation*; or increasing clockwise = *negative orientation*.

$P_j \in \mathbb{C}$: Momentum of body j .

$a_j \in \mathbb{R}$: Symmetry-reduced coordinate, length of the side of $X_1 X_2 X_3$ opposite to body j such that $|X_l - X_k| = a_j$.

$p_j \in \mathbb{R}$: Canonically conjugated momentum with respect to a_j .

$\phi_j \in \mathbb{R}$: Angle of the side of $X_1 X_2 X_3$ opposite to m_j such that $X_l - X_k = a_j e^{i\phi_j}$.

$\alpha_j \in \mathbb{R}$: Regularised variables with relationship to side lengths: $a_j = \alpha_k^2 + \alpha_l^2$; or $\alpha_j = \pm \sqrt{\sigma - a_j}$. Orientation corresponds to the sign of the product $\alpha_1 \alpha_2 \alpha_3$.

$\pi_j \in \mathbb{R}$: Canonically conjugated momentum with respect to α_j .

$t \in \mathbb{R}$: Scaled time, necessary for regularisation. Related to \tilde{t} by $\frac{dt}{d\tilde{t}} = a_1 a_2 a_3$.

$\alpha \in \mathbb{R}^+$: Square root of semiperimeter: $\alpha^2 := \sum \alpha_j^2 = \frac{1}{2} \sum a_j$.

$O \in \mathbb{C}$: Centre of mass: $O = \frac{1}{m} \sum m_j X_j$, with all X_j, P_j chosen so that $O = 0$ for all time.

$C \in \mathbb{C}$: Incentre of $X_1 X_2 X_3$: $C = \frac{1}{\sigma} \sum a_j X_j$.

$A \in \mathbb{R}$: Signed area of $X_1 X_2 X_3$: $A = \alpha_1 \alpha_2 \alpha_3 \alpha$.

$\phi \in \mathbb{R}$: An angle introduced by symmetry reduction such that $\phi = \frac{1}{3} \sum \phi_j$. Required for reconstruction.

$p_\phi \in \mathbb{R}$: Angular momentum, conserved quantity canonically conjugated with respect to ϕ : $p_\phi = \text{Im} \sum \bar{X}_j P_j$. After symmetry reduction we choose $p_\phi = 0$.

$\Delta G \in \mathbb{R}$: Geometric phase.

x' : Derivative with respect to physical time: $\frac{dx}{d\tilde{t}}$.

\dot{x} : Derivative with respect to scaled time: $\frac{dx}{dt}$.

Contents

1	Introduction	1
1.1	Overview	1
1.2	Hamiltonian systems	4
1.3	The 3-body problem	11
1.4	Regularisation	21
2	Discrete symmetries	34
2.1	Definition of the symmetry groups	34
2.2	Structure of the symmetry group	35
2.3	Fixed sets	37
2.4	Subgroup structure	45
2.5	Conclusion	49
3	Symbolic dynamics	51
3.1	Overview	51
3.2	Classical symbolic dynamics in the 3-body problem	51
3.3	Symmetry-reduced symbolic dynamics	54
3.4	Reduced symbolic dynamics and symmetric orbits	62
4	Geometric phase	64
4.1	Introduction	64
4.2	A criterion for vanishing geometric phase	65

CONTENTS	xi
5 Numerical methods	71
5.1 Introduction	71
5.2 Symplectic integration	71
5.3 Finding periodic orbits	81
6 “Experimental” Results and Discussion	87
6.1 Introduction	87
6.2 Known periodic orbits	87
6.3 Common modes of behaviour	90
6.4 Stability	106
6.5 Choreographies	106
6.6 Geometric phase	113
7 Conclusion	117
A Reconstruction	126
A1 Exterior angles and side angles	126
A2 Positions and momenta	127
B Momenta and velocities near collision	131
C Stages of the explicit integrator	133
D Coefficients for higher order methods	136
E Extra relative partial choreographies	138
F Bestiary of periodic orbits	143

List of Tables

2.1	Summary of symmetries	36
2.2	Factorisations of cyclic subgroups of Γ into direct products.	46
2.3	Factorisations of subgroups of Γ isomorphic to V_4 into direct products.	47
2.4	Factorisations of non-cyclic subgroups of Γ of order 6 or higher into direct products.	50
2.5	Factorisations of non-cyclic subgroups of Γ (that cannot be factored into direct products) into semidirect products.	50
3.1	Boundaries of the fundamental domain for unequal masses.	56
3.2	Boundaries of the fundamental domain for $m_2 = m_3$	58
3.3	Boundaries of the fundamental domain for equal masses.	59
6.1	Bestiary orbits similar to classes from [73].	88
6.2	Orbit modes	93
6.3	Reversing symmetries in the M -mode.	100
6.4	Symmetries in the B -mode.	102
6.5	Symmetries in the E -mode.	105
6.6	Stable orbits.	107
6.7	Sequence types corresponding to simple or partial choreographic motion, and rotating frames revealing or preserving choreography.	110

List of Figures

1.1	The planar 3-body problem for vanishing angular momentum.	11
1.2	The shape sphere.	16
1.3	Symmetry-reduced variables.	18
1.4	The Hill region in shape space.	21
1.5	Regularised variables.	24
1.6	The regularised shape sphere.	30
1.7	The regularised free fall boundary.	33
2.1	Illustration of a solution in an invariant subspace and possessing reversing symmetries.	38
2.2	Configuration space reconstructions of points in physically meaningful non-reversing fixed sets for equal masses; invariant subspaces.	39
2.3	Configuration space reconstruction of points in physically meaningful reversing fixed sets for equal masses.	42
3.1	The fundamental domain chosen for equal masses.	55
3.2	Fundamental domain on the shape spheres, unequal masses.	57
3.3	Fundamental domain on the shape spheres, $m_2 = m_3$	58
3.4	Fundamental domain on the shape spheres, equal masses.	59
3.5	Mapping back into the fundamental domain.	60
4.1	Integral of geometric phase formula over a fraction of one period in the non-reversing case.	69
4.2	Integral of geometric phase formula over a fraction of one period in the reversing case.	70

5.1	Work-precision diagram	77
5.2	Figure-8 tests	78
5.3	Pythagorean orbit tests	79
5.4	Collision orbit tests	80
6.1	Three modes.	92
6.2	Symmetry of modes.	92
6.3	Two distinct types of isosceles orbits.	95
6.4	Comparison of two winding orbits in the <i>B</i> -mode.	97
6.5	Comparison of two ‘L’-shaped orbits in the <i>B</i> -mode.	98
6.6	Comparison of two ‘L’-shapes orbits without winding.	98
6.7	Isosceles reversing symmetries.	100
6.8	<i>M</i> -mode reversing symmetries.	101
6.9	Rectilinear reversing symmetries.	103
6.10	<i>B</i> -mode reversing symmetries.	104
6.11	<i>E</i> -mode reversing symmetries.	105
6.12	Extra relative partial choreographies.	112
6.13	An orbit with large geometric phase in a slower rotating frame.	114
6.14	Orbit with the greatest ω drawn in the inertial frame.	115
A.1	Relationship between ψ_j and $\phi_{k,l}$	128
E.1	Type-0 , sequence class $(B\Omega M\Omega')^2$	139
E.2	Type-0 , sequence class $(B\Omega M\Omega')^4$	140
E.3	Isosceles, sequence classes $(B\Omega M\Omega')^2$ (a), $(F\Omega M\Omega')^2$ (b-d).	141
E.4	Rectilinear, sequence classes $(B\Omega M\Omega')^4$ (a), $(F\Omega M\Omega')^2$ (b-g).	142

1 Introduction

1.1 Overview

The 3-body problem was first described by Newton [54], and is one of the classical problems of mathematics, physics, and astronomy. To review the 3-body problem in its entirety would be impossible, and is indeed unnecessary. Many tomes are devoted to the topic, to the n -body problem in general, and to celestial dynamics; see, for example, [35, 68, 62, 10]. Many methods have been used to simplify the 3-body problem and understand its dynamics. Such techniques have included restriction to fewer dimensions, as in the planar, isosceles, and rectilinear 3-body problems; the restricted (spatial and planar, circular and elliptical) 3-body problem, in which one body is treated as having negligible mass; and the search for (relative) equilibria, and for periodic motions in all possible simplified versions of the problem and in the full problem. Much of the focus of study in the 3-body problem has been to understand whether or not our own solar system is stable; although it appears to have lasted for thousands of millions of years, it is natural, after all, to wonder if it will continue to last in a state similar to the present, or for how long it will do so. Laskar, in work expanding upon that by Ito and Tanikawa [27], who performed extremely long term (10^9 years) integrations of a simplified solar system, has in recent times done considerable work to this end, showing that the solar system is chaotic and that the inner solar system could even, with a probability of about one per cent, be disrupted catastrophically in the remaining life of the sun; for example, see [31, 32].

Poincaré most famously proved the non-integrability of the 3-body problem [56] and made great early investigations into chaos. In light of his results, it seems that periodic orbits may be one of our clearest windows into the 3-body problem.

What makes these periodic solutions so precious is that they are, so to say, the only breach we can use to penetrate into a region reputed to be unapproachable. -Henri Poincaré [57]

This thesis is concerned with relative periodic orbits for equal masses and vanishing angular momentum, and with geometric phase for general masses and vanishing angular momentum. Our goal is to understand how symmetry affects the geometric phase,

and to find relative periodic orbits with large rates of rotation per period.

Geometric phase can explain a rotation independent of angular momentum, typically as a result of a non-rigid body or system of bodies deforming and returning to the same shape as at some earlier time. The most classic example of such motion is the problem of the falling cat, in which a cat, dropped from an inverted position with no angular momentum, is able to land on its feet. The motion of the cat in this instance is—more or less—periodic [39], in the sense that it starts in one shape, moves its limbs and upper and lower torso in relation to one another, and finally returns to (roughly) the same shape as that in which it began. That is, in an idealised sense, it undergoes a periodic motion in its space of allowable shapes, or *shape space*. This rotation is not achieved by aerodynamical effects; it is purely due to the geometry of the deformations involved, and has been studied in detail by several authors (see Montgomery [46], and references therein), and explained in a very readable review of the phenomenon of geometric phase in general by Batterman [3].

The 3-body problem is similar to the cat in that it describes a system of bodies capable of changing shape, and, when restricted to zero angular momentum, the dynamic phase (an integral of the instantaneous angular velocity and moment of inertia over an orbit) vanishes: the rotation of a relative periodic orbit with vanishing angular momentum is purely due to the geometry of its motion. In 1984 Berry [4] described a path-dependent phase change for quantal systems undergoing an adiabatic change, which became known as “Berry’s phase”. Through several works [20, 28] the Berry phase was adapted by Wu [86] to develop a similar result for the 3-body problem. Montgomery picked up the story in [47], after his work on the falling cat, resulting in a one-form that can be integrated over a periodic orbit of the 3-body problem to calculate its geometric phase.

We begin this thesis with an overview of the frameworks in which we shall reside, introducing terminology and important concepts that are more general than the specific problem posed. Initially this will take us through Hamiltonian systems, concepts of symmetry—of both continuous and discrete types—and the “reductions” of the problem that simplify it as much as possible and reveal its underlying structure. Special discrete symmetries are involutions, including reflections and “time reversal”. The section concludes by describing a method of reducing a continuous system to a discrete map, the Poincaré map. We continue by working our way to the 3-body problem itself, taking a broad look at the structure of the problem. Specific ideas that we will develop include reduction by continuous symmetries (resulting in the *shape space* and *shape sphere*) and regularisation of binary collisions (with a corresponding shape space and shape sphere that are enlarged versions of the preceding ones).

After transformation into a suitable frame of reference (namely the centre of mass

frame), *relative periodic orbits* of the un-reduced system are orbits that, after some specific length of time called the period, are related to their original configuration by a rigid rotation about the centre of mass. Reduction by continuous symmetries causes all relative and absolute periodic orbits to become periodic in the reduced space. The reduced space (shape space) can be considered as the set of congruence classes of oriented triangles, and the shape sphere the set of similarity classes of oriented triangles.

Symmetry is fundamental to two of our main problems: first, that of geometric phase; second, that of classification of periodic orbits. Chapter 2 is devoted to the discrete symmetries that remain in the problem after reduction by continuous symmetries. We examine the symmetries for general masses, two equal masses and all equal masses, the fixed sets of all possible symmetries and the element structure of the symmetry group, as well as the subgroup structure that becomes relevant particularly when studying periodic orbits with symmetries.

Chapter 3 discusses a method of, in essence, “naming” each possible solution through the assignment of symbols to particular events along a solution curve, and it concludes with a different look at some of the symmetries of the 3-body problem, which suggests a classification scheme for the symbol sequences of periodic orbits. We develop a simple way to classify the symmetry group of an orbit up to isomorphism.

In Chapter 4 we investigate geometric phase. What symmetries are associated with its presence or its absence? It all becomes clear: simply by the presence of certain symmetries in the symmetry group of a periodic orbit we can deduce that its geometric phase vanishes! This is one of our main results, Theorem 4.5. We obtain a simple classification scheme using its symbol sequence to quickly determine if an orbit is absolutely periodic.

Chapter 5 takes a different direction, where we discuss the numerical methods and programs with which we will find periodic orbits. First, we must find a way to approximate solutions “politely”; that is, respecting the symplectic structure of Hamiltonian systems, which is not respected by traditional integration methods. Attempting to use non-symplectic methods may result in totally inaccurate results. In contrast, symplectic numerical methods can give very good “global” accuracy for the solutions they approximate, at the cost of possible greater computational complexity or lower local accuracy. This gives the first explicit symplectic integrator for the symmetry reduced and regularised 3-body problem with vanishing angular momentum. The second part of this chapter discusses our methods, making use of the integrator now developed, for finding periodic solutions of the regularised and symmetry-reduced problem.

Chapter 6 is where we present and discuss the “experimental” findings of our search. It is paired with the rather bulky appendix F (the “Bestiary”, as we call it), in which

are listed 363 relative periodic orbits of the equal mass 3-body problem with vanishing angular momentum, unique up to symmetry, and their “vital statistics”. In summary, we present 221 collisionless orbits—some known in current literature, but many new—with varying levels of symmetry, and many linearly stable, including several absolute and relative choreographies, and relative partial choreographies, which we believe are heretofore unknown for vanishing angular momentum. The Bestiary also includes 82 collision orbits, divided into two categories: 75 in which the collisions occur between only one pair of bodies and 7 in which the collisions occur between two different pairs of bodies. Remarkably, some in each camp are stable. The remaining orbits live in special invariant subspaces of the dynamics: 5 are isosceles, and 55 are collinear. All but two particularly simple orbits (one from each) of the invariant subspaces are unstable. Among our main findings are that most periodic orbits can easily be classified by their paths in the regularised shape space relating them to collinear, isosceles or choreographic motion, and that with these modes of behaviour are restrictions on the symmetries they possess. Returning to the geometric phase, we also show the relative periodic orbit which has the largest rate of rotation per period, albeit at angular momentum zero.

1.2 Hamiltonian systems

Hamiltonian dynamics is a framework for the study of dynamical systems with a certain underlying structure common to many physical systems (for example, see [2]), of which the problem of mutually gravitating particles is but one class. A Hamiltonian system is derived from a smooth scalar function $H(z, t)$, called the *Hamiltonian*, and represented by a system of first order differential equations (called *Hamilton’s equations*):

$$\dot{z} = J \nabla H(z, t), \quad J = \begin{pmatrix} 0 & I \\ -I & 0 \end{pmatrix}, \quad (1.1)$$

where $z \in \Omega$ is a vector of length $2n$ (the set Ω is the *phase space* and is for us \mathbb{R}^{2n} , with n being the number of degrees of freedom of the system), $t \in \mathbb{R}$ and J is the *symplectic matrix*, with I the $n \times n$ identity matrix. The phase space vector is naturally split like $z = (q, p)$, where $q, p \in \mathbb{R}^n$ are canonically conjugated variables, q representing configuration in some sense and p representing the canonically conjugated momenta with respect to q . Note that $J^{-1} = J^T = -J$, with T indicating transposition.

The system of differential equations can thus be represented by

$$\dot{q} = \nabla_p H, \quad \dot{p} = -\nabla_q H. \quad (1.2)$$

The Hamiltonian usually represents the total energy of a system, with $H = T(p, q) + V(q)$, where T is kinetic energy and V is the potential energy. Very often it is the case that T is a quadratic form in the momenta. That is, we can write

$$T(p) = \frac{1}{2} p^T M p, \quad (1.3)$$

where $M = M(q)$ is the *mass matrix*. For a mechanical system describing the motion of point particles whose Hamiltonian is written in Cartesian coordinates, M is diagonal, with the entries equal to the masses of each body corresponding to the respective components of p .

When the time variable t is absent, the Hamiltonian is described as *autonomous*, and the value $h = H(z)$ of the Hamiltonian along any given solution of equation (1.1) is a constant of motion. Should a Hamiltonian be dependent on t , we can expand the phase space so that t becomes a coordinate with canonically conjugated momentum $p_t = -h$, introducing a “fictional” time variable \tilde{t} such that $\frac{dt}{d\tilde{t}} = \dot{t} = \frac{\partial H}{\partial p_t}$ and $\frac{dp_t}{d\tilde{t}} = \dot{p}_t = -\frac{\partial H}{\partial t}$, and the resulting system can be considered autonomous with respect to the new time variable.

Hamiltonian systems also possess what is called a *symplectic* structure. A real $2n \times 2n$ matrix A is called symplectic if

$$A^T J A = J. \quad (1.4)$$

Every symplectic matrix is invertible with determinant +1, with inverse given by $A^{-1} = J^{-1} A^T J$. The flow map of a Hamiltonian system is a symplectic map, which means that its Jacobian matrix is a symplectic matrix. A symplectic integrator in an approximation of the flow by a time stepping map that is symplectic.

1.2.1 Change of coordinates and generating functions

Given a Hamiltonian H written in terms of canonical coordinates (q, p) , we may wish to choose different coordinates (Q, P) that preserve the structure of Hamilton’s equations for that system and result in a new Hamiltonian K , simpler or more advantageous in some way than the original. We wish to obtain $Q = Q(q, p, t)$ and $P = P(q, p, t)$. This is done through the use of a *generating function* $G: \mathbb{R}^{2n+1} \rightarrow \mathbb{R}$, a relationship between some old quantities, some new quantities, and possibly time. There are four classes of generating functions:

- a) $G_1(q, Q, t) : p = \frac{\partial G_1}{\partial q}; P = -\frac{\partial G_1}{\partial Q}$.
- b) $G_2(q, P, t) : p = \frac{\partial G_2}{\partial q}; Q = \frac{\partial G_2}{\partial P}$.

$$c) \ G_3(p, Q, t) : q = -\frac{\partial G_3}{\partial p}; \ P = -\frac{\partial G_3}{\partial Q}.$$

$$d) \ G_4(p, P, t) : q = -\frac{\partial G_4}{\partial p}; \ Q = \frac{\partial G_4}{\partial P}.$$

Substitution and rearrangement/inversion gives precise form of the relationships between new and old quantities, and in each case the new Hamiltonian is $K(Q, P, t) = H(q, p) + \frac{\partial G_i}{\partial t}$.

Using a generating function to construct a coordinate transformation ensures that the transformation is a symplectic map.

1.2.2 Orbits and the flow of Hamiltonian systems

1.2.2.1 Solutions

The differential equation (1.1) are in general too complicated to solve analytically. Nevertheless, as a system of first order differential equations the existence and uniqueness of their solutions for some time is guaranteed if H is smooth. Solutions may terminate at *singularities*, where at least one of the values of coordinates or momenta tends to infinity in finite time. Such singularities may or may not be related to singularities of the vector field, respectively the Hamiltonian. The vector field of the Hamiltonian H induces a flow parameterised by time t , denoted φ_H^t , that acts on the phase space, such that $\varphi_H^0 = I$. Given an initial condition $z_0 \in \Omega$ we can denote a trajectory by $z(t) = \varphi_H^t z_0$, or we can evolve a set of initial points $A_0 \subset \Omega$ by the flow, so that $A(t) = \varphi_H^t A_0$. The flow is itself a one-parameter symplectic transformation. We consider an *orbit* to be the set $Z_{z_0} = \{z \in \Omega : z = \varphi_H^t z_0, \forall t \in \mathbb{R}\}$, or for as long as it is defined.

1.2.2.2 Singularities

As mentioned, some solutions to a system may terminate in singularities. Such solutions (or the sets of points leading to singularities) must be “removed” from the phase space; however, in some cases the singularities themselves are removable by some procedure (called *regularisation*) which reformulates the problem in some way such that trajectories in the reformulated or regularised space are smooth when their reconstructed analogues in the original space are not.

1.2.2.3 Periodic orbits

Most systems admit solutions with the noteworthy property that for some minimal $T \in \mathbb{R}^+$ it is the case that $z(t) = z(t+T)$ (then for any integer multiple of T this holds). These solutions are *periodic*, and they are of great use in studying complex dynamical systems.

Stability analysis, which is discussed in section 1.2.4, of periodic solutions allows us to understand the behaviour of non-periodic solutions that are in some sense “nearby”.

1.2.3 Poincaré mapping

Consider a dynamical system D (which in general need not be Hamiltonian) with phase space Ω , with a smooth vector field defined by $\dot{z} = F(z)$ inducing a continuous (and reversible) flow φ_D^t . We choose a suitable equation $S(z) = 0$ and define $X = \{z \in \Omega : S(z) = 0\}$, which we call the *Poincaré section* or *surface of section*. Now we define the *Poincaré map* to be the map $P_D : X \rightarrow X$ induced by φ_D^t such that for all $x_0 \in X$, $x_1 = P_D(x_0)$ is the point on solution $z(t) = \varphi_D^t z_0$ with the least positive t that intersects with X . Often intersection with X for which $\dot{S}(x_1)$ has different sign from $\dot{S}(x_0)$ are discarded.

Thus the continuous system is replaced by a discrete map with one fewer degrees of freedom but, importantly, displaying its key features if the surface of section S was chosen well. We replace $z(t) = \varphi_D^t z_0$ by $z_i = P_D^i(z_0)$, where $z_0 \in X$, the i -th composition of P_D with itself. The resulting set $X_{z_0} = \{z \in X : z_i = P_D^i(z_0) \forall i \in \mathbb{Z}\}$ is the orbit of z_0 .

In this setting, a periodic orbit is a solution for which $z_i = z_{i+k}$ for which $k \in \mathbb{Z}^+$ is the smallest value of k for which this holds. That is, periodic orbits are fixed points of the map P_D^k ; it is much easier to find the fixed points of such a map than it is to find a periodic orbit in the continuous setting.

For an autonomous Hamiltonian system we must take extra care, as there is one additional constraint that the value of the Hamiltonian is constant along any solution. This means that when searching for periodic orbits in a Hamiltonian system we must fix $H(z_0) = h$, and our surface of section becomes a surface of codimension 2 in the original phase space. In practise this means that we must choose one of the phase space variables to be fixed by the others using the extra constraint.

1.2.4 Stability of periodic orbits

Stability of periodic orbits of Hamiltonian systems is treated generally by Birkhoff [5], and Hadjimetriou [22] discusses the stability of periodic orbits of the 3-body problem in particular. If z^* is a k -periodic point of the Poincaré map $P_D : X \rightarrow X$, we have that z^* is a fixed point of the iterated map P_D^k . We thus linearise P_D^k about z^* to determine the stability of z^* :

$$\xi_{i+1} = D P_D^k(z^*) \xi_i. \quad (1.5)$$

The eigenvalues of $D P_D^k$ indicate the stability of the solution given by z^* . If the modulus of any of the eigenvalues exceeds one, the orbit z^* is unstable. Conversely, if all the moduli of the eigenvalues are less than one the solution is asymptotically stable. However, the product of the eigenvalues of periodic orbits in Hamiltonian systems must equal one (as the map $D P_D^i$ is symplectic); therefore, at best, all eigenvalues lie on the unit circle, and the solution is linearly stable, but not asymptotically so.

1.2.5 Symmetry

Two classes of symmetries are of note: 1) continuous symmetries, which are associated with constants of motion by Noether's Theorem, and may be eliminated by an appropriate canonical transformation; and 2) discrete symmetries, in which the dynamics in one region of phase space may be identified with the dynamics in another.

Define a map γ to be a symmetry of a system with vector field $\dot{z} = F(z)$ if $\gamma \circ F(z) = F \circ \gamma(z)$. If γ depends on a continuous parameter, we say that γ is a *continuous symmetry*; otherwise, we say it is a *discrete symmetry*. If every γ is invertible, the set $G = \{\gamma\}$ of symmetries form a group under composition.

Typically, we eliminate continuous spatial symmetries by appropriate canonical transformations, so that the essential dynamics are captured without redundant expression of information. Therefore, unless specified otherwise, we use the term *symmetry group* to refer only to the group of discrete symmetries.

A fundamental feature of a symmetry is that if $z(t) = \varphi_H^t z_0$ is a solution of the system H , so also is $S(z(t)) = S(\varphi_H^t z_0) = \varphi_H^t S(z_0)$. That is, symmetries map solutions to solutions, and, moreover, if a symmetry maps a solution to a different solution, the two solutions are dynamically equivalent.

An additional symmetry is *phase-shifting*. That is, if $z(t)$ is a solution of some continuous system, so is $z(t - t_0)$, simply shifting the origin of the time coordinate. If $z(t)$ is periodic with period T , phase shifts themselves form a group under addition

modulo T . This is better expressed as a fraction of the period. This motivates the following theorem [66].

Theorem 1.6. *Suppose H is a Hamiltonian system possessing symmetry group G . Suppose also that $z(t)$ is a solution of Hamilton's equations for H such that $z(0) = z_0$ and $z(t_0) = \gamma(z_0)$ for some $\gamma \in G$, some minimal $t_0 > 0$, and γ is of order k . Then $z(t)$ is periodic with period $T = kt_0$.*

Proof. The statement that $z(t_0) = \gamma(z(0))$ is equivalent to $\varphi_H^{t_0}z_0 = \gamma(z_0)$. Thus $z(2t_0) = \varphi_H^{2t_0}z_0 = \varphi_H^{t_0} \circ \varphi_H^{t_0}z_0 = \varphi_H^{t_0}(z(t_0)) = \varphi_H^{t_0}\gamma(z_0) = \gamma(\varphi_H^{t_0}) = \gamma^2(z_0)$. By iteration k times we obtain $z(kt_0) = \gamma^k(z(0)) = z(0)$.

By phase-shifting we have $z(t + kt_0) = z(t)$ for all t . Therefore $z(t)$ is periodic with period $T = kt_0$. \square

We denote such symmetries of solutions by $(\gamma, \pm \frac{1}{k} \bmod 1)$, where $\gamma \in G$ and $\gamma^k = I$, such that $(\gamma, \pm \frac{1}{k})(z(t)) = \gamma(z(t + \frac{T}{k}))$. That is, after $\frac{T}{k}$ the solution is in a configuration related to its configuration at time t by symmetry γ .

We now introduce the idea of the fixed set of a symmetry; important because fixed sets of involutions play an important role in the dynamics of systems with symmetry [59, 30].

Definition 1.7. *The fixed set of a symmetry is the set of points $z \in \Omega$ fixed by $\gamma \in G$, where $\gamma: \Omega \rightarrow \Omega$, is*

$$\text{Fix}(\gamma) = \{z: \gamma(z) = z\}.$$

Involutions are discrete symmetries of order 2—that is, $\gamma_i = \gamma_i^{-1}$. These are interesting because of their fixed sets, which may impose interesting structure on solutions with points in their fixed sets.

A map R that sends orbits into time-reversed orbits is called a *reversing symmetry*. Such a map satisfies $R \circ F(z) = -F \circ R(z)$, and its fixed set $\text{Fix}(R)$ is defined the same way as for a non-reversing symmetry. Autonomous Hamiltonian systems that are even functions of momentum are symmetric under simultaneous reversal of the signs of the momentum variables and the direction of the flow of time, so we take reversing the signs of the momenta to be the “atomic” time-reversing (or just *reversing*) symmetry, an involution whose fixed set is the set of points in phase space such that $p = 0$. Composing the reversor, the map that sends $p \rightarrow -p$, with another symmetry creates another reversing symmetry.

The composition of a non-reversing symmetry with a reversing symmetry is a reversing symmetry. The composition of two reversing symmetries is a non-reversing symmetry.

The *reversing symmetry group* $\Gamma = G \cup RG$ is the group comprising all reversing and non-reversing symmetries, c.f. Lamb and Quispel [30]. The comprehensive review by Roberts and Quispel [59] and references therein give the following theorem, which is a sufficient condition for periodic orbits of a system with reversing symmetries.

Theorem 1.8. *Consider a solution $z(t)$ to a dynamical system with reversing symmetry group Γ and spatial symmetry group G , with reversing involutions $R_1, R_2 \in \Gamma \setminus G$, such that $z(0) \in \text{Fix}(R_1)$ and $z(\frac{t_0}{2}) \in \text{Fix}(R_2)$, and for no $t \in (0, \frac{t_0}{2})$ is any point of $z(t)$ in the fixed set of any other reversing symmetry.*

The solution $z(t)$ is periodic with period $T = kt_0$, where k is the order of the non-reversing element $R_2R_1 \in G$.

Proof. As $z(0) \in \text{Fix}(R_1)$, we have

$$R_1(z(t)) = z(-t).$$

Similarly, we have

$$R_2(z(t)) = z(t_0 - t),$$

so that $R_2(z(\frac{t_0}{2})) = z(\frac{t_0}{2})$ as required. By composition, observe that

$$\begin{aligned} R_2R_1(z(t)) &= R_2(z(-t)) \\ &= z(t_0 + t). \end{aligned}$$

This is exactly the case that Theorem 1.6 applies, with $\gamma = R_2R_1$ of order k . Thus $z(t)$ is periodic with period $T = kt_0$. \square

The Mirror Theorem [61] is an example of a special case of Theorem 1.8 for the n -body problem with general masses, where the reversing symmetries are either a) collinear configurations with all velocities perpendicular to the given line, or b) planar configurations with all velocities perpendicular to the given plane. The Mirror Theorem is restated by Broucke and Boggs [7] as a sufficient condition for periodicity of orbits in the general 3-body problem.

Theorems 1.6 and 1.8 give us some idea about the behaviour of solutions with symmetry. One more case is of interest to specify: the fixed set of a non-reversing symmetry $\text{Fix}(\gamma)$ forms an invariant subspace of the dynamics of a system. If a solution $z(t)$ begins in $\text{Fix}(\gamma)$, then γ fixes every point of $z(t)$, with $\gamma(z(t)) = z(t)$. If the dimension of $\text{Fix}(\gamma)$ is sufficiently large, interesting dynamics may occur, including periodic solutions possessing symmetry beyond that γ itself, to which Theorems 1.6 and 1.8 apply.

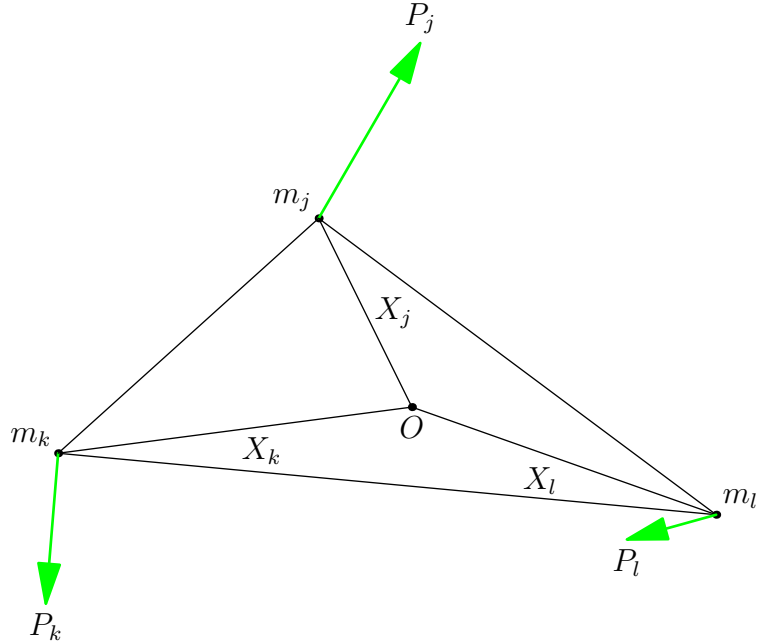


Figure 1.1: The planar 3-body problem for vanishing angular momentum.

1.3 The 3-body problem

1.3.1 A problem in classical dynamics

The 3-body problem is the classical problem of celestial mechanics of three bodies moving under their mutual gravitational forces, see, for example, [41, 35] and many others. It may be expressed as a Hamiltonian system in Cartesian coordinates, illustrated in figure 1.1. In this figure the bodies, denoted by subscripted indices, have masses m_i and positions relative to the origin O of an inertial frame of reference denoted by X_i , with momenta P_i . The origin in this figure is chosen to be the centre of mass, and the momenta satisfy $P_j + P_k + P_l = 0$. The force of gravity acts between bodies i and j (with $i \neq j$) such that $F_{ij} = -F_{ji} = \frac{Gm_i m_j (X_j - X_i)}{|X_j - X_i|^2}$.

The Hamiltonian of the classical N -body problem in dimension d is

$$H = T(P_1, \dots, P_N) + V(X_1, \dots, X_N), \quad (1.9)$$

in which T is kinetic energy and V is potential energy, given by

$$T = \sum_{i=1}^N \frac{\|P_i\|^2}{2m_i} \text{ and} \quad (1.10)$$

$$V = - \sum_{i=1}^{N-1} \sum_{j=i+1}^N \frac{G m_i m_j}{\|X_j - X_i\|} \quad (1.11)$$

where $P_i, X_i \in \mathbb{R}^d$ and $m_i \in \mathbb{R}^+$ for all $i = 1, \dots, N$ and $G \in \mathbb{R}^+$ is the gravitational constant. We choose $N = 3$ and $d = 2$, units such that $G = 1$, and consider $P_i, X_i \in \mathbb{C}$ rather than in \mathbb{R}^2 . Thus the Hamiltonian we consider is

$$H = \sum \frac{|P_j|^2}{2m_j} - \sum \frac{m_k m_l}{|X_l - X_k|}, \quad (1.12)$$

with notation chosen to provide a shorthand throughout this document: (j, k, l) are cyclic permutations of $(1, 2, 3)$ and summation (and taking products) without index is over the permutations of j, k and l . That is, (j, k, l) are replaced in such expressions by $(1, 2, 3)$, $(2, 3, 1)$ and $(3, 1, 2)$ in turn and the resulting expressions are added (or multiplied). Time is denoted by \tilde{t} .

The moment of inertia is

$$I = \sum m_j |X_j|^2. \quad (1.13)$$

Define *reduced masses* $\mu_j \in \mathbb{R}^+$:

$$\frac{1}{\mu_j} = \frac{1}{m_k} + \frac{1}{m_l} = \frac{m_k + m_l}{m_k m_l}. \quad (1.14)$$

Define also the *total mass* $m = \sum m_j$.

1.3.2 Symmetries of the 3-body problem

1.3.2.1 Continuous symmetries

The equations of motion

$$\dot{X}_j = \frac{\partial H}{\partial P_j}, \quad \dot{P}_j = -\frac{\partial H}{\partial X_j} \quad (1.15)$$

of (1.12) contain many symmetries. In general, the equations of motion are invariant under spatial and temporal translations, and rotations. The phase space is 12-dimensional, and by fixing the centre of mass and centre of momentum (as was shown in figure 1.1), the energy $H = h$ and angular momentum $p_\phi = \text{Im} \sum \bar{X}_j P_j$, we reduce to a phase space of dimension 6, where solutions evolve on manifolds of constant energy, dimension 5.

Spatial translations are of the form $X_j \rightarrow X_j + a$, where $a \in \mathbb{C}$ constant for each $j = 1, 2, 3$. In the potential, $|X_l - X_k| \rightarrow |X_l + a - X_k - a| = |X_l - X_k|$. The potential

$V(X)$ is homogeneous in space. We thus may choose the centre of mass to be the origin of an inertial coordinate system, without loss of generality.

Time translations are of the form $t \rightarrow t + a$, where $a \in \mathbb{R}$ constant. Since H is independent of t the system is invariant under time translations and energy is conserved.

Rotations take the form $(X_j, P_j) \rightarrow (e^{i\theta} X_j, e^{i\theta} P_j)$, for constant $\theta \in \mathbb{R}$ for each $j = 1, 2, 3$. As $|e^{i\theta}| = 1$, $|e^{i\theta} X_l - e^{i\theta} X_k| = |e^{i\theta}| |X_l - X_k| = |X_l - X_k|$ and $|e^{i\theta} P_j| = |e^{i\theta}| |P_j| = |P_j|$.

Because of spatial translation invariance we have that total momentum $\sum P_j = P$ constant. Without loss of generality, choose $\sum P_j = 0$, which sets the velocity of the centre of mass to zero.

Homogeneity implies a scaling law. The potential energy has degree -1 in coordinates, while the kinetic energy has degree 2 in momenta. Thus if we scale the total energy by $\lambda \in \mathbb{R}^+$, we may scale momenta by $\lambda^{\frac{1}{2}}$ and coordinates by λ^{-1} to obtain a dynamically equivalent solution. Solutions related by such a parameter are said to be *homothetic*. As we are interested in only the negative-energy case, we thus normalise the energy to $h = -1$.

1.3.2.2 Discrete symmetries

Discrete symmetries depend on the values of the masses: if all three masses are equal, then any permutation of the indices is a symmetry; if two masses are equal, then permutations of the corresponding indices are symmetries; and if all masses are not equal, there are no permutation symmetries. In every case, however, the equations of motion are invariant under spatial reflection of positions and momenta.

For equal masses, define

$$\begin{aligned}\sigma_j(X_j, X_k, X_l, P_j, P_k, P_l) &= (X_j, X_l, X_k, P_j, P_l, P_k) \\ c(X_j, X_k, X_l, P_j, P_k, P_l) &= (X_k, X_l, X_j, P_k, P_l, P_j) \\ \rho(X_j, X_k, X_l, P_j, P_k, P_l) &= (\bar{X}_j, \bar{X}_k, \bar{X}_l, \bar{P}_j, \bar{P}_k, \bar{P}_l).\end{aligned}$$

In order, σ_j is pairwise permutation of coordinates and momenta of bodies k and l , $c = \sigma_l \circ \sigma_k$ is a cyclic permutation of all coordinates and momenta, and ρ is a reflection.

The set $\{I, \sigma_1, \sigma_2, \sigma_3, c, c^2\}$ form the symmetric group S_3 , of order 6, where I is the identity and $c^2 = c^{-1}$. The reflection symmetry ρ generates $R_2 \cong \mathbb{Z}_2$ and commutes with all elements of S_3 . The group $G = R_2 \times S_3$ is the spatial symmetry group, of order 12, with centre R_2 .

Because the Hamiltonian is autonomous and even in the momenta, it possesses the reversing symmetry τ such that $\tau(X_j, X_k, X_l, P_j, P_k, P_l) = (X_j, X_k, X_l, -P_j, -P_k, -P_l)$,

generating $T_2 \cong \mathbb{Z}_2$. This symmetry (which commutes with all elements of G) may be composed with the preceding discrete symmetries to obtain other reversing symmetries, as in section 1.2.5. The reversing symmetry group is $\Gamma \cong C_4 \times S_3$, where $C_4 = T_2 \times R_2 \cong V_4$ is the centre of Γ , isomorphic to the Klein 4-group.

When $m_k = m_l \neq m_j$, only the permutation σ_j remains of the permutation subgroup, so we have $\Gamma = C_4 \times S_2 \cong E_8 \cong \mathbb{Z}_2^3$. In the case of unequal masses, no permutation is a symmetry, so in that case $\Gamma = C_4 \times \{I\} \cong V_4$. In general, denote the symmetry group by $\Gamma = C_4 \times S$, where S is chosen to be the appropriate permutation group.

1.3.3 Reduction by continuous symmetries

Moeckel and Montgomery [44] give a comprehensive overview of symmetry reduction and regularisation of collisions in the 3-body problem.

We reduce the continuous symmetries of equation (1.15) by canonical changes of coordinates. We make use of two approaches: first, Jacobi coordinates (to reduce by translations) followed by the Hopf map (to reduce by rotations), which gives the classical *shape space*, or the set of congruence classes of oriented triangles (in turn, scaling by moment of inertia reduces to the *shape sphere*, the set of similarity classes of triangles); and second, Murnaghan's symmetric coordinates, which reduces by both translations and rotations. The second method does not distinguish between positively and negatively oriented triangles; however, this is acceptable as the process of regularisation (section 1.4) in fact restores the distinction.

1.3.3.1 Jacobi coordinates, the Hopf map and the shape sphere

Jacobi coordinates [36] are commonly used to represent n -body systems, reducing the number of degrees of freedom in a hierarchical way. We first choose one pair of masses (say, X_1 and X_3) and construct $\xi_1 = X_1 - X_3$. The location of the third mass is then given with respect to the barycentre of the first pair: $\xi_2 = X_2 - \frac{m_1 X_1 + m_3 X_3}{m_1 + m_3}$. These coordinates are invariant under translations, but not rotations. We scale these by reduced masses defined by $\frac{1}{\tilde{\mu}_1} = \frac{1}{\mu_2} = \frac{1}{m_1} + \frac{1}{m_3}$ and $\frac{1}{\tilde{\mu}_2} = \frac{1}{m_2} + \frac{1}{m_1 + m_3}$. Define $\zeta_1 = \sqrt{\tilde{\mu}_1} \xi_1$ and $\zeta_2 = \sqrt{\tilde{\mu}_2} \xi_2$. Note that while $\tilde{\mu}_1 = \mu_2$, $\tilde{\mu}_2$ is the reduced mass with respect to the pair of bodies 1 and 3. The difference in notation is chosen so that the subscripts of the new variables correspond to one another.

The Hopf map [26] allows us to reduce by rotations to obtain the shape sphere [29, 42]. Define w_1, w_2, w_3, w_4 as follows:

$$w_1 = |\zeta_1|^2 - |\zeta_2|^2$$

$$\begin{aligned} w_2 + iw_3 &= 2\bar{\zeta}_1\zeta_2 \\ w_4 &= |\zeta_1|^2 + |\zeta_2|^2. \end{aligned}$$

In this way, we have $w_1^2 + w_2^2 + w_3^2 = w_4^2$, where $w_4 = \frac{1}{m} \sum m_j |X_j|^2$ is the moment of inertia. By normalising so that $w_4 = \frac{1}{2}$ we obtain $S_c = \{(w_1, w_2, w_3) : w_1^2 + w_2^2 + w_3^2 = \frac{1}{4}\}$, the classical shape sphere, with radius one half, or set of similarity classes of triangles. Leaving these coordinates un-normalised we have the shape space, in which each oriented triangle is represented by a point. Of note is that $w_3 = 4\sqrt{\frac{M}{m}}|X_3 - X_2||X_1 - X_3|\sin(\theta_3)$, where θ_3 is the exterior angle at X_3 . In other words, $w_3 = 4\sqrt{\frac{M}{m}}A$, where $M = m_1 m_2 m_3$, is proportional to the signed area $A = |X_3 - X_2||X_1 - X_3|\sin(\theta_3)$ of the triangle formed by the three bodies.

Montgomery has made extensive use of the shape sphere in his work on the 3-body problem [50], and it is for closed loops on the shape sphere that the geometric phase is defined, though we do not deal with geometric phase specifically until Chapter 4.

For equal masses the shape sphere has the following properties:

- the north and south poles represent equilateral configurations;
- the equator contains all collinear configurations;
- three points on the equator (each $\frac{2\pi}{3}$ apart) represent binary collisions;
- the great circles joining each collision point to the north and south poles are isosceles configurations.

For exactly two equal masses only one of the isosceles lines of symmetry remains a great circle, and the points representing the equilateral triangles move from the north and south poles. For general masses, only the set of collinear configuration remains a great circle.

Figure 1.2 shows the shape sphere and labels its important features in the case of equal masses. The notation of these features, with \pm referring to the orientation of the triangle, is as follows:

E^\pm : the \pm -oriented equilateral point;

B_{kl} : the collision between bodies k and l ;

M_j : the midpoint of the arc of the equator between B_{jk} and B_{lj} , isosceles collinear with m_j in syzygy;

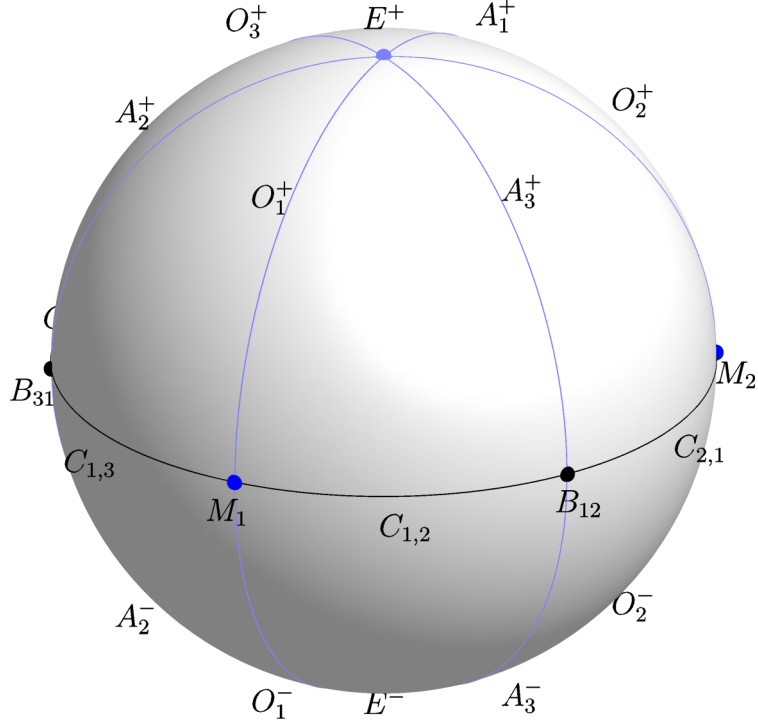


Figure 1.2: The shape sphere with symmetry lines depicted for equal masses. Blue circles represent isosceles configurations (A, O), the black circle represents collinear configurations (C). The light blue dots represent equilateral configurations (E), dark blue dots represent isosceles collinear configurations (M) and black dots represent the binary collisions (B).

$C_{j,k}$: the set of collinear configurations with body j in syzygy and closer to collision with body k ;

A_j^\pm : the acute isosceles configurations between E^\pm and B_{kl} (that is, with m_j on the symmetry axis);

O_j^\pm : the obtuse isosceles configurations between E^\pm and M_j (again, with m_j on the symmetry axis).

Discrete symmetries act on shape space as follows:

σ_j : rotates by π about the line joining M_j with B_{kl} through the centre of the shape sphere;

c : composes $\sigma_k \circ \sigma_j$, rotating a point clockwise by $\frac{2\pi}{3}$ about the axis joining the poles E^\pm ;

ρ : reflects across the equator.

1.3.3.2 Symmetric coordinates

Murnaghan's symmetric coordinates [53] eliminate the nodes, describing the triangle in terms of its side lengths and an extra angle that describes the rotation of the triangle with respect to an inertial frame. Define $a_j, \phi_j \in \mathbb{R}$ such that

$$X_l - X_k = a_j e^{i\phi_j}. \quad (1.16)$$

That is, a_j is the length of the side of the triangle opposite m_j and ϕ_j is its angle in an inertial frame. Define $\phi = \frac{1}{3}(\phi_1 + \phi_2 + \phi_3)$. *Reconstruction* is the process of recovering the original coordinates and momenta from the reduced coordinates and momenta.

Reconstruction from symmetric coordinates to configuration space is given in Waldvogel [85]:

$$mX_j = m_l a_k e^{i\phi_k} - m_k a_l e^{i\phi_l}, \quad (1.17)$$

where $m = m_1 + m_2 + m_3$.

Figure 1.3a illustrates the symmetric coordinates and absolute and relative angles and their relationship to the positions relative to the centre of mass O .

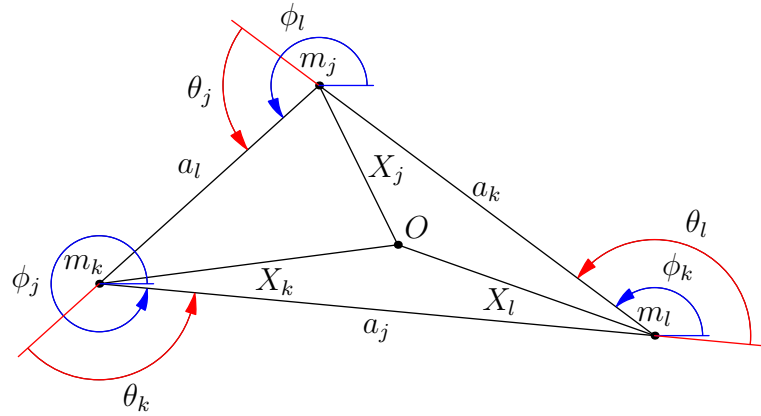
Canonically conjugate momenta are $p_j, p_\phi \in \mathbb{R}$. The generating function of the second type

$$G(X_1, X_2, X_3, p_1, p_2, p_3, p_\phi) = a_1 p_1 + a_2 p_2 + a_3 p_3 + \phi p_\phi, \quad (1.18)$$

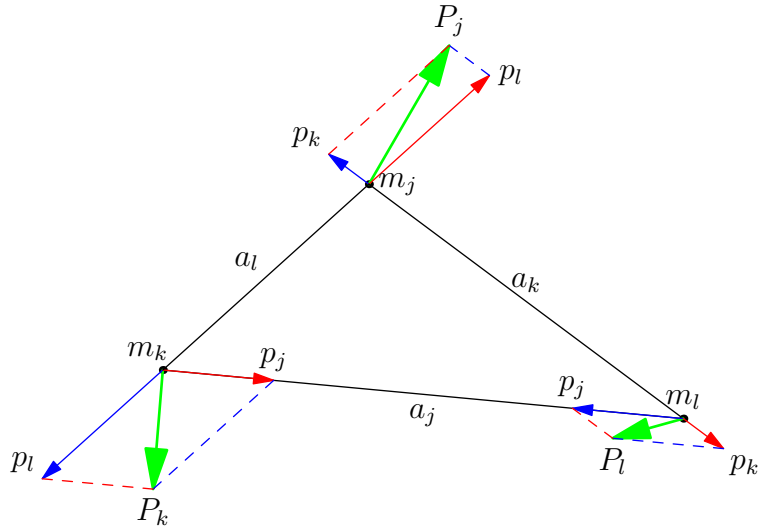
gives

$$P_j = \frac{\partial G}{\partial X_j} = p_k e^{i\phi_k} - p_l e^{i\phi_l} + \frac{ip_\phi}{3} \left(\frac{e^{i\phi_k}}{a_k} - \frac{e^{i\phi_l}}{a_l} \right), \quad (1.19)$$

illustrated for $p_\phi = 0$ in figure 1.3b, showing how the reduced momenta are the lengths of projections of the physical momenta in the directions of the sides onto the adjacent sides. There is some slight subtlety to be observed here, in that neither the original complex coordinates X_1, X_2, X_3 , nor the original momenta P_1, P_2, P_3 are linearly independent; there are four reduced real coordinates a_1, a_2, a_3 , and ϕ , and corresponding reduced momenta. While the equations (1.18) and (1.19) are expressed symmetrically, it is better to use the constraints $m_1 X_1 + m_2 X_2 + m_3 X_3 = 0$ and $P_1 + P_2 + P_3 = 0$ to eliminate one pair of coordinates and momenta, so that the number of degrees of freedom match. Equation (1.19) can be used to reconstruct the two momenta, and the constraints can be used to obtain the position and momentum of the third body.



- (a) Symmetry-reduced coordinates a_j (the side lengths of the triangle opposite each body j), absolute side angles ϕ_j , and exterior angles θ_j in relationship with Cartesian coordinates X_j .



- (b) Symmetry-reduced momenta p_j in relationship with physical momenta P_j . Blue colouring represents when the reduced momentum is the first term of equation (1.19) and red represents when it is the second. The dashed lines are parallel to the arrowed vectors of corresponding colour, showing the relationship as projections of P_j in the directions of the adjacent sides.

Figure 1.3: Symmetry-reduced variables.

We carry along p_ϕ because while we intend to fix its value to zero for subsequent work, we still require the equation of motion for ϕ to allow reconstruction of the original configuration and momenta.

Substituting equations (1.16) and (1.19) into H gives a new Hamiltonian

$$H = \frac{1}{2} \sum \frac{1}{m_j} \left(p_k^2 + p_l^2 - p_k p_l \frac{a_j^2 - a_k^2 - a_l^2}{a_k a_l} \right) + \frac{2p_\phi}{3} \sum \frac{1}{m_j} \left(\frac{p_k}{a_l} - \frac{p_l}{a_k} \right) \frac{A}{a_k a_l} + \frac{p_\phi^2}{9} \sum \frac{1}{m_j} \frac{a_k^2 + a_l^2 - \frac{1}{2} a_j^2}{a_k a_l} \quad (1.20)$$

in which the angle ϕ is ignorable, so $\frac{dp_\phi}{dt} = 0$. Hamilton's equations give the equations of motion for each a_j and p_j , but also

$$\frac{d\phi}{d\tilde{t}} = \frac{\partial H}{\partial p_\phi} = \frac{2}{3} \sum \frac{A}{m_j a_k a_l} \left(\frac{p_k}{a_l} - \frac{p_l}{a_k} \right) + \frac{2}{9} p_\phi \sum \frac{a_k^2 + a_l^2 - \frac{1}{2} a_j^2}{m_j a_k^2 a_l^2}, \quad (1.21)$$

for the angle ϕ needed during reconstruction. Shape dynamics are separated from rotation dynamics.

Note that reflections along the lines with slope $\phi + \frac{k\pi}{3}$ for $k = 0, 1, 2$ preserve ϕ .

For reconstruction, define exterior angles

$$\theta_j = \phi_l - \phi_k \mod 2\pi. \quad (1.22)$$

Then

$$\cos \theta_j = \frac{a_j^2 - a_k^2 - a_l^2}{2a_k a_l}, \quad (1.23)$$

$$\sin \theta_j = \frac{2A}{a_k a_l}, \text{ and} \quad (1.24)$$

$$\tan \frac{\theta_j}{2} = \frac{4A}{a_j^2 - (a_k - a_l)^2}, \quad (1.25)$$

where $A = \sqrt{\sigma(\sigma - a_1)(\sigma - a_2)(\sigma - a_3)}$ is the area and $\sigma = \frac{1}{2}(a_1 + a_2 + a_3)$ is the semiperimeter. The inverse transformation is

$$\phi_j = \phi + \frac{1}{3} (\theta_k - \theta_l). \quad (1.26)$$

Note that these coordinates, while elegant due to their symmetry, are undesirable, as singularities are introduced to the momenta when the system approaches any syzygy (that is, any configuration where $a_j = a_k + a_l$). These singularities arise from the projections of the physical momenta in the directions of the sides of the triangle, which all coincide at such points of degeneracy. We use coordinates a_j, p_j , however, as a stepping stone to regularisation of the binary collisions in section 1.4.

1.3.4 Central configurations

Special configurations of the 3-body problem deserve some mention at this point; namely, *central configurations*, discussed, for example, by Marchal [37, 38]. These are special configurations in which the acceleration of each body is proportional to its distance from the centre of mass of the system, or $\frac{F_j}{m_j} = \lambda X_j$ for each j , with $\lambda > 0$. Two possible cases must be considered: all X_j are collinear; or they are not.

The first case gives rise to Euler configurations, where the distances between the bodies is related to the masses. Without loss of generality, align the bodies such that $\text{Im}(X_j) = 0$ for each j , and set $X_1 = 0$, $X_2 = 1$, and $X_3 = 1 + r$, for $r > 0$. Then the central configurations for the collinear 3-body problem are governed by a fifth degree polynomial in r , with the masses as parameters, with only one positive real root.

Lagrange proved in the second case that the only central configuration for the non-collinear 3-body problem is an equilateral configuration. This result holds for any masses.

The importance of central configurations is that if released from rest such configurations proceed to total collapse to the centre of mass. If given appropriate velocities, such configurations evolve in Keplerian orbits about the centre of mass; however, such orbits have non-vanishing angular momentum. Moreover, it is only possible to approach triple collision by tending towards a central configuration [83, 84, 42].

Interestingly, the equilateral configuration only corresponds to the points $(0, 0, \pm 1)$ on the shape sphere when $m_1 = m_2 = m_3$. In general, the equilateral point is given by

$$\begin{aligned} w_1 &= \frac{m_1 m_3 \left(1 + \frac{2m_2}{m_1+m_3}\right) - m_2 m_3 - m_1 m_2}{m_2 m_3 + m_3 m_1 + m_1 m_2} \\ w_2 &= \frac{\sqrt{mM} \left(1 - \frac{2m_1}{m_1+m_3}\right)}{m_2 m_3 + m_3 m_1 + m_1 m_2} \\ w_3 &= \pm \frac{\sqrt{3mM}}{m_2 m_3 + m_3 m_1 + m_1 m_2}, \end{aligned}$$

where the sign of w_3 is given by the orientation of the triangle. The triangle corresponding to the poles $(w_1, w_2, w_3) = (0, 0, \pm 1)$ has side lengths $a_j = \lambda \sqrt{m_j(m_k + m_l)}$, for some positive scale factor λ .

1.3.5 The energy surface and the Hill region

The energy surface is a 5-dimensional surface in the 6-dimensional phase space. As energy is fixed along each trajectory and any orbit can be scaled so that its energy

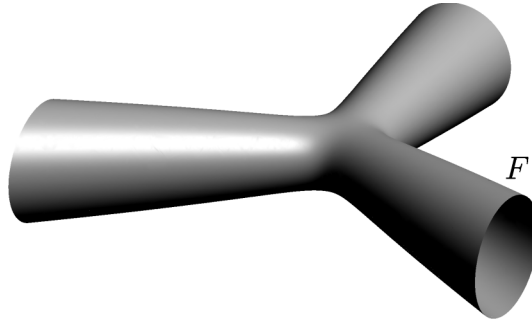


Figure 1.4: The Hill region in shape space.

takes an arbitrary value (of the same sign), fix energy to $h = -1$. The energy surface is given by $H = T + V = h$. To understand what this surface looks like, set all momenta to zero: now we have a 2D boundary in \mathbb{R}^3 , which we call the *free fall boundary*, inside which motion may occur. Now fix points inside the boundary (away from collisions) and observe that the quadratic structure of T implies that the momenta live on ellipsoids that shrink to points towards the free fall boundary.

The region $\{z : V(z) \leq h\}$ contained by the free fall boundary is called the *Hill region*, illustrated in figure 1.4.

1.4 Regularisation

All formulations to this point contain singularities at the collisions, where the velocities become infinite. While the triple collision cannot be regularised (Siegel [69] showed that no real analytic continuation of a trajectory through triple collision is possible), the binary collisions can be. We do this following the method in [85], himself following Lemaître[34]. The regularised coordinates naturally give rise to a *regularised shape sphere*, and map to the classical shape sphere, albeit with some differences. In particular, regularisation introduces new coordinates that produce a four-fold cover of the normal shape sphere, and these regularised coordinates are not mass-weighted.

1.4.1 Transformations

Following [85], introduce regularised variables $\alpha_j \in \mathbb{R}$ such that

$$a_j = \alpha_k^2 + \alpha_l^2. \quad (1.27)$$

The inverse transformation gives

$$\alpha_j = \pm \sqrt{\alpha^2 - a_j},$$

where $\alpha := \sqrt{\alpha_1^2 + \alpha_2^2 + \alpha_3^2}$. Geometrically, the squares of the new variables are the distances between the masses and tangent points of the incircle with the sides adjacent to corresponding masses (figure 1.5a). Because the new coordinates are the square roots of the distances, any choice of signs of α_j s represents a triangle's shape, producing an eight-fold cover of the space of Murnagan's symmetric coordinates. While Heron's formula in terms of the symmetric coordinates takes only a positive sign, it may be modified in the new coordinates to represent the signed area in a natural way:

$$A = \alpha_1 \alpha_2 \alpha_3 \alpha. \quad (1.28)$$

Regularised canonically conjugated momenta $\pi_j \in \mathbb{R}$ are introduced by another generating function of the second type

$$G(a_1, a_2, a_3, \pi_1, \pi_2, \pi_3) = \sum \alpha_j \pi_j.$$

Thus

$$p_j = \frac{\partial G}{\partial a_j} = \frac{1}{4} \left(-\frac{\pi_j}{\alpha_j} + \frac{\pi_k}{\alpha_k} + \frac{\pi_l}{\alpha_l} \right). \quad (1.29)$$

Substituting equations (1.27) and (1.29) into the symmetry reduced Hamiltonian equation (1.20) produces a (still not regularised) Hamiltonian $H(\alpha_1, \alpha_2, \alpha_3, \phi, \pi_1, \pi_2, \pi_3, p_\phi)$.

To obtain a geometric understanding of the new momenta, substitute equations (1.27) and (1.29) into equation (1.19) to obtain

$$P_j = \frac{1}{4} \left((e^{i\phi_k} - e^{i\phi_l}) \frac{\pi_j}{\alpha_j} + (e^{i\phi_k} + e^{i\phi_l}) \left(\frac{\pi_l}{\alpha_l} - \frac{\pi_k}{\alpha_k} \right) \right) + \frac{ip_\phi}{3} \left(\frac{e^{i\phi_k}}{\alpha_k} - \frac{e^{i\phi_l}}{\alpha_l} \right). \quad (1.30)$$

Note that the complex numbers $(e^{i\phi_k} - e^{i\phi_l})$ and $(e^{i\phi_k} + e^{i\phi_l})$, interpreted as vectors in \mathbb{R}^2 , are perpendicular for any ϕ_k, ϕ_l . Define the *incentre* of the triangle to be

$$C = \frac{\sum a_j X_j}{2\alpha^2} \quad (1.31)$$

It happens that $\text{Arg}(e^{i\phi_k} - e^{i\phi_l}) = \text{Arg}(X_j - C) =: \psi_j$, so each momentum is naturally decomposed into two orthogonal vectors, as illustrated in figure 1.5b. The reconstruction formula for the physical coordinates is the same as equation (1.17), where we now substitute equation (1.27) for each a_j , and the physical momenta are reconstructed by equation (1.30). Full details of the reconstruction procedure are given in

appendix A, as some care is required in order to reconstruct solutions, rather than single points in the configuration space. We reproduce here the reconstruction of the physical momenta

$$P_j = \frac{e^{i\psi_j}}{2\sqrt{a_k a_l}} \left(\alpha \pi_j + i(\alpha_k \pi_l - \alpha_l \pi_k) + \frac{p_\phi}{3a_k a_l} ((a_k - a_l) \alpha_k \alpha_l + i(a_k + a_l) \alpha_j \alpha) \right). \quad (1.32)$$

The regularised coordinates “more space” around the collisions, but we must rescale time in order that the singularities be removed; the velocities still become infinite at collision with the transformations thus far. Our wish is to create a new time variable, with respect to which the velocities in the system remain finite at binary collision.

Recall section 1.2, in which we discussed the transformation to turn a non-autonomous Hamiltonian autonomous by the introduction of an extra degree of freedom. “Poincaré’s trick” bears some resemblance to the method of extending phase space, but both begins and ends with an autonomous Hamiltonian. Earlier the Hamiltonian was $H = H(q, p, \tilde{t})$, explicitly a function of the time variable (now denoted \tilde{t}), which was made into a dependent variable by the introduction of a fictional time t and a canonically conjugated momentum $p_{\tilde{t}}$. A new Hamiltonian became $K = \tilde{H}(q, p, \tilde{t}, p_{\tilde{t}}) = H + p_{\tilde{t}}$. This resulted in extra equations of motion $\frac{d\tilde{t}}{dt} = \frac{\partial K}{\partial p_{\tilde{t}}} = 1$ and $\frac{dp_{\tilde{t}}}{dt} = -\frac{\partial K}{\partial \tilde{t}} = -\frac{\partial H}{\partial t}$. That is, the fictional time flows at the same rate as the physical time, but the energy is not a constant of motion.

Here we begin with an autonomous Hamiltonian and wish for our modified Hamiltonian to remain so, but also vary the rate of flow between the fictional and physical times as a function of the configuration. Introduce a fictional time t , now such that $\frac{d\tilde{t}}{dt} = g(q, p)$. Our new Hamiltonian must be constructed such that

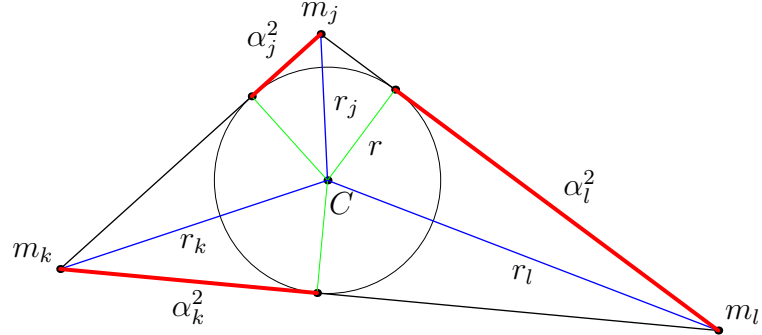
$$\frac{d\tilde{t}}{dt} = \frac{\partial K}{\partial p_{\tilde{t}}} = g(q, p) \quad (1.33)$$

$$\frac{dp_{\tilde{t}}}{dt} = -\frac{\partial K}{\partial \tilde{t}} = 0. \quad (1.34)$$

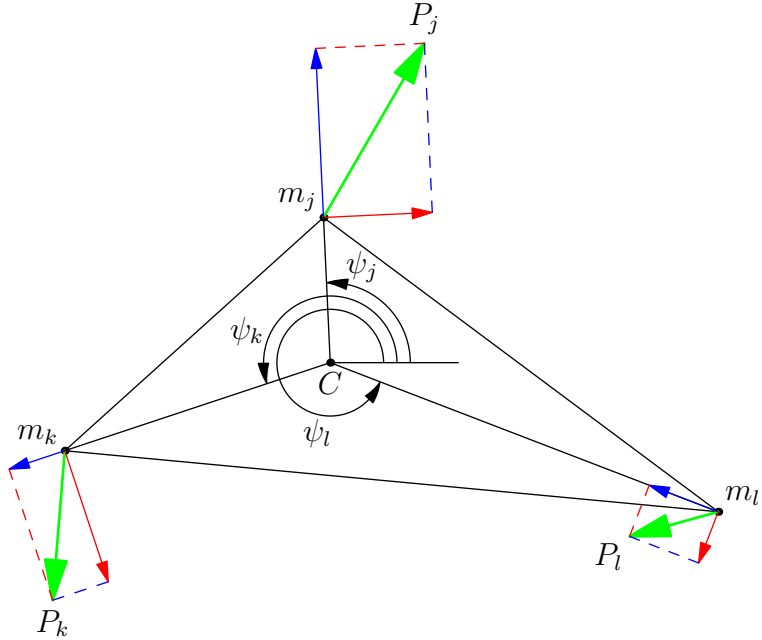
We thus require from equation (1.33) $K = p_{\tilde{t}}g(q, p) + F(q, p, \tilde{t})$ and from equation (1.34) K is independent of \tilde{t} . The only choice of function satisfying the boundary conditions and our requirements is $K = (H(q, p) + p_{\tilde{t}})g(q, p)$. Since the energy $h = H(q_0, p_0) = -p_{\tilde{t}}$ for initial conditions (q_0, p_0) is a constant of motion we can also write the modified Hamiltonian $K = (H - h)g(q, p) \equiv 0$ for any trajectory of the original system.

In our case choose t such that

$$\frac{d\tilde{t}}{dt} = a_1 a_2 a_3, \quad (1.35)$$



(a) Geometric interpretation of regularised coordinates (squared, red), incentre-vertex distances $r_j = \frac{\alpha_j \alpha}{\sqrt{a_k a_l}}$ (blue), and incircle radius $r = \frac{\alpha_1 \alpha_2 \alpha_3}{\alpha}$ (indicated in green).



(b) Decomposition of physical momenta as in equation (A.12) and indication of the incentre-vertex angles ψ_j . The blue component of each momentum vector is $\frac{\alpha \pi_j}{\sqrt{8a_k a_l}} e^{i\psi_j}$ and the red component is $-\frac{(\alpha_k \pi_l - \alpha_l \pi_k)}{\sqrt{8a_k a_l}} e^{i(\psi_j + \frac{\pi}{2})}$.

Figure 1.5: Regularised variables.

and use Poincaré's trick to construct

$$K = (H - h) a_1 a_2 a_3 = K_0 - h a_1 a_2 a_3. \quad (1.36)$$

The term K_0 coming from the original Hamiltonian multiplied by the time scaling still contains singularities in terms containing p_ϕ and p_ϕ^2 , but when we fix $p_\phi = 0$ it becomes

$$K_0 = \frac{1}{8} \boldsymbol{\pi}^T B(\boldsymbol{\alpha}) \boldsymbol{\pi} - \sum m_k m_l a_k a_l, \quad (1.37)$$

where

$$\begin{aligned} \boldsymbol{\pi} &= (\pi_1, \pi_2, \pi_3)^T, \\ \boldsymbol{\alpha} &= (\alpha_1, \alpha_2, \alpha_3)^T, \\ B(\boldsymbol{\alpha}) &= \begin{pmatrix} A_1 & B_3 & B_2 \\ B_3 & A_2 & B_1 \\ B_2 & B_1 & A_3 \end{pmatrix}, \\ A_j &= \frac{a_j}{m_j} \alpha^2 + \frac{a_k}{m_k} \alpha_l^2 + \frac{a_l}{m_l} \alpha_k^2, \text{ and} \\ B_j &= -\frac{a_j}{m_j} \alpha_k \alpha_l. \end{aligned}$$

The result of our choice $p_\phi = 0$ is that K is a polynomial of degree 6 without singularities at binary collision.

The symmetry-reduced, regularised equations of motion are thus

$$\dot{\boldsymbol{z}} = \begin{pmatrix} \dot{\boldsymbol{\alpha}} \\ \dot{\boldsymbol{\pi}} \end{pmatrix} = J_3 \nabla K. \quad (1.38)$$

Henceforth, differentiation of any quantity x with respect to physical time \tilde{t} shall be denoted by a prime x' , and with respect to scaled time t by a dot \dot{x} .

By the chain rule the geometric rotation angle evolves in scaled time by

$$\begin{aligned} \dot{\phi} &= \frac{d\phi}{d\tilde{t}} \frac{d\tilde{t}}{dt} = \frac{2}{3} \sum \frac{a_j A}{m_j} \left(\frac{p_k}{a_l} - \frac{p_l}{a_k} \right) \\ &= \frac{1}{6} \sum \frac{a_j \alpha}{m_j a_k a_l} \left(\alpha_k \alpha_l (\alpha_l^2 - \alpha_k^2) \pi_j + \alpha_j (\alpha_j^2 + \alpha^2) (\alpha_k \pi_l - \alpha_l \pi_k) \right). \end{aligned} \quad (1.39)$$

Even after regularisation equation (1.39) is not clearly going to be well-behaved at collision. So while we have a reconstruction formula (appendix A) that we know works for collisionless orbits, will this continue to work through collisions? To find out, we look briefly at the dynamics at collision.

Lemma 1.40. *The momentum sphere is degenerate at 23-collision and becomes a cylinder with axis aligned with the π_1 axis and radius $R_1 := 2\sqrt{2\mu_1 m_2 m_3}$, with no constraints on π_1 .*

Proof. Without loss of generality, substitute $\alpha_2 = \alpha_3 = 0$ into equation (1.36). After rearrangement this yields

$$\pi_2^2 + \pi_3^2 = \frac{8m_2^2 m_3^2}{m_2 + m_3} = 8\mu_1 m_2 m_3 = R_1^2. \quad (1.41)$$

□

By permutation of indices, we obtain analogous results for the other collisions.

From lemma 1.40 we may parameterise the regularised momenta at collision by an angle θ such that $\pi_2 = R_1 \cos \theta$ and $\pi_3 = R_1 \sin \theta$. The Hamiltonian vector field at 23-collision $z_B = (\alpha_1, 0, 0, \pi_1, \pi_2, \pi_3)$ may be written as

$$\dot{z}|_{z_B} = \begin{pmatrix} 0 \\ \frac{1}{4\mu_1} \alpha_1^4 \pi_2 \\ \frac{1}{4\mu_1} \alpha_1^4 \pi_3 \\ 0 \\ \frac{\alpha_1^3 \pi_1 \pi_2}{4m_3} \\ \frac{\alpha_1^3 \pi_1 \pi_3}{4m_2} \end{pmatrix} = \begin{pmatrix} 0 \\ \frac{R_1}{4\mu_1} \alpha_1^4 \cos \theta \\ \frac{R_1}{4\mu_1} \alpha_1^4 \sin \theta \\ 0 \\ \frac{R_1}{4m_3} \alpha_1^3 \pi_1 \cos \theta \\ \frac{R_1}{4m_2} \alpha_1^3 \pi_1 \sin \theta \end{pmatrix}. \quad (1.42)$$

The second time derivative is

$$\ddot{z}|_{z_B} = \begin{pmatrix} -\frac{1}{2} (m_2 \cos^2 \theta + m_3 \sin^2 \theta) \alpha_1^7 \\ 0 \\ 0 \\ -\frac{1}{2} (m_2 \cos^2 \theta + m_3 \sin^2 \theta) \alpha_1^6 \pi_1 \\ \frac{R_1}{2} (C + (m_3 - m_2) \sin^2 \theta) \alpha_1^6 \cos \theta \\ \frac{R_1}{2} (C + (m_2 - m_3) \cos^2 \theta) \alpha_1^6 \cos \theta \end{pmatrix}, \quad (1.43)$$

where

$$C = \frac{1}{\mu_1} (m_1 (m_2 + m_3) + h\alpha_1^2) - \frac{1}{8} \left(\frac{1}{m_2 m_3} + \frac{1}{m_1 \mu_1} \right) \pi_1^2,$$

and $\mu_1 = \frac{m_2 m_3}{m_2 + m_3}$.

Consider a solution passing near collision with $z_\epsilon = (\alpha_1, \epsilon \cos \vartheta, \epsilon \sin \vartheta, \pi_1, \pi_2, \pi_3)$, with $\alpha_1 \neq 0$ and $0 < \epsilon \ll 1$. From equation (1.42), we see that at collision the velocities $\dot{\alpha}_2 \propto \pi_2$ and $\dot{\alpha}_3 \propto \pi_3$. Decompose the velocities $\dot{\alpha}_2 = v_{\parallel} \cos \vartheta - v_{\perp} \sin \vartheta$, $\dot{\alpha}_3 = v_{\parallel} \sin \vartheta +$

$v_\perp \cos \vartheta$ with $v_\parallel = \dot{\epsilon}$ and $v_\perp = \epsilon \dot{\theta}$, components parallel to the radial direction from the origin of the $\alpha_2\alpha_3$ -plane and perpendicular to it, and v_\parallel and v_\perp are rather messy functions of the regularised coordinates and momenta. Equate these velocities to the corresponding components of the full vector field to obtain expressions for π_2 , π_3 in terms of $\alpha_1, \pi_1, \epsilon, \vartheta, \dot{\epsilon}, \epsilon \dot{\theta}$ and the masses. Details for this are given in appendix B.

The decomposition of the solution into radial and angular components gives us a way to understand the behaviour of $\dot{\phi}$ as we approach collision on a “true” collision solution, or if the trajectory merely makes a very close approach.

Consider first the choice that $v_\parallel = 0$, $v_\perp \neq 0$. We find the second derivatives of ϵ and ϑ :

$$\begin{aligned}\ddot{\epsilon} &= v_\perp^2 + \frac{m_2 - m_3}{4m_2 m_3} \alpha_1^3 \pi_1 v_\perp \sin(2\vartheta) \epsilon \\ \ddot{\vartheta} &= \frac{1}{2} (m_2 - m_3) \left(\alpha_1^6 + \frac{v_\perp^2}{(m_2 + m_3) \alpha_1^2} \right) \sin(2\vartheta),\end{aligned}$$

assuring us that this choice means ϵ is the distance of closest approach of a trajectory in the neighbourhood of z_ϵ . We choose this because from $v_\perp = \epsilon \dot{\vartheta}$ we see that $v_\perp = \dot{\epsilon} \dot{\vartheta} + \epsilon \ddot{\vartheta}$, from which $\frac{v_\perp}{\epsilon}$ gives us the angular acceleration of the trajectory about the collision axis, as we have chosen $v_\perp = \epsilon \dot{\theta} = 0$.

We construct the Taylor series about $\epsilon = 0$ of $\dot{\epsilon} \dot{\vartheta}$ for a trajectory that avoids collision with minimal regularised distance ϵ :

$$\epsilon \dot{\phi} = -\frac{2}{3} \operatorname{sgn}(\alpha_1) v_\perp + \frac{m_3 - m_2}{12m_2 m_3} |\alpha_1^3| \pi_1 \sin(2\vartheta) \epsilon + 0\epsilon^2 + \mathcal{O}(\epsilon^3). \quad (1.44)$$

Observe that in non-collision trajectories $\dot{\phi} \sim \frac{1}{\epsilon}$ as $\epsilon \rightarrow 0$, if the speed of the trajectory v_\perp at that point is given. Note that the physical distance between the two bodies is $a_1 = \epsilon^2$, and the absolute values of the physical momenta $P_2, P_3 \sim \frac{1}{\epsilon}$.

Consider now the case where $v_\perp = 0$, $v_\parallel \neq 0$. We hope that $\dot{\phi}$ at least does not blow up on solutions passing exactly through collision! (Indeed, it is exactly the case that $\lim_{\epsilon \rightarrow 0} \epsilon \dot{\phi} = 0$ on this trajectory.)

Without restriction on the velocities or momenta, the Taylor expansion of $\dot{\epsilon} \dot{\vartheta}$ for a trajectory passing through collision is

$$\epsilon \dot{\phi} = \frac{\operatorname{sgn}(\alpha_1) \alpha_1^4}{6\mu_1} (\pi_2 \sin \vartheta - \pi_3 \cos \vartheta) + 0\epsilon + 0\epsilon^2 + \mathcal{O}(\epsilon^3), \quad (1.45)$$

whose condition to vanish is that $\pi_2 = \lambda \cos \vartheta$ and $\pi_3 = \lambda \sin \vartheta$ for some $\lambda \neq 0$ and some ϑ . As 23-collision requires that $\pi_2 = R_1 \cos \theta$, $\pi_3 = R_1 \sin \theta$, we have $\lambda = R_1$, and $\phi(t)$ is

defined for all time on binary collision solutions, guaranteeing that our reconstruction will still work through collision.

1.4.2 Regularised symmetries

The process of regularisation induces an eightfold cover of Murnagan’s symmetric coordinates—a fourfold cover of the shape sphere (respecting oriented triangles). Alternating the sign of any combination of the regularised coordinates leaves the side lengths invariant. Changing the signs of the corresponding momenta simultaneously with the coordinates leaves the physical momenta invariant. We note that alternating the signs of two coordinates at once (and their corresponding momenta) is preserves the sign of the oriented area of the configuration triangle, so we define $s_j : \alpha_k \rightarrow -\alpha_k, \alpha_l \rightarrow -\alpha_l, \pi_k \rightarrow -\pi_k, \pi_l \rightarrow -\pi_l$. As each s_j is an involution and $s_j = s_k s_l = s_l s_k$, we see that $F_4 := \{I, s_1, s_2, s_3\} \cong V_4$.

Generators of the regularised non-reversing symmetry group for equal masses may be chosen as follows:

$$\begin{aligned}\rho(z) &= -z \\ \sigma_1(z) &= (-\alpha_1, -\alpha_3, -\alpha_2, -\pi_1, -\pi_3, -\pi_2) \\ \sigma_2(z) &= (-\alpha_3, -\alpha_2, -\alpha_1, -\pi_3, -\pi_2, -\pi_1) \\ s_3(z) &= (-\alpha_1, -\alpha_2, \alpha_3, -\pi_1, -\pi_2, \pi_3),\end{aligned}$$

with the actions of ρ and σ_j being chosen so that their meaning in configuration space is preserved—respectively reflecting across a line through the centre of mass, and swapping a pair of coordinates and momenta (which reverses orientation). The two pairwise permutations generate S_3 as before, and the other “sign flip” symmetries are generated by conjugations $s_1 = \sigma_2 s_3 \sigma_2$ and $s_2 = \sigma_1 s_3 \sigma_1$.

Observe that $s_j \sigma_k = \sigma_k s_l$, and the order of $\sigma_j s_k$ is 4, while $\sigma_j s_j = s_j \sigma_j$. The structure of the subgroup involving only permutation symmetries and sign flip symmetries is a semidirect product $S_3 \rtimes F_4$ with multiplication rule $(\sigma, \phi)(\sigma', \phi') = (\sigma\sigma', \sigma'^{-1}\phi\sigma'\phi')$, where $\sigma, \sigma' \in S_3$ and $\phi, \phi' \in F_4$.

The resulting regularised symmetry group is defined to be $\tilde{\Gamma} = C_4 \times S \rtimes F_4 \cong V_4 \times S_4$. The symmetry group, and the fixed sets of the symmetries, are discussed further in sections 2.1 and 2.3.

1.4.3 Regularised shape space and the regularised shape sphere

Each point in α -space represents an oriented triangle, so α -space is already a space of shapes of triangles. Note that the shape of triangle corresponding to any point in α -space does not depend on the choice of masses. Here we call it the *regularised shape space*. Similar to the shape space in section 1.3.3.1, the origin represents the triple collision; however, the distance from the origin is no longer the moment of inertia but the square root of the semiperimeter. Projecting all points onto a sphere of radius 1 forms the *regularised shape sphere* $S_r = \{(\alpha_1, \alpha_2, \alpha_3) : \alpha_1^2 + \alpha_2^2 + \alpha_3^2 = 1\}$.

Figure 1.6 illustrates the regularised shape sphere. Similar to figure 1.2 the important features may be labelled as follows, being derived from the discrete symmetries for equal masses in section 1.4.2; however, to avoid visual clutter we only display labels over one octant to illustrate the notation:

$$\begin{aligned} C_{j,k}^{\pm\pm} &= \{\alpha_j = 0, |\alpha_k| < |\alpha_l|\} \\ A_j^{\pm\pm\pm} &= \{|\alpha_j| > |\alpha_k| = |\alpha_l|\} \\ O_j^{\pm\pm\pm} &= \{|\alpha_j| < |\alpha_k| = |\alpha_l|\} \\ B_{jk}^{\pm} &= \{\alpha_j = \alpha_k = 0, \alpha_l \neq 0\} \\ E^{\pm\pm\pm} &= \{|\alpha_j| = |\alpha_k| = |\alpha_l|\} \\ M_j^{\pm\pm} &= \{\alpha_j = 0, |\alpha_k| = |\alpha_l|\} \end{aligned}$$

Here the superscripted signs indicate the signs of the coordinates dictating in which octant of space (when there are three signs), which quadrant of a coordinate plane (when there are two), or which side of a coordinate axis (where there is one) the particular point or great circle of symmetry lies.

Each $E^{\pm\pm\pm}$ lives in the centre of one octant of the regularised shape sphere, the binary collision points B_{kl}^{\pm} are on the intersections of the regularised shape sphere and the coordinate axes, the isosceles collinear configurations $M_j^{\pm\pm}$ lie on the coordinate planes exactly between the binary collision points, while the edges $C_{j,k}^{\pm\pm}$ as before join B_{kl}^{\pm} to $M_j^{\pm\pm}$, $O_j^{\pm\pm\pm}$ connects $M_j^{\pm\pm}$ to $E^{\pm\pm\pm}$, and $A_j^{\pm\pm\pm}$ connects B_{kl}^{\pm} to $E^{\pm\pm\pm}$. Concerning the map back to the un-regularised shape sphere, the product of signs gives the corresponding symbol with orientation.

1.4.4 Derivation of the classical shape sphere in regularised coordinates

While it is possible to put a regularised trajectory onto the classical shape sphere by use of the reconstruction described in appendix A and then following the traditional

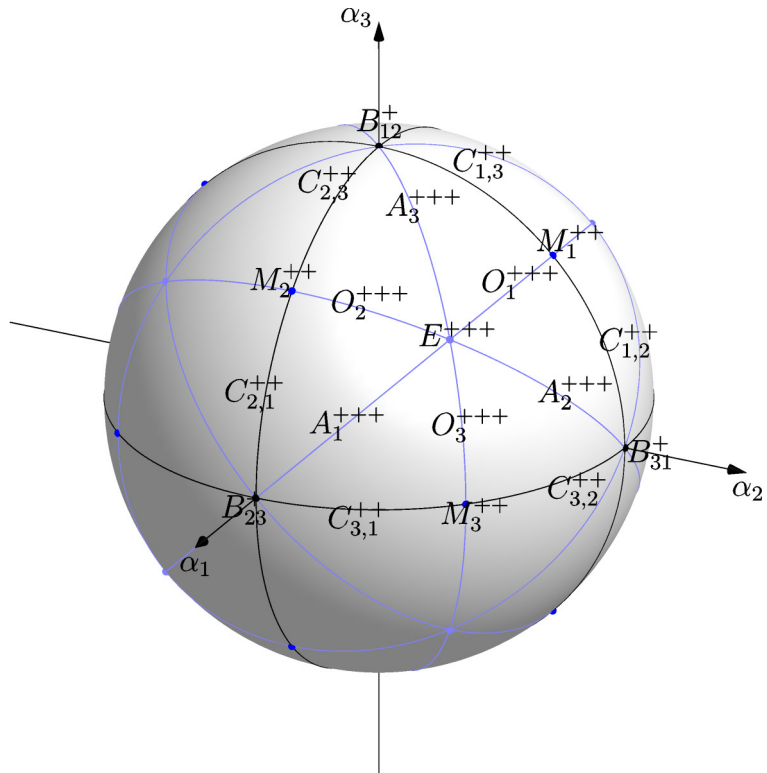


Figure 1.6: The regularised shape sphere, indicating lines and points of symmetry for equal masses. Light blue lines represent isosceles configurations, black lines collinear configurations. Light blue points represent equilateral configurations, dark blue isosceles collinear and black collisions.

method of reducing to Jacobi coordinates and applying the Hopf map, we desire an explicit expression in terms of the regularised variables for the purpose of calculating the geometric phase.

Define reduced masses $\tilde{\mu}_1, \tilde{\mu}_2$ as before:

$$\begin{aligned}\frac{1}{\tilde{\mu}_1} &= \frac{1}{m_1} + \frac{1}{m_3} \\ \frac{1}{\tilde{\mu}_2} &= \frac{1}{m_2} + \frac{1}{m_1 + m_3}.\end{aligned}$$

Thus

$$\begin{aligned}\tilde{\mu}_1 &= \frac{m_1 m_3}{m_1 + m_3} \\ \tilde{\mu}_2 &= \frac{m_2(m_1 + m_3)}{m_1 + m_2 + m_3} \text{ and} \\ \tilde{\mu}_1 \tilde{\mu}_2 &= \frac{m_1 m_2 m_3}{m_1 + m_2 + m_3} = \frac{M}{m},\end{aligned}$$

where $M = m_1 m_2 m_3$ and $m = m_1 + m_2 + m_3$.

Apply the Jacobi map

$$\begin{aligned}\xi_1 &= X_1 - X_3 = a_2 e^{i\phi_2} \\ \xi_2 &= X_2 - \frac{m_1 X_1 + m_3 X_3}{m_1 + m_3} \\ &= X_2 - \frac{m_1(X_1 - X_3) + (m_3 + m_1)X_3}{m_1 + m_3} \\ &= X_2 - X_3 - \frac{m_1}{m_3 + m_1} a_2 e^{i\phi_2} \\ &= -a_1 e^{i\phi_1} - \frac{\tilde{\mu}_1}{m_3} \xi_2\end{aligned}$$

and the mass-reduced Jacobi coordinates are defined also as before.

Consequently,

$$\zeta_1 \bar{\zeta}_1 = \tilde{\mu}_1 a_2^2 \tag{1.46}$$

$$\zeta_2 \bar{\zeta}_2 = \tilde{\mu}_2 \left(\left(1 - \frac{\tilde{\mu}_1}{m_3} \right) a_1^2 + \frac{\tilde{\mu}_1}{m_3} \left(\frac{\tilde{\mu}_1}{m_3} - 1 \right) a_2^2 + \frac{\tilde{\mu}_1}{m_3} a_3^2 \right) \tag{1.47}$$

$$\zeta_1 \bar{\zeta}_2 + \bar{\zeta}_1 \zeta_2 = \sqrt{\frac{M}{m}} \left(a_1^2 + \left(1 - \frac{2}{m_1 + m_3} \right) a_2^2 - a_3^2 \right) \tag{1.48}$$

$$\zeta_1\bar{\zeta}_2 - \bar{\zeta}_1\zeta_2 = 4\sqrt{\frac{M}{m}}A, \quad (1.49)$$

where $A = \frac{1}{2}a_1a_2 \sin \theta_3 = \alpha_1\alpha_2\alpha_3\alpha$ is the signed area of the triangle.

Now we apply the Hopf map: define w_1, w_2, w_3, w_4 such that

$$w_1 = \zeta_1\bar{\zeta}_1 - \zeta_2\bar{\zeta}_2 \quad (1.50)$$

$$w_2 + iw_3 = 2\bar{\zeta}_1\zeta_2 \quad (1.51)$$

$$w_4 = \zeta_1\bar{\zeta}_1 + \zeta_2\bar{\zeta}_2, \quad (1.52)$$

and $w_1^2 + w_2^2 + w_3^2 = w_4^2$.

Substituting equations (1.46)–(1.49) into equations (1.50)–(1.52) and simplifying, we obtain

$$\begin{aligned} w_1 &= -\frac{1}{m} \left(m_2m_3a_1^2 - m_1m_3 \left(1 + \frac{2m_2}{m_1 + m_3} \right) a_2^2 + m_1m_2a_3^2 \right) \\ w_2 &= \sqrt{\frac{M}{m}} \left(a_1^2 + \left(1 - \frac{2m_1}{m_1 + m_3} \right) a_2^2 - a_3^2 \right) \\ w_3 &= 4\sqrt{\frac{M}{m}}\alpha_1\alpha_2\alpha_3\alpha \\ w_4 &= \frac{1}{m} (m_2m_3a_1^2 + m_3m_1a_2^2 + m_1m_2a_3^2) = I, \end{aligned} \quad (1.53)$$

and we obtain the shape sphere with half-unit radius and coordinates (w_1, w_2, w_3) by normalising so that $w_4 = \frac{1}{2}$.

1.4.5 Regularised free fall boundary and Hill region

If $k \in \mathbb{R}$, we can scale distances in the 3-body problem by k^2 , momenta scale as k^{-1} and the energy by k^{-2} and obtain dynamically equivalent orbits. As the energy is a parameter of the regularised Hamiltonian, we choose to normalise the energy of all orbits to $h = -1$ (that is, choose $k^2 = |h|$). If all momenta are set to zero, we obtain a surface that we call the *free fall boundary*

$$F = \{(\alpha_1, \alpha_2, \alpha_3) \in \mathbb{R}^3 : V(\alpha_1, \alpha_2, \alpha_3) = -h\}. \quad (1.54)$$

The potential energy of the 3-body problem is

$$V = \frac{m_2m_3}{a_1} + \frac{m_3m_1}{a_2} + \frac{m_1m_2}{a_3}.$$

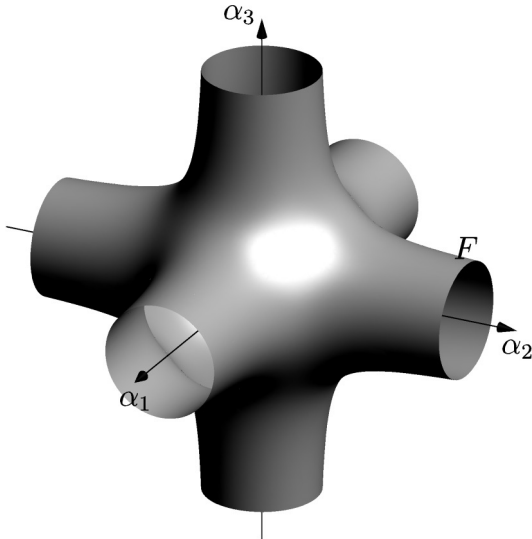


Figure 1.7: Regularised free fall boundary for $m_1 = m_2 = m_3 = -h = 1$.

Choosing $h = -V = -1$ gives the free fall boundary, shown for equal unit masses and negative unit energy in regularised shape space in figure 1.7, where the “arms” encircling each coordinate axis asymptote to cylinders of radius $\sqrt{m_k m_l}$.

As before, the Hill region is the volume of coordinate space inside the free fall boundary. Now, as the binary collisions are regularised, the collision axes may be included. It is important to note that the map of the free fall boundary to the regularised shape sphere does *not* include collision points, as lemma 1.40 shows that brake points are not possible at collision.

2 Discrete symmetries

2.1 Definition of the symmetry groups

Earlier, in sections 1.3.2.2 and 1.4.2, we introduced the discrete (reversing) symmetries of the 3-body problem in the un-regularised and regularised settings. In this chapter we recall these groups and examine their structure and the actions of their elements and subgroups on solutions, building a foundation for the work in subsequent chapters. We will mainly treat the case of equal masses, making note of when and how the cases of exactly two masses equal and unequal masses differ from the equal mass case.

Recall that the un-regularised problem permits spatial symmetries that are reflections of the configuration and momenta through some given line in the plane, represented by ρ , generating the group $R_2 \cong \mathbb{Z}_2$, and permutations of equal masses, generating S . The spatial symmetries form a group $R_2 \times S$. In the case of unequal masses no non-trivial permutation is allowed, so $S = \{I\}$; when exactly two masses are equal (say, $m_k = m_l$) we have $S = S_{2,j} = \{I, \sigma_j\}$, where σ_j swaps the positions and momenta of bodies k and l , leaving body j invariant; when all three masses are equal, we have $S = S_3 = \{I, \sigma_1, \sigma_2, \sigma_3, c, c^2\}$, in which all pairwise permutations σ_j and cyclic permutations c and $c^{-1} = c^2$ are allowed. Depending on the symmetry in the masses, the spatial symmetry group has order 2, 4, or 12. Of particular note is that R_2 is the centre of $G = R_2 \times S$ if G is not abelian (that is, when all three masses are equal).

The time reversing transformation τ , acts by flipping the signs of all momenta and generates the group $T_2 \cong \mathbb{Z}_2$. Together with the spatial symmetries this generates the reversing symmetry group $\Gamma = T_2 \times G$. Both τ and ρ commute with all elements, so in the context of the reversing symmetry group, it will at times be more convenient to think of $\Gamma = C_4 \times S$, where $C_4 = R_2 \times T_2 \cong V_4$ is the Klein-4 group generated by τ and ρ , and C_4 is the centre of Γ .

Once the binary collisions are regularised simultaneously, per section 1.4, new symmetries s_j are introduced, corresponding to flipping the signs of pairs of regularised coordinates α_k, α_l and their corresponding momenta π_k, π_l , chosen so that the oriented area $A = \alpha_1 \alpha_2 \alpha_3 \alpha$ is invariant under the action of each s_j . These operations form a group $F_4 = \{I, s_1, s_2, s_3\} \cong V_4$, where each $s_j^2 = I$ and $s_k s_l = s_l s_k = s_j$. At this point it is essential to remind ourselves of the definitions of the symmetries acting on

the regularised coordinates and momenta (chosen so that they preserve their meaning after reconstruction to the physical coordinates). Let $z = (\alpha_1, \alpha_2, \alpha_3, \pi_1, \pi_2, \pi_3)$:

$$\begin{aligned}\sigma_1(z) &= (-\alpha_1, -\alpha_3, -\alpha_2, -\pi_1, -\pi_3, -\pi_2) \\ \sigma_2(z) &= (-\alpha_3, -\alpha_2, -\alpha_1, -\pi_3, -\pi_2, -\pi_1) \\ s_3(z) &= (-\alpha_1, -\alpha_2, \alpha_3, -\pi_1, -\pi_2, \pi_3) \\ \rho(z) &= -z \\ \tau(z) &= (\alpha_1, \alpha_2, \alpha_3, -\pi_1, -\pi_2, -\pi_3).\end{aligned}$$

We observe that composition of sign flip symmetries and pairwise permutations with non-matching indices (and thus also the cyclic permutations) do not commute: $s_k\sigma_j = \sigma_js_l$ and $s_j\sigma_j = \sigma_js_j$. Indeed, the subgroup of allowed permutations and sign flip symmetries is a semidirect product $S \rtimes F_4$ with multiplication rule $(\sigma, \phi)(\sigma', \phi') = (\sigma\sigma', \sigma'\phi\sigma'^{-1}\phi')$. Observe also that τ and ρ are still generators of the centre. As a result, we have the regularised reversing symmetry group $\tilde{\Gamma} = C_4 \times S \rtimes F_4$. In the case of equal masses, $S \rtimes F_4 = S_3 \rtimes F_4 \cong S_4$, and the order of $\tilde{\Gamma} \cong V_4 \times S_4$ is 96. When exactly two masses are equal we have $S \rtimes F_4 = S_{2,j} \rtimes F_4 \cong D_4$, and the order of $\tilde{\Gamma} \cong V_4 \times D_4$ is 32. Finally, when all masses are unequal, we have $S \rtimes F_4 = \{I\} \rtimes F_4 \cong V_4$, and the order of $\tilde{\Gamma} \cong V_4 \times V_4 \cong \mathbb{Z}_2^4$ is 16.

Having established the structure of the regularised reversing symmetry group, we decide how to represent elements of the group. With the given product structure we can represent an element $\gamma \in \tilde{\Gamma}$ by the ordered tuple $\gamma = (\tau, \rho, \sigma, \phi)$, with $\tau \in T_2$, $\rho \in R_2$, $\sigma \in S$, and $\phi \in F_4$. In general, we will use a shorthand notation $\gamma = \tau\rho\sigma\phi$, which uniquely represents each element of $\tilde{\Gamma}$ under the usual composition rules. In this notation where any component is the identity element of its corresponding factor of the whole group, that component is not written unless every component is the identity, in which case we write $\gamma = I$. Thus, for example, if $\gamma = \tau\rho s_2$ and $\gamma' = \rho\sigma_1$, the resulting composition $\gamma\gamma' = \tau\rho s_2 \rho\sigma_1 = \tau\sigma_1 s_3$, and the composition $\gamma'\gamma = \rho\sigma_1 \tau \rho s_2 = \tau\sigma_1 s_2$.

In the rest of this chapter we will discuss the consequences of the symmetries on the dynamics of the system.

2.2 Structure of the symmetry group

Elements of the reversing symmetry group are listed in table 2.1, to provide a clearer idea of the group's structure. Blocks of rows correspond to symmetries in the masses. The centre of the group goes across table 2.1; the top row contains the subgroup $C_4 = \{I, \rho, \tau, \tau\rho\}$. The first column gives the regularised permutation group $\tilde{S} = S_3 \rtimes F_4$.

Each major column also contains information on the order of the element in the group, its representation, and, where such is the case, the symmetry of the configuration in parentheses (reversing if in columns 3 or 4, non-reversing if in columns 1 or 2).

The symbols are listed according to the symbolic dynamics discussed in Chapter 3: B indicates a binary collision, M an isosceles collinear configuration, C a collinear configuration, I an isosceles configuration, whereas F represents a free-fall point that can happen anywhere in the domain or its boundary. Colouration is provided to aid clarity, with two darkened columns indicating symmetries that contain a ρ or τ , but not both. These will be important in relation to vanishing geometric phase in Chapter 4.

The symmetry group of the regularised vector field has order 96 in the case of equal masses, comprising all row blocks. In the case that exactly two masses are equal, the first row block and the corresponding one of the three middle row blocks comprise the symmetry group. In the case of unequal masses, only the first row block comprises symmetries of the vector field.

Masses	Symmetry of regularised vector field			
Unequal masses	1 I	2 ρ	2 τ	2 $\tau\rho$
	2 s_1 (B)	2 ρs_1 (C)	2 τs_1 (B)	2 $\tau\rho s_1$ (C)
	2 s_2 (B)	2 ρs_2 (C)	2 τs_2 (B)	2 $\tau\rho s_2$ (C)
$m_2 = m_3$	2 s_3 (B)	2 ρs_3 (C)	2 τs_3 (B)	2 $\tau\rho s_3$ (C)
	2 σ_1 (M)	2 $\rho\sigma_1$ (I)	2 $\tau\sigma_1$ (M)	2 $\tau\rho\sigma_1$ (I)
	2 $\sigma_1 s_1$ (M)	2 $\rho\sigma_1 s_1$ (I)	2 $\tau\sigma_1 s_1$ (M)	2 $\tau\rho\sigma_1 s_1$ (I)
	4 $\sigma_1 s_2$	4 $\rho\sigma_1 s_2$	4 $\tau\sigma_1 s_2$	4 $\tau\rho\sigma_1 s_2$
$m_3 = m_1$	4 $\sigma_1 s_3$	4 $\rho\sigma_1 s_3$	4 $\tau\sigma_1 s_3$	4 $\tau\rho\sigma_1 s_3$
	2 σ_2 (M)	2 $\rho\sigma_2$ (I)	2 $\tau\sigma_2$ (M)	2 $\tau\rho\sigma_2$ (I)
	2 $\sigma_2 s_2$ (M)	2 $\rho\sigma_2 s_2$ (I)	2 $\tau\sigma_2 s_2$ (M)	2 $\tau\rho\sigma_2 s_2$ (I)
	4 $\sigma_2 s_3$	4 $\rho\sigma_2 s_3$	4 $\tau\sigma_2 s_3$	4 $\tau\rho\sigma_2 s_3$
$m_1 = m_2$	4 $\sigma_2 s_1$	4 $\rho\sigma_2 s_1$	4 $\tau\sigma_2 s_1$	4 $\tau\rho\sigma_2 s_1$
	2 σ_3 (M)	2 $\rho\sigma_3$ (I)	2 $\tau\sigma_3$ (M)	2 $\tau\rho\sigma_3$ (I)
	2 $\sigma_3 s_3$ (M)	2 $\rho\sigma_3 s_3$ (I)	2 $\tau\sigma_3 s_3$ (M)	2 $\tau\rho\sigma_3 s_3$ (I)
	4 $\sigma_3 s_1$	4 $\rho\sigma_3 s_1$	4 $\tau\sigma_3 s_1$	4 $\tau\rho\sigma_3 s_1$
$m_1 = m_2 = m_3$	4 $\sigma_3 s_2$	4 $\rho\sigma_3 s_2$	4 $\tau\sigma_3 s_2$	4 $\tau\rho\sigma_3 s_2$
	3 c	6 ρc	6 τc	6 $\tau\rho c$
	3 cs_1	6 ρcs_1	6 τcs_1	6 $\tau\rho cs_1$
	3 cs_2	6 ρcs_2	6 τcs_2	6 $\tau\rho cs_2$
	3 cs_3	6 ρcs_3	6 τcs_3	6 $\tau\rho cs_3$
	3 c^2	6 ρc^2	6 τc^2	6 $\tau\rho c^2$
	3 $c^2 s_1$	6 $\rho c^2 s_1$	6 $\tau c^2 s_1$	6 $\tau\rho c^2 s_1$
	3 $c^2 s_2$	6 $\rho c^2 s_2$	6 $\tau c^2 s_2$	6 $\tau\rho c^2 s_2$
	3 $c^2 s_3$	6 $\rho c^2 s_3$	6 $\tau c^2 s_3$	6 $\tau\rho c^2 s_3$

Table 2.1: Elements of the symmetry group. Columns 1-2 are non-reversing symmetries, columns 3-4 are reversing symmetries. Descending row blocks correspond to increasing symmetry in the masses, with the three labelled by each $m_k = m_l$ being having an equivalent degree of symmetry.

2.3 Fixed sets of symmetries and reversing symmetries

In this section we provide a list of fixed sets of all regularised symmetries and reversing symmetries for equal masses. Recall definition 1.7, the set of points fixed by a given symmetry. Fixed sets are parameterised by $a_i \in \mathbb{R}$, so the largest index indicates the dimension of the set. For example, $\text{Fix}(\rho s_1) = \{z = (0, a_1, a_2, 0, a_3, a_4)\}$ is parameterised by four real numbers, and thus is of dimension 4.

The list is sorted first by whether or not the fixed set is physically interesting, then by the dimension of the fixed set, then by class (isosceles, collinear, etc.), with the order n of each symmetry listed after its fixed set. Here, by ‘‘physically interesting’’ or ‘‘physically meaningful’’ we mean that the fixed set satisfies the regularised Hamiltonian $K \equiv 0$ and that the set is of sufficiently high dimension that if the symmetry is non-reversing it contains complicated dynamics, or if it is reversing that the dynamics of solutions with points in the set may be complicated. For example, $\text{Fix}(\tau c) = \{z = (a_1, a_1, a_1, 0, 0, 0)\}$ is of dimension 1; after fixing energy $h = -1$ the parameter a_1 is fixed, and solution is an equilateral configuration that collapses to triple collision.

Observe that all physically interesting reversing fixed sets have dimension 3. All physically meaningful non-reversing fixed sets with dimension 2 or lower lead to triple collision in finite time—indeed, the invariant equilateral configurations represent a central configuration for any masses, and the invariant isosceles collinear configurations are central whenever the outer bodies have equal masses, and their dynamics are well known.

The properties/classification of the elements of this list do not change in the case of different mass ratios, but certain members would not be symmetries of the associated problem, as is made clear in table 2.1. Colouring is assigned to match this table. If $m_k = m_l \neq m_j$ we exclude all symmetries involving c , σ_k , σ_l , which reduces to 32 members, and if no mass equals any other we exclude the symmetries involving the remaining permutation symmetry, reducing to a list of only 16 members. The involutions, in particular, tend to have interesting fixed sets. In the case of non-reversing symmetries, these fixed sets form invariant subspaces, to which a solution is restricted if it has one point in that set. Fixed sets of reversing involutions, in contrast, are not invariant subspaces; instead, a solution containing a point in such a set appears reflected about the corresponding invariant subspace—see figure 2.1 for an illustration of a solution that is symmetric with two points in $\text{Fix}(\tau s_1)$ (and additionally lying in $\text{Fix}(\rho \sigma_1)$).

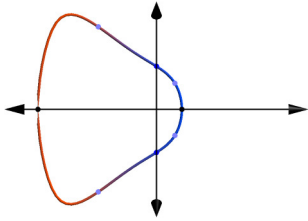


Figure 2.1: Illustration of a solution in an invariant subspace and possessing reversing symmetries.

2.3.1 Fixed sets of non-reversing involutions

Only four sets of non-reversing symmetries are physically meaningful, in the case of equal masses; that is, fixed sets which form invariant subspaces. The first of these is the set of collinear subspaces, given by $\text{Fix}(\rho s_j)$. The second is the set of isosceles subspaces, given by $\text{Fix}(\rho \sigma_j)$ and $\text{Fix}(\rho \sigma_j s_j)$. The third and fourth form central configurations which are bounded forwards and backwards in time by triple collision: Euler (collinear) configurations, given by $\text{Fix}(\sigma_j)$ and $\text{Fix}(\sigma_j s_j)$, and Lagrange (equilateral) configurations, given by $\text{Fix}(c)$, $\text{Fix}(c^2)$, $\text{Fix}(cs_j)$ and $\text{Fix}(c^2 s_j)$ (which are not involutions but have order 3). Points from each of these four sets are illustrated with physical reconstructions in figure 2.2.

Figure 2.2a shows the reconstruction of a point in one collinear invariant subspace. All bodies are in a line, and all momenta are parallel to the line. Figure 2.2b shows the reconstruction a point in an isosceles invariant subspace. Here the momentum vector of the body on the axis of symmetry is aligned with the axis of symmetry, and the other two momenta are related by a reflection across the axis of symmetry. Figure 2.2c shows the reconstruction of a point in the equilateral invariant subspace, in which all momenta are aligned radially from the centre of mass, which coincides with the incentre of the triangle, and of equal magnitude. Figure 2.2d shows the reconstruction of a point in the isosceles collinear invariant subspace, where the central body is at rest and the outer bodies have equal and opposite momenta parallel to the line formed by the three bodies.

When only two of the masses are equal, only one isosceles subspace remains, and this is lost when all three masses are unequal. However, the collinear subspaces remain intact in every case. The equilateral subspace is not symmetric when the masses are not equal, but remains a subspace of the general problem (Lagrange configuration). The isosceles collinear subspace exists only when the outer masses are equal.

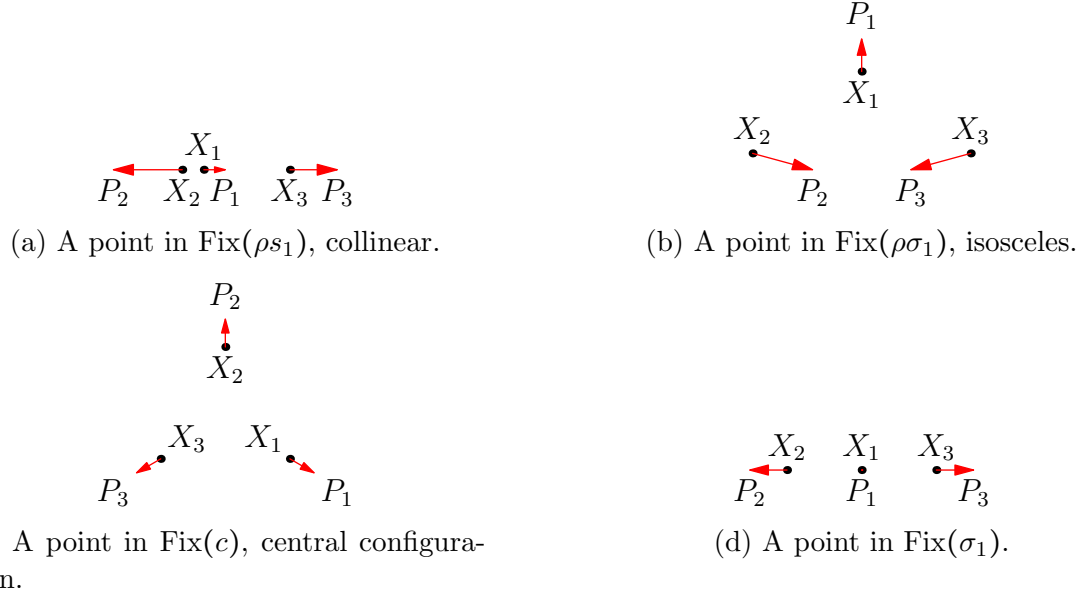


Figure 2.2: Configuration space reconstructions of points in physically meaningful non-reversing fixed sets for equal masses; invariant subspaces.

Dimension 4: Isosceles (Invariant)

$\text{Fix}(\rho \sigma_1)$	$= \{z = (a_1, a_2, a_2, a_3, a_4, a_4)\},$	$n = 2$
$\text{Fix}(\rho \sigma_1 s_1)$	$= \{z = (a_1, -a_2, a_2, a_3, -a_4, a_4)\},$	$n = 2$
$\text{Fix}(\rho \sigma_2)$	$= \{z = (a_2, a_1, a_2, a_4, a_3, a_4)\},$	$n = 2$
$\text{Fix}(\rho \sigma_2 s_2)$	$= \{z = (-a_2, a_1, a_2, -a_4, a_3, a_4)\},$	$n = 2$
$\text{Fix}(\rho \sigma_3)$	$= \{z = (a_2, a_2, a_1, a_4, a_4, a_3)\},$	$n = 2$
$\text{Fix}(\rho \sigma_3 s_3)$	$= \{z = (-a_2, a_2, a_1, -a_4, a_4, a_3)\},$	$n = 2$

Dimension 4: Collinear (Invariant)

$\text{Fix}(\rho s_1)$	$= \{z = (0, a_1, a_2, 0, a_3, a_4)\},$	$n = 2$
$\text{Fix}(\rho s_2)$	$= \{z = (a_1, 0, a_2, a_3, 0, a_4)\},$	$n = 2$
$\text{Fix}(\rho s_3)$	$= \{z = (a_1, a_2, 0, a_3, a_4, 0)\},$	$n = 2$

Dimension 2: Equilateral (Invariant)

$$\begin{aligned}
 \text{Fix}(c) &= \{z = (a_1, a_1, a_1, a_2, a_2, a_2)\}, & n = 3 \\
 \text{Fix}(cs_1) &= \{z = (a_1, -a_1, a_1, a_2, -a_2, a_2)\}, & n = 3 \\
 \text{Fix}(cs_2) &= \{z = (a_1, a_1, -a_1, -a_2, -a_2, a_2)\}, & n = 3 \\
 \text{Fix}(cs_3) &= \{z = (-a_1, a_1, a_1, -a_2, a_2, a_2)\}, & n = 3 \\
 \text{Fix}(c^2) &= \{z = (a_1, a_1, a_1, a_2, a_2, a_2)\}, & n = 3 \\
 \text{Fix}(c^2s_1) &= \{z = (a_1, a_1, -a_1, -a_2, -a_2, a_2)\}, & n = 3 \\
 \text{Fix}(c^2s_2) &= \{z = (-a_1, a_1, a_1, -a_2, a_2, a_2)\}, & n = 3 \\
 \text{Fix}(c^2s_3) &= \{z = (a_1, -a_1, a_1, a_2, -a_2, a_2)\}, & n = 3
 \end{aligned}$$

Dimension 2: Isosceles collinear (Invariant)

$$\begin{aligned}
 \text{Fix}(\sigma_1) &= \{z = (0, -a_1, a_1, 0, -a_2, a_2)\}, & n = 2 \\
 \text{Fix}(\sigma_1s_1) &= \{z = (0, a_1, a_1, 0, a_2, a_2)\}, & n = 2 \\
 \text{Fix}(\sigma_2) &= \{z = (-a_1, 0, a_1, -a_2, 0, a_2)\}, & n = 2 \\
 \text{Fix}(\sigma_2s_2) &= \{z = (a_1, 0, a_1, a_2, 0, a_2)\}, & n = 2 \\
 \text{Fix}(\sigma_3) &= \{z = (-a_1, a_1, 0, -a_2, a_2, 0)\}, & n = 2 \\
 \text{Fix}(\sigma_3s_3) &= \{z = (a_1, a_1, 0, a_2, a_2, 0)\}, & n = 2
 \end{aligned}$$

2.3.2 Fixed sets of reversing involutions

The fixed sets of reversing symmetries are not invariant subspaces. Rather, solutions with points $\{z(t_0), z(t_1), \dots\}$ in the fixed sets of reversing involutions are symmetric with respect to time reversal and some non-reversing involutions at those points. Figure 2.3 illustrates points in the fixed sets of several interesting reversing symmetries in the case of equal masses. Five reversing fixed sets take our interest: the set of reversing collinear configurations, given by $\text{Fix}(\tau\rho s_j)$; the set of reversing isosceles configurations, given by $\text{Fix}(\tau\rho\sigma_j)$ and $\text{Fix}(\tau\rho\sigma_js_j)$; the set of *brake-collision* configurations, given by $\text{Fix}(\tau s_j)$; the set of reversing isosceles collinear configurations, given by $\text{Fix}(\tau\sigma_j)$ and $\text{Fix}(\tau\sigma_js_j)$; and the set of free-fall or brake configurations, given by $\text{Fix}(\tau)$.

The reversing isosceles collinear configuration has been used to find periodic orbits in the equal-mass 3-body problem [73], as after fixing the size of the configuration the only two parameters are the direction to which all momenta are aligned, and the magnitudes of the momentum vectors, subject to $P_k = P_l = -\frac{1}{2}P_j$. Restricting to such initial conditions makes the search space manageable and yet turns up many interesting orbits.

Figure 2.3a shows the reconstruction of a point in the reversing collinear fixed set, in which the three bodies form a line and all momenta are perpendicular to the line. This fixed set exists in the case of all mass ratios, and the solutions before and after are

related by a reflection, as well as time reversal. Figure 2.3b shows the reconstruction of a point in the reversing fixed set of a collision (with the momenta of the colliding bodies normalised to unit length). Here the colliding momenta are equal and opposite, and the momentum of the non-colliding body is zero. The solutions on either side of such a point are related by time reversal. Figure 2.3c shows the reconstruction of a point in a reversing isosceles fixed set. Here the momentum vector of the body on the axis of symmetry is perpendicular to the axis of symmetry, and the other two momenta are aligned along the sides of the triangle, with one pointing toward the body on the axis of symmetry and one pointing away. Solutions evolving on either side of such a point are time reversed under the exchange of the two off-axis bodies, and this configuration is only symmetric if the corresponding masses are equal. Figure 2.3d shows the reconstruction of a point on the free fall boundary, where all three bodies are momentarily at rest. Finally, figure 2.3e shows the reconstruction of a point in the reversing fixed set of collinear isosceles configurations, requiring that the outer masses be equal. In this configuration all momenta are parallel, and the outer two velocities are equal.

Dimension 3: Arbitrary free-fall (Reversing)

$$\text{Fix}(\tau) = \{z = (a_1, a_2, a_3, 0, 0, 0)\}, \quad n = 2$$

Dimension 3: Isosceles collinear (Reversing)

$$\text{Fix}(\tau\sigma_1) = \{z = (0, -a_1, a_1, a_2, a_3, a_3)\}, \quad n = 2$$

$$\text{Fix}(\tau\sigma_1s_1) = \{z = (0, a_1, a_1, a_2, -a_3, a_3)\}, \quad n = 2$$

$$\text{Fix}(\tau\sigma_2) = \{z = (-a_1, 0, a_1, a_3, a_2, a_3)\}, \quad n = 2$$

$$\text{Fix}(\tau\sigma_2s_2) = \{z = (a_1, 0, a_1, -a_3, a_2, a_3)\}, \quad n = 2$$

$$\text{Fix}(\tau\sigma_3) = \{z = (-a_1, a_1, 0, a_2, a_2, a_3)\}, \quad n = 2$$

$$\text{Fix}(\tau\sigma_3s_3) = \{z = (a_1, a_1, 0, -a_2, a_2, a_3)\}, \quad n = 2$$

Dimension 3: Brake-collision (Reversing)

$$\text{Fix}(\tau s_1) = \{z = (a_1, 0, 0, 0, a_2, a_3)\}, \quad n = 2$$

$$\text{Fix}(\tau s_2) = \{z = (0, a_1, 0, a_3, 0, a_2)\}, \quad n = 2$$

$$\text{Fix}(\tau s_3) = \{z = (0, 0, a_1, a_2, a_3, 0)\}, \quad n = 2$$

Dimension 3: Isosceles (Reversing)

$$\text{Fix}(\tau\rho\sigma_1) = \{z = (a_1, a_2, a_2, 0, -a_3, a_3)\}, \quad n = 2$$

$$\text{Fix}(\tau\rho\sigma_1s_1) = \{z = (a_1, -a_2, a_2, 0, a_3, a_3)\}, \quad n = 2$$

$$\text{Fix}(\tau\rho\sigma_2) = \{z = (a_2, a_1, a_2, -a_3, 0, a_3)\}, \quad n = 2$$

$$\text{Fix}(\tau\rho\sigma_2s_2) = \{z = (-a_2, a_1, a_2, a_3, 0, a_3)\}, \quad n = 2$$

$$\text{Fix}(\tau\rho\sigma_3) = \{z = (a_2, a_2, a_1, -a_3, a_3, 0)\}, \quad n = 2$$

$$\text{Fix}(\tau\rho\sigma_3s_3) = \{z = (-a_2, a_2, a_1, a_3, a_3, 0)\}, \quad n = 2$$

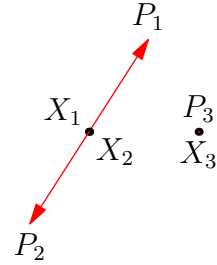
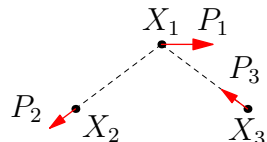
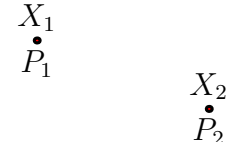
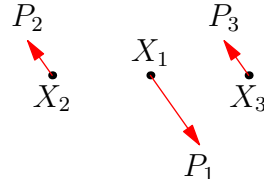
(a) A point in $\text{Fix}(\tau\rho s_1)$.(b) A point in $\text{Fix}(\tau s_3)$. Magnitudes $|P_1| = |P_2| = \infty$ and $\arg P_1 = \arg P_2 + \pi$; $P_3 = 0$.
$$\begin{matrix} X_3 \\ P_3 \end{matrix}$$
(c) A point in $\text{Fix}(\tau\rho\sigma_1)$. Two momenta P_2, P_3 point towards/away from X_1 with $|P_2| = |P_3|$; P_1 is perpendicular to the axis of symmetry.(d) A point in $\text{Fix}(\tau)$. All momenta are instantaneously zero.(e) A point in $\text{Fix}(\tau\sigma_1)$, central configuration. All momenta are parallel with $P_2 = P_3 = -\frac{P_1}{2}$.

Figure 2.3: Configuration space reconstruction of points in physically meaningful reversing fixed sets for equal masses.

Dimension 3: Collinear (Reversing)

$\text{Fix}(\tau\rho s_1)$	=	$\{z = (0, a_1, a_2, a_3, 0, 0)\}$,	$n = 2$
$\text{Fix}(\tau\rho s_2)$	=	$\{z = (a_2, 0, a_1, 0, a_3, 0)\}$,	$n = 2$
$\text{Fix}(\tau\rho s_3)$	=	$\{z = (a_1, a_2, 0, 0, 0, a_3)\}$,	$n = 2$

2.3.3 Other fixed sets

Other reversing fixed sets have physical meaning but are “too small” to be of interest and are not shown. In particular, $\text{Fix}(\tau c) = \{a_1, a_1, a_1, 0, 0, 0\} \subset \text{Fix}(\tau)$ and similar collapse to triple collision and do nothing else.

Dimension 1: Free-fall equilateral (Reversing)

$\text{Fix}(\tau c)$	=	$\{z = (a_1, a_1, a_1, 0, 0, 0)\}$,	$n = 6$
$\text{Fix}(\tau c s_1)$	=	$\{z = (a_1, -a_1, a_1, 0, 0, 0)\}$,	$n = 6$
$\text{Fix}(\tau c s_2)$	=	$\{z = (a_1, a_1, -a_1, 0, 0, 0)\}$,	$n = 6$
$\text{Fix}(\tau c s_3)$	=	$\{z = (-a_1, a_1, a_1, 0, 0, 0)\}$,	$n = 6$
$\text{Fix}(\tau c^2)$	=	$\{z = (a_1, a_1, a_1, 0, 0, 0)\}$,	$n = 6$
$\text{Fix}(\tau c^2 s_1)$	=	$\{z = (a_1, a_1, -a_1, 0, 0, 0)\}$,	$n = 6$
$\text{Fix}(\tau c^2 s_2)$	=	$\{z = (-a_1, a_1, a_1, 0, 0, 0)\}$,	$n = 6$
$\text{Fix}(\tau c^2 s_3)$	=	$\{z = (a_1, -a_1, a_1, 0, 0, 0)\}$,	$n = 6$

But what about all the other reversing symmetries? Many of these symmetries do not have “valid” physical meaning, in the sense that they correspond to points of phase space that do not satisfy the Hamiltonian $K \equiv 0$, or they do so trivially (for example, triple collision and zero momenta). All the fixed sets with no valid physical meaning are listed here.

Dimension 3: Triple collision, arbitrary momenta (Reversing)

$\text{Fix}(\tau\rho)$	=	$\{z = (0, 0, 0, a_1, a_2, a_3)\}$,	$n = 2$
------------------------	---	--------------------------------------	---------

Dimension 2: Binary collision

$\text{Fix}(s_1)$	$= \{z = (a_1, 0, 0, a_2, 0, 0)\},$	$n = 2$
$\text{Fix}(s_2)$	$= \{z = (0, a_1, 0, 0, a_2, 0)\},$	$n = 2$
$\text{Fix}(s_3)$	$= \{z = (0, 0, a_1, 0, 0, a_2)\},$	$n = 2$
$\text{Fix}(\sigma_1 s_2)$	$= \{z = (a_1, 0, 0, a_2, 0, 0)\},$	$n = 4$
$\text{Fix}(\sigma_1 s_3)$	$= \{z = (a_1, 0, 0, a_2, 0, 0)\},$	$n = 4$
$\text{Fix}(\sigma_2 s_1)$	$= \{z = (0, a_1, 0, 0, a_2, 0)\},$	$n = 4$
$\text{Fix}(\sigma_2 s_3)$	$= \{z = (0, a_1, 0, 0, a_2, 0)\},$	$n = 4$
$\text{Fix}(\sigma_3 s_1)$	$= \{z = (0, 0, a_1, 0, 0, a_2)\},$	$n = 4$
$\text{Fix}(\sigma_3 s_2)$	$= \{z = (0, 0, a_1, 0, 0, a_2)\},$	$n = 4$

Dimension 1: Binary collision brake (Reversing)

$\text{Fix}(\tau \sigma_1 s_2)$	$= \{z = (a_1, 0, 0, 0, 0, 0)\},$	$n = 4$
$\text{Fix}(\tau \sigma_1 s_3)$	$= \{z = (a_1, 0, 0, 0, 0, 0)\},$	$n = 4$
$\text{Fix}(\tau \sigma_2 s_1)$	$= \{z = (0, a_1, 0, 0, 0, 0)\},$	$n = 4$
$\text{Fix}(\tau \sigma_2 s_3)$	$= \{z = (0, a_1, 0, 0, 0, 0)\},$	$n = 4$
$\text{Fix}(\tau \sigma_3 s_1)$	$= \{z = (0, 0, a_1, 0, 0, 0)\},$	$n = 4$
$\text{Fix}(\tau \sigma_3 s_2)$	$= \{z = (0, 0, a_1, 0, 0, 0)\},$	$n = 4$

Dimension 1: Triple collision (Reversing)

$\text{Fix}(\tau \rho \sigma_1 s_2)$	$= \{z = (0, 0, 0, a_1, 0, 0)\},$	$n = 4$
$\text{Fix}(\tau \rho \sigma_1 s_3)$	$= \{z = (0, 0, 0, a_1, 0, 0)\},$	$n = 4$
$\text{Fix}(\tau \rho \sigma_2 s_1)$	$= \{z = (0, 0, 0, 0, a_1, 0)\},$	$n = 4$
$\text{Fix}(\tau \rho \sigma_2 s_3)$	$= \{z = (0, 0, 0, 0, a_1, 0)\},$	$n = 4$
$\text{Fix}(\tau \rho \sigma_3 s_1)$	$= \{z = (0, 0, 0, 0, 0, a_1)\},$	$n = 4$
$\text{Fix}(\tau \rho \sigma_3 s_2)$	$= \{z = (0, 0, 0, 0, 0, a_1)\},$	$n = 4$
$\text{Fix}(\tau \rho c)$	$= \{z = (0, 0, 0, a_1, a_1, a_1)\},$	$n = 6$
$\text{Fix}(\tau \rho c s_1)$	$= \{z = (0, 0, 0, a_1, -a_1, a_1)\},$	$n = 6$
$\text{Fix}(\tau \rho c s_2)$	$= \{z = (0, 0, 0, a_1, a_1, -a_1)\},$	$n = 6$
$\text{Fix}(\tau \rho c s_3)$	$= \{z = (0, 0, 0, -a_1, a_1, a_1)\},$	$n = 6$
$\text{Fix}(\tau \rho c^2)$	$= \{z = (0, 0, 0, a_1, a_1, a_1)\},$	$n = 6$
$\text{Fix}(\tau \rho c^2 s_1)$	$= \{z = (0, 0, 0, a_1, a_1, -a_1)\},$	$n = 6$
$\text{Fix}(\tau \rho c^2 s_2)$	$= \{z = (0, 0, 0, -a_1, a_1, a_1)\},$	$n = 6$
$\text{Fix}(\tau \rho c^2 s_3)$	$= \{z = (0, 0, 0, a_1, -a_1, a_1)\},$	$n = 6$

Dimension 0: Triple collision brake		
$\text{Fix}(\rho)$	$= \{z = (0, 0, 0, 0, 0, 0)\}$,	$n = 2$
$\text{Fix}(\rho\sigma_1 s_2)$	$= \{z = (0, 0, 0, 0, 0, 0)\}$,	$n = 4$
$\text{Fix}(\rho\sigma_1 s_3)$	$= \{z = (0, 0, 0, 0, 0, 0)\}$,	$n = 4$
$\text{Fix}(\rho\sigma_2 s_3)$	$= \{z = (0, 0, 0, 0, 0, 0)\}$,	$n = 4$
$\text{Fix}(\rho\sigma_2 s_1)$	$= \{z = (0, 0, 0, 0, 0, 0)\}$,	$n = 4$
$\text{Fix}(\rho\sigma_3 s_1)$	$= \{z = (0, 0, 0, 0, 0, 0)\}$,	$n = 4$
$\text{Fix}(\rho\sigma_3 s_2)$	$= \{z = (0, 0, 0, 0, 0, 0)\}$,	$n = 4$
$\text{Fix}(\rho c)$	$= \{z = (0, 0, 0, 0, 0, 0)\}$,	$n = 6$
$\text{Fix}(\rho c s_1)$	$= \{z = (0, 0, 0, 0, 0, 0)\}$,	$n = 6$
$\text{Fix}(\rho c s_2)$	$= \{z = (0, 0, 0, 0, 0, 0)\}$,	$n = 6$
$\text{Fix}(\rho c s_3)$	$= \{z = (0, 0, 0, 0, 0, 0)\}$,	$n = 6$
$\text{Fix}(\rho c^2)$	$= \{z = (0, 0, 0, 0, 0, 0)\}$,	$n = 6$
$\text{Fix}(\rho c^2 s_1)$	$= \{z = (0, 0, 0, 0, 0, 0)\}$,	$n = 6$
$\text{Fix}(\rho c^2 s_2)$	$= \{z = (0, 0, 0, 0, 0, 0)\}$,	$n = 6$
$\text{Fix}(\rho c^2 s_3)$	$= \{z = (0, 0, 0, 0, 0, 0)\}$,	$n = 6$

2.4 Subgroup structure

2.4.1 The “small” group

The small symmetry group (the natural symmetry group acting on the un-regularised system), of order 24 for equal masses, is isomorphic to $C_4 \times S_3$. We list the subgroups and their number, up to isomorphism:

- a) 15, $\mathbb{Z}_2 \cong D_1$;
- b) 1, \mathbb{Z}_3 ;
- c) 3, \mathbb{Z}_6 ;
- d) 19, $V_4 \cong D_2$;
- e) 4, $S_3 \cong D_3$;
- f) 3, $E_8 \cong \mathbb{Z}_2^3$;
- g) 1, $\mathbb{Z}_6 \times \mathbb{Z}_2$;
- h) 6, D_6 .

	Subgroup	Normal factor	Central factor
\mathbb{Z}_2	$\{I, \sigma_1\}$	$\{I, \sigma_1\}$	$\{I\}$
	$\{I, \sigma_2\}$	$\{I, \sigma_2\}$	$\{I\}$
	$\{I, \sigma_3\}$	$\{I, \sigma_3\}$	$\{I\}$
	$\{I, \rho\}$	$\{I\}$	$\{I\rho\}$
	$\{I, \tau\}$	$\{I\}$	$\{I\tau\}$
	$\{I, \tau\rho\}$	$\{I\}$	$\{I\tau\rho\}$
	$\{I, \rho\sigma_1\}$	$\{I\}$	$\{I, \rho\sigma_1\}$
	$\{I, \rho\sigma_2\}$	$\{I\}$	$\{I, \rho\sigma_2\}$
	$\{I, \rho\sigma_3\}$	$\{I\}$	$\{I, \rho\sigma_3\}$
	$\{I, \tau\sigma_1\}$	$\{I\}$	$\{I, \tau\sigma_1\}$
	$\{I, \tau\sigma_2\}$	$\{I\}$	$\{I, \tau\sigma_2\}$
	$\{I, \tau\sigma_3\}$	$\{I\}$	$\{I, \tau\sigma_3\}$
	$\{I, \tau\rho\sigma_1\}$	$\{I\}$	$\{I, \tau\rho\sigma_1\}$
	$\{I, \tau\rho\sigma_3\}$	$\{I\}$	$\{I, \tau\rho\sigma_3\}$
	$\{I, \tau\rho\sigma_4\}$	$\{I\}$	$\{I, \tau\rho\sigma_4\}$
\mathbb{Z}_3	$\{I, c, c^2\}$	$\{I, c, c^2\}$	$\{I\}$
\mathbb{Z}_6	$\{I, \rho c, c^2, \rho, c, \rho c^2\}$	$\{I, c, c^2\}$	$\{I, \rho\}$
	$\{I, \tau c, c^2, \tau, c, \tau c^2\}$	$\{I, c, c^2\}$	$\{I, \tau\}$
	$\{I, \tau\rho c, c^2, \tau\rho, c, \tau\rho c^2\}$	$\{I, c, c^2\}$	$\{I, \tau\rho\}$

Table 2.2: Factorisations of cyclic subgroups of Γ into direct products of normal and central factors.

Subgroups of this group may all be written in the form $G_S \times C$ or $G_S \rtimes C$, where G_S is a subgroup of S_3 , and C is isomorphic to a subgroup of the centre C_4 , containing elements of the form $r\gamma$, where $r \in C_4$, and $\gamma \in S_3$ such that $\gamma^2 = I$. The subgroups with the semidirect product structure are the D_3 subgroups with central elements of the form $r\sigma_j$, or D_6 with cyclic elements of the form rc , where $r \in \{\tau, \rho, \tau\rho\}$. Tables 2.2–2.5 give the decompositions of each subgroup according to these rules.

So each subgroup is either cyclic, dihedral (D_1 , D_2 , D_3 , or D_6), or something else (E_8 , or $\mathbb{Z}_6 \times \mathbb{Z}_2$). In the latter two cases, the subgroups are both of the form $G \times \mathbb{Z}_2$, where G is cyclic or dihedral.

2.4.2 The “big” group

The large symmetry group $\tilde{\Gamma}$ is the group of symmetries acting on the regularised vector field, order 96 for equal masses, isomorphic to $C_4 \times S_3 \rtimes F_4$. This group has many more subgroups, due to the factor $S_3 \rtimes F_4 \cong S_4$, including nine subgroups of order 4 not present in the smaller group, isomorphic to \mathbb{Z}_4 and generated by $r\sigma_j s_k$,

	Subgroup	Normal factor	Central factor
V_4	$\{I, \rho, \tau, \tau\rho\}$	$\{I\}$	$\{I, \rho, \tau, \tau\rho\}$
	$\{I, \rho, \sigma_1, \rho\sigma_1\}$	$\{I, \sigma_1\}$	$\{I, \rho\}, \{I, \rho\sigma_1\}$
	$\{I, \rho, \sigma_2, \rho\sigma_2\}$	$\{I, \sigma_2\}$	$\{I, \rho\}, \{I, \rho\sigma_2\}$
	$\{I, \rho, \sigma_3, \rho\sigma_3\}$	$\{I, \sigma_3\}$	$\{I, \rho\}, \{I, \rho\sigma_3\}$
	$\{I, \tau, \sigma_1, \tau\sigma_1\}$	$\{I, \sigma_1\}$	$\{I, \tau\}, \{I, \tau\sigma_1\}$
	$\{I, \tau, \sigma_2, \tau\sigma_2\}$	$\{I, \sigma_2\}$	$\{I, \tau\}, \{I, \tau\sigma_2\}$
	$\{I, \tau, \sigma_3, \tau\sigma_3\}$	$\{I, \sigma_3\}$	$\{I, \tau\}, \{I, \tau\sigma_3\}$
	$\{I, \tau\rho, \sigma_1, \tau\rho\sigma_1\}$	$\{I, \sigma_1\}$	$\{I, \tau\rho\}, \{I, \tau\rho\sigma_1\}$
	$\{I, \tau\rho, \sigma_2, \tau\rho\sigma_2\}$	$\{I, \sigma_2\}$	$\{I, \tau\rho\}, \{I, \tau\rho\sigma_2\}$
	$\{I, \tau\rho, \sigma_3, \tau\rho\sigma_3\}$	$\{I, \sigma_3\}$	$\{I, \tau\rho\}, \{I, \tau\rho\sigma_3\}$
	$\{I, \rho, \tau\sigma_1, \tau\rho\sigma_1\}$	$\{I\}$	$\{I, \rho, \tau\sigma_1, \tau\rho\sigma_1\}$
	$\{I, \rho, \tau\sigma_2, \tau\rho\sigma_2\}$	$\{I\}$	$\{I, \rho, \tau\sigma_2, \tau\rho\sigma_2\}$
	$\{I, \rho, \tau\sigma_3, \tau\rho\sigma_3\}$	$\{I\}$	$\{I, \rho, \tau\sigma_3, \tau\rho\sigma_3\}$
	$\{I, \rho\sigma_1, \tau, \tau\rho\sigma_1\}$	$\{I\}$	$\{I, \rho\sigma_1, \tau, \tau\rho\sigma_1\}$
	$\{I, \rho\sigma_2, \tau, \tau\rho\sigma_2\}$	$\{I\}$	$\{I, \rho\sigma_2, \tau, \tau\rho\sigma_2\}$
	$\{I, \rho\sigma_3, \tau, \tau\rho\sigma_3\}$	$\{I\}$	$\{I, \rho\sigma_3, \tau, \tau\rho\sigma_3\}$
	$\{I, \rho\sigma_1, \tau\sigma_1, \tau\rho\}$	$\{I\}$	$\{I, \rho\sigma_1, \tau\sigma_1, \tau\rho\}$
	$\{I, \rho\sigma_2, \tau\sigma_2, \tau\rho\}$	$\{I\}$	$\{I, \rho\sigma_2, \tau\sigma_2, \tau\rho\}$
	$\{I, \rho\sigma_3, \tau\sigma_3, \tau\rho\}$	$\{I\}$	$\{I, \rho\sigma_3, \tau\sigma_3, \tau\rho\}$

Table 2.3: Factorisations of subgroups of Γ isomorphic to V_4 into direct products of normal and central factors. Where the factorisation is non-unique, all factors are given.

where $r \in C_4$, and also subgroups of order 8, including eighteen isomorphic to D_4 and nine isomorphic to $\mathbb{Z}_4 \times \mathbb{Z}_2$, of which in both cases \mathbb{Z}_4 is a normal subgroup.

We can project $\tilde{\Gamma}$ to the small group Γ by the homomorphism $\Pi_0 : \tilde{\Gamma} \rightarrow \Gamma$ such that $\Pi_0(\phi, \sigma, s) = (\phi, \sigma)$, for $\phi \in C_4$, $\sigma \in S$, and $s \in F_4$. Under this projection, for example, we have $\Pi_0(\{I, \sigma_j s_k, s_j, \sigma_j s_l\}) = \{I, \sigma_j\}$. In this way, every subgroup of $\tilde{\Gamma}$ with a 4-cycle is mapped to a subgroup of Γ with a 2-cycle involving a pairwise permutation.

The consequence of these involutions s_j is that periodic orbits of the regularised system which possess such a “naked” sign flip symmetry are doubly-periodic when projected back to the un-regularised system. We have found a number of such orbits, including *rectilinear*(16, 1), all orbits in appendices F1.2 and F3.1, and *t0*(4, 13), whose isotropy subgroups contain \mathbb{Z}_4 as a subgroup (in the latter case its isotropy subgroup is isomorphic to \mathbb{Z}_4), and *t0*(2, 12), whose isotropy subgroup is $\{(I, 0), (s_2, \frac{1}{2})\}$.

2.4.3 Isotropy subgroups

Recall Theorems 1.6 and 1.8, classifying two types of behaviour and symmetry of periodic orbits. In particular, if a solution is periodic with a cyclic symmetry group generated by γ , the shift associated with γ is $\frac{T}{k}$, where k is the order of γ , and if a solution is periodic with a dihedral symmetry group generated by R_1 and R_2 , we may phase shift so that $R_1(z(t)) = z(-t)$ we thus have $R(z(t)) = z(\frac{T}{2k} - t)$, where k is the order of $R_2 R_1$. The shift associated with every other symmetry in the group can be calculated by addition of the shifts. We denote the symmetries of solutions by (γ, t_0) , where $\gamma \in \tilde{\Gamma}$ and t_0 is the associated shift.

Consider a T -periodic solution $z(t)$ of the regularised system with cyclic symmetry group, such as *t0*(4, 13), with symmetry $\sigma_1 s_3$ of order 4 such that $\sigma_1 s_3(z(t)) = z(t + \frac{T}{4})$. Then we have that $(\sigma_1 s_3)^2(z(t)) = s_1(z(t)) = z(t + \frac{T}{2})$ and $(\sigma_1 s_3)^3(z(t)) = \sigma_1 s_2(z(t)) = z(t + \frac{3T}{4}) = z(t - \frac{T}{4})$. The *isotropy subgroup* of $z(t)$ is

$$\Sigma_z = \{(I, 0), (\sigma_1 s_3, \frac{1}{4}), (s_1, \frac{1}{2}), (\sigma_1 s_2, \frac{3}{4})\}.$$

The solution is divided into k portions, where the each k -th of the orbit is identical up to spatial symmetry γ^i , for $i = 0, \dots, k - 1$.

The case for a solution with reversing symmetries is similar, but takes slightly more care. We take R_1 and R_2 and initial conditions such that $R_1(z(t)) = z(-t)$ and $R_2(z(t)) = z(\frac{T}{k} - t)$. By theorem 1.8, this is equivalent to $z(0) \in \text{Fix}(R_1)$ and $z(\frac{T}{2k}) \in \text{Fix}(R_2)$. Now the solution is divided into $2k$ portions, where each $2k$ -th is identical to its immediate neighbours, up a spatial symmetry and time reflection. For example, consider a solution $z(t)$ such as *t0*(4, 1), with $z(0) \in \text{Fix}(\tau \rho \sigma_3)$ and $z(\frac{T}{4}) \in \text{Fix}(\tau \rho s_3)$.

The isotropy subgroup must therefore be

$$\Sigma_z = \{(I, 0), (\tau\rho\sigma_3, 0), (\tau\rho s_3, \frac{1}{2}), (\sigma_3 s_3, \frac{1}{2})\},$$

with a cyclic permutation that swaps the roles of bodies 1 and 2 after half the period.

Given the isotropy subgroup of an orbit with dihedral symmetry (including the shift associated with each symmetry), we can determine which reversing symmetries may be taken to be R_1 and R_2 . Each reversing symmetry is an involution, but their product must be equal to the degree of the dihedral group, and the difference between their shifts must be $\frac{1}{k}$, where k is the degree. In the “Bestiary” (Appendix F), the generators may therefore be taken to be the two unique elements which appear as $(R_1, 0)$, $(R_2, \frac{1}{k})$.

2.5 Conclusion

The work in this chapter lays the foundation for two further ideas. One is the use of discrete symmetry information to develop an appropriate symmetry-reduced symbolic dynamics for each mass ratio in Chapter 3. The other, making use of both this chapter’s work and the symbolic dynamics, to study in Chapter 4 the geometric phase and determine from the symmetries alone under which circumstances the geometric phase must vanish.

	Subgroup	Normal factor	Central factor
S_3	$\{I, \sigma_1, \sigma_2, \sigma_3, c, c^2\}$	$\{I, \sigma_1, \sigma_2, \sigma_3, c, c^2\}$	$\{I\}$
E_8	$\{I, \rho, \tau, \tau\rho, \sigma_1, \rho\sigma_1, \tau\sigma_1, \tau\rho\sigma_1\}$ $\{I, \rho, \tau, \tau\rho, \sigma_2, \rho\sigma_2, \tau\sigma_2, \tau\rho\sigma_2\}$ $\{I, \rho, \tau, \tau\rho, \sigma_3, \rho\sigma_3, \tau\sigma_3, \tau\rho\sigma_3\}$	$\{I, \sigma_1\}$ $\{I, \sigma_2\}$ $\{I, \sigma_3\}$	$\{I, \rho, \tau, \tau\rho\}, \{I, \rho\sigma_1, \tau, \tau\rho\sigma_1\}, \{I, \rho, \tau\sigma_1, \tau\rho\sigma_1\}, \{I, \rho\sigma_1, \tau\sigma_1, \tau\rho\}$ $\{I, \rho, \tau, \tau\rho\}, \{I, \rho\sigma_2, \tau, \tau\rho\sigma_2\}, \{I, \rho, \tau\sigma_2, \tau\rho\sigma_2\}, \{I, \rho\sigma_2, \tau\sigma_2, \tau\rho\}$ $\{I, \rho, \tau, \tau\rho\}, \{I, \rho\sigma_3, \tau, \tau\rho\sigma_3\}, \{I, \rho, \tau\sigma_3, \tau\rho\sigma_3\}, \{I, \rho\sigma_3, \tau\sigma_3, \tau\rho\}$
$\mathbb{Z}_6 \times \mathbb{Z}_2$	$\{I, \rho, \tau, \tau\rho, c, \rho c, \tau c, \tau\rho c, c^2, \rho c^2, \tau c^2, \tau\rho c^2\}$	$\{I, c, c^2\}$	$\{I, \rho, \tau, \tau\rho\}$
D_6	$\{I, c, c^2, \sigma_1, \sigma_2, \sigma_3, \rho, \rho c, \rho c^2, \rho\sigma_1, \rho\sigma_2, \rho\sigma_3\}$ $\{I, c, c^2, \sigma_1, \sigma_2, \sigma_3, \tau, \tau c, \tau c^2, \tau\sigma_1, \tau\sigma_2, \tau\sigma_3\}$ $\{I, c, c^2, \sigma_1, \sigma_2, \sigma_3, \tau\rho, \tau\rho c, \tau\rho c^2, \tau\rho\sigma_1, \tau\rho\sigma_2, \tau\rho\sigma_3\}$	$\{I, \sigma_1, \sigma_2, \sigma_3, c, c^2\}$ $\{I, \sigma_1, \sigma_2, \sigma_3, c, c^2\}$ $\{I, \sigma_1, \sigma_2, \sigma_3, c, c^2\}$	$\{I, \rho\}$ $\{I, \tau\}$ $\{I, \tau\rho\}$

Table 2.4: Factorisations of non-cyclic subgroups of Γ of order 6 or higher into direct products of normal and central factors. Where the factorisation is non-unique, all factors are given.

	Subgroup	Normal factor	Central factor
D_3	$\{I, c, c^2, \rho\sigma_1, \rho\sigma_2, \rho\sigma_3\}$ $\{I, c, c^2, \tau\sigma_1, \tau\sigma_2, \tau\sigma_3\}$ $\{I, c, c^2, \tau\rho\sigma_1, \tau\rho\sigma_2, \tau\rho\sigma_3\}$	$\{I, c, c^2\}$ $\{I, c, c^2\}$ $\{I, c, c^2\}$	$\{I, \rho\sigma_1\}, \{I, \rho\sigma_2\}, \{I, \rho\sigma_3\}$ $\{I, \tau\sigma_1\}, \{I, \tau\sigma_2\}, \{I, \tau\sigma_3\}$ $\{I, \tau\rho\sigma_1\}, \{I, \tau\rho\sigma_2\}, \{I, \tau\rho\sigma_3\}$
D_6	$\{I, c, c^2, \rho\sigma_1, \rho\sigma_2, \rho\sigma_3, \tau, \tau c, \tau c^2, \tau\rho\sigma_1, \tau\rho\sigma_2, \tau\rho\sigma_3\}$ $\{I, c, c^2, \tau\sigma_1, \tau\sigma_2, \tau\sigma_3, \rho, \rho c, \rho c^2, \tau\rho\sigma_1, \tau\rho\sigma_2, \tau\rho\sigma_3\}$ $\{I, c, c^2, \rho\sigma_1, \rho\sigma_2, \rho\sigma_3, \tau, \tau c, \tau c^2, \tau\sigma_1, \tau\sigma_2, \tau\sigma_3\}$	$\{I, c, c^2\}$ $\{I, c, c^2\}$ $\{I, c, c^2\}$	$\{I, \rho\sigma_1, \tau, \tau\rho\sigma_1\}, \{I, \rho\sigma_2, \tau, \tau\rho\sigma_2\}, \{I, \rho\sigma_3, \tau, \tau\rho\sigma_3\}$ $\{I, \rho, \tau\sigma_1, \tau\rho\sigma_1\}, \{I, \rho, \tau\sigma_2, \tau\rho\sigma_2\}, \{I, \rho, \tau\sigma_3, \tau\rho\sigma_3\}$ $\{I, \rho\sigma_1, \tau\sigma_1, \tau\rho\}, \{I, \rho\sigma_2, \tau\sigma_2, \tau\rho\}, \{I, \rho\sigma_3, \tau\sigma_3, \tau\rho\}$

Table 2.5: Factorisations of non-cyclic subgroups of Γ (that cannot be factored into direct products) into semidirect products of normal and central factors. Where the factorisation is non-unique, all factors are given.

3 Symbolic dynamics

3.1 Overview

Consider a continuous dynamical system D whose phase space Ω is partitioned into finitely many regions. Let $T:\Omega\longrightarrow\Omega$ be a (possibly invertible) map from the phase space to itself. We assign a symbol s to each of the regions of phase space such that repeated applications of $T(x)$ (or its inverse) produces an infinite (or bi-infinite) string of symbols $.s_0s_1s_2\dots$ (or $\dots s_{-2}s_{-1}.s_0s_1s_2\dots$), where the subscript indicates the number of applications of T or its inverse. The set $\{s\}$ of symbols is called the *alphabet*. This construction, first used by Hadamard in 1898 [21] but only studied rigorously as an object in its own right since Morse and Hedlund [52], reduces the continuous dynamics of D to a discrete dynamical system whose qualitative properties reflect the properties of D . The string of symbols associated to a particular solution of D is called the *symbol sequence* of the solution.

3.2 Classical symbolic dynamics in the 3-body problem

Symbolic dynamics has been applied to the 3-body problem in various forms, with periodic sequences playing an important role. The rectilinear 3-body problem was explored by Tanikawa and Mikkola [77], using the collisions as symbols, to systematically discover unrealisable sequences. It was thus found that the realisable sequences form a Cantor set. In [78] symbolic dynamics was used to discover orbits of the rectilinear 3-body problem that begin and end in triple collision. The work was continued by Saito and Tanikawa [63, 64], wherein the roles of the triple collision point and of periodic orbits are explored. Meanwhile, Moeckel [43] constructs a chaotic invariant set and uses symbolic dynamics to prove the existence of solutions with interesting behaviour, such as close approaches to triple collision and excursions near infinity (meaning either that all three are widely separated or, particularly in the case of negative energy, one is far from the other two and those two are bound in a tight binary).

Symbolic dynamics is also used in the study of the free-fall 3-body problem by Tanikawa and Mikkola [79], wherein solutions start on the free fall boundary in a minimal set of dynamically equivalent configurations (called the fundamental domain). Syzygies were used as symbols to divide the space of initial conditions and ask the question, what kind of orbits correspond to the boundaries between different words of length n in the space of initial conditions? Regions that map to particular syzygies are of course bounded by binary collision curves, whose intersection points correspond to initial conditions leading to triple collision. An interesting result is a picture of how the “syzygy map” of previously free-fall initial conditions changes when angular momentum is non-zero.

In this thesis symbolic dynamics is used as a means of classification for periodic orbits, as the symmetries of the symbolic dynamics reflect the symmetries of the orbits themselves. In this section we will first describe a symbolic dynamics that has been proposed before, why such a symbolic dynamics is unsuitable for our problem, and then develop a system that makes use of the symmetry information at our disposal to produce a more fine-grained symbolic dynamics.

In [49] Montgomery showed that all orbits but one¹ of the 3-body problem with zero angular momentum suffer syzygies. It has been proposed for collisionless orbits, by Tanikawa and Mikkola [79], to use the sequence of syzygies as a symbolic dynamics for the 3-body problem, where the index of the mass passing between the other two is used as a symbol.

In Tanikawa and Mikkola’s symbolic dynamics, if the signed area A evolves from positive to negative with body j in syzygy, record j ; should the signed area evolves from negative to positive with j in syzygy, record $j + 3$. On the shape sphere this is equivalent to taking note of through which arc of the equator the trajectory passes and in which direction.

The orientation of the configuration triangle is preserved through collisions. As collision implies two of the regularised coordinates are simultaneously zero, either one is identically zero and the other changes sign (in which case the orbit is in the collinear subspace and the orientation is undefined, with zero area), or two regularised coordinates change sign together. In the latter case, this means that just before and just after collision the sign of the product of regularised coordinates is the same. The symbolic dynamics proposed by Tanikawa and Mikkola may be extended to include collisions by just three new symbols: one for each collision, allowing us to use this symbolic dynamics in the regularised setting². This we will call the *oriented syzygy*

¹This one orbit is Lagrange’s homothetic solution, which for zero angular momentum evolves by scaling only, beginning and ending in triple collision, with an equilateral configuration at all times.

²This symbolic dynamics may be used without the addition of new symbols by considering a

sequence.

Working with j and $j + 3$ is not strictly necessary, as the $+3$ is simply alternating, for collisionless orbits. In the case of collision orbits, the $+3$ alternates for non-collision symbols (because orientation is preserved through collisions). Simpler than the oriented syzygy sequence proposed by Tanikawa and Mikkola, then, is just the *syzygy sequence*, which consists of the alphabet $(1, 2, 3, a, b, c)$.

While the syzygy sequence (oriented or otherwise) is laudable for studying the topology of solutions, it does not distinguish neighbouring solutions with distinct symmetries. As an example, consider the figure-8 choreography $t_0(12, 1)$ and its neighbour $t_0(4, 23)$. Both form very similar loops on the shape sphere, and both have very similar periods (the former 2.22181372 the latter 2.22181404). But the figure-8 choreography has a symmetry group of order 12, while its “shadow” has symmetry of only order 4, and it is not choreographic. The oriented syzygy sequences of both orbits are the same: 153426, indicating the same topology and similar length, mapping to the syzygy sequence 123123.

3.2.1 Discrete symmetries in symbolic dynamics

Symmetries of an orbit are reflected in the oriented syzygy sequence. For example, the figure-8 choreography, with oriented syzygy sequence 152426, which is symmetric under cyclic permutations of $(1, 2, 3)$ and $(4, 5, 6)$, under reversal of orientation (swapping 1 and 4, 2 and 5, and 3 and 6), and under pairwise permutations and “time reversal of the sequence” (that is, reading the sequence in reverse), in each case with an appropriate cyclic shift to bring it back to 152426. While the figure-8’s “shadow” does not possess all these symmetries, there exist separate solutions that are identical up to symmetry. Our goal now is to develop a symbolic dynamics that is reduced with respect to discrete symmetries for each case of symmetry in the masses, so that orbits related by symmetry have the same symbol sequences, and, as much as is possible, no two different orbits will have the same symbol sequence.

collision as a limit of non-collision cases, as is done by Tanikawa and Mikkola [80]. However, we argue that combining the two limiting collinearity symbols into one collision symbol is conceptually simpler, especially where our purposes differ from those of others.

3.3 Symmetry-reduced symbolic dynamics

3.3.1 The regularised fundamental domain and reduced symbolic dynamics

The values of the masses determine which permutation group is a factor of the full symmetry group. While we are concerned primarily with equal masses, it is little extra effort to consider every possible case of symmetry in the masses. Recall that the regularised spatial symmetry group is $\tilde{G} = R_2 \times S \rtimes F_4$, where $R_2 \cong \mathbb{Z}_2$ is generated by spatial reflection ρ and is the centre of \tilde{G} , S is the permutation group, determined by the number of equal masses, and $F_4 \cong V_4$ is the group of “sign flip” symmetries induced by regularisation. For three equal masses we have $S = S_3$, for two equal masses we have $S = S_2 \cong \mathbb{Z}_2$, and for unequal masses $S = \{I\}$, the trivial group.

The reflecting involutions of \tilde{G} and its projection down to the un-regularised group $G = R_2 \times S$ acting on coordinates divides each respective shape space into n dynamically equivalent regions, where n is the order of each symmetry group (respectively 48 and 12). One such region is singled out and referred to as the *fundamental domain*; a solution beginning in the fundamental domain can be mapped back into the fundamental domain at its boundary by a reflection on the appropriate part of the boundary. A symmetry-reduced symbolic dynamics therefore uses the boundaries of the fundamental domain as its symbols.

Another way to phrase the description of our symbolic dynamics is to consider the fundamental region of shape space bounded by the invariant subspaces and the boundary of the Hill region. Each time a solution touches a boundary a symbol is recorded, and the trajectory is reflected back into the fundamental domain. The fundamental domain in shape space for equal masses is shown in figure 3.1, including the symbols we record on the walls (C collinear, A acute isosceles, O obtuse isosceles configurations), the edges where the walls intersect (M “midpoint” isosceles collinear, E equilateral, B binary collision configurations), and the free fall boundary (F any brake—or free-fall—point).

Reduction by discrete symmetries makes the symbolic dynamics invariant under the action of the spatial symmetry group. Time reversal, τ , is another discrete symmetry that reverses the direction of the flow on the fundamental domain. Most reversing symmetries occur on each part of the boundary of the fundamental domain; however, τ can occur for any non-collision configuration. If τ occurs, the trajectory has touched the edge of the free fall boundary. As the free fall boundary is itself a boundary of the fundamental domain in shape space (albeit “invisible” on the shape sphere) and

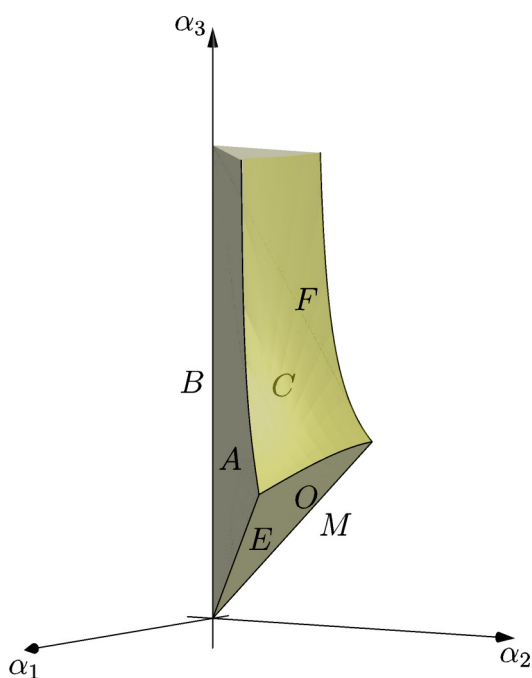


Figure 3.1: The lower portion of fundamental domain chosen for unit masses. The domain extends for arbitrarily large α_3 , and the boundary F tends towards a segment of the cylinder $\alpha_1^2 + \alpha_2^2 = 1$

corresponds to a reversing involution, we assign to it the symbol F .

We now discuss the fundamental domains in each distinct case of symmetry in the masses and describe the reduced symbolic dynamics.

3.3.1.1 Unequal masses

The least symmetric case, with all masses different, is only symmetric under the reflection symmetry ρ , or ρs_j for each j . In such a case the fundamental domain is one hemisphere of the shape sphere (bounded by the equator), or one octant of the regularised shape sphere (figures 3.2a and 3.2b). We choose the fundamental domain such that every $\alpha_j \geq 0$.

In this case the symbolic dynamics is just the syzygy sequence with the addition of a symbol for brake-points. Thus we choose the alphabet

$$\{1, 2, 3, a, b, c, F\},$$

where the numerals represent syzygies, the lower case Roman letters indicate collisions as before, and F represents a brake point in the trajectory (table 3.1).

Symbol	Boundary in regularised coordinates
1	$\{0 = \alpha_1 < \alpha_2, \alpha_3\}$
2	$\{0 = \alpha_2 < \alpha_3, \alpha_1\}$
3	$\{0 = \alpha_3 < \alpha_1, \alpha_2\}$
a	$\{0 = \alpha_2 = \alpha_3 < \alpha_1\}$
b	$\{0 = \alpha_3 = \alpha_1 < \alpha_2\}$
c	$\{0 = \alpha_1 = \alpha_2 < \alpha_3\}$
F	$\{0 = \pi_1 = \pi_2 = \pi_3\}$

Table 3.1: Boundaries of the fundamental domain for unequal masses.

Trajectories that leave the fundamental domain are mapped back into it at each symbol by the following symmetries:

$$\begin{array}{lll} 1 : \rho s_1, & 2 : \rho s_2, & 3 : \rho s_3, \\ a : s_1, & b : s_2, & c : s_3. \end{array}$$

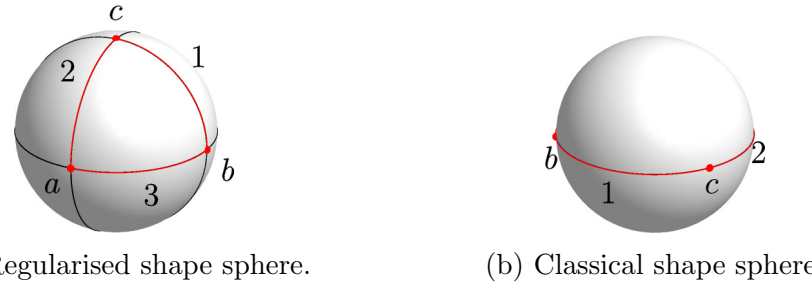


Figure 3.2: The fundamental domain on (a) the regularised shape sphere, and (b) the classical shape sphere, with unequal masses.

3.3.1.2 Two masses equal

The next most symmetric case, in which exactly two masses are equal (say, $m_2 = m_3$), allows the pairwise permutation symmetry σ_1 . In this case, the fundamental domain becomes one quarter of the shape sphere, bounded by the equator and by the great circle defined by $\text{Fix}(\sigma_1)$, or half of one octant of the regularised shape sphere, bounded by three great circles: for example, the smaller region bounded by great circles connecting B_{23}^+ to B_{12}^+ to M_1^{++} (figures 3.3a and 3.3b).

Here an alphabet for the symbolic dynamics could be given as

$$\{1, 2, i, a, M, c, F\},$$

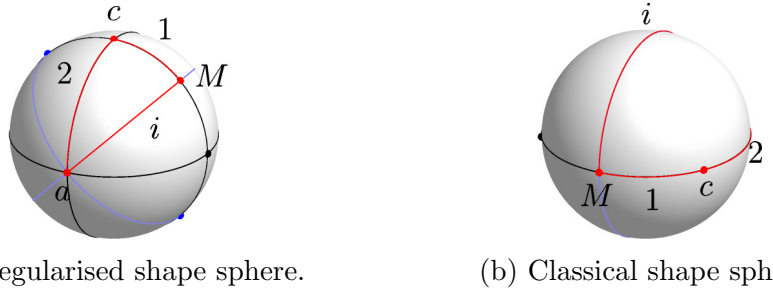
where the different symbols are i , representing isosceles configurations where $\alpha_2 = \alpha_3$, and M , isosceles collinear configurations with $\alpha_1 = 0$ and $\alpha_2 = \alpha_3$ (table 3.2).

We point out that in the equal-mass case we will distinguish between acute and obtuse isosceles configurations (separated by the equilateral configuration), but here the equilateral configuration is not distinguished by symmetry, so only one symbol i is used for the one corresponding arc of symmetry on the shape sphere.

Trajectories that leave the fundamental domain are mapped back into it at each symbol by the following symmetries:

$1 : \rho s_1,$	$2 : \rho s_2,$	$i : \rho \sigma_1,$
$a : s_1,$	$M : \sigma_1 s_1,$	$c : s_3.$

Symbol	Boundary in regularised coordinates
1 :	$\{0 = \alpha_1 < \alpha_2 < \alpha_3\}$
2 :	$\{0 = \alpha_2 < \alpha_3, \alpha_1 \neq 0\}$
$i :$	$\{0 < \alpha_1, 0 < \alpha_2 = \alpha_3\}$
$a :$	$\{0 = \alpha_2 = \alpha_3 < \alpha_1\}$
$M :$	$\{0 = \alpha_1 < \alpha_2 = \alpha_3\}$
$c :$	$\{0 = \alpha_1 = \alpha_2 < \alpha_3\}$
$F :$	$\{\pi_1 = \pi_2 = \pi_3 = 0\}$

Table 3.2: Boundaries of the fundamental domain for $m_2 = m_3$.Figure 3.3: The fundamental domain on (a) the regularised shape sphere, and (b) the classical shape sphere, with $m_2 = m_3$.

3.3.1.3 Equal masses

Finally, if all three masses are equal, all possible symmetries are achieved, reducing the fundamental domain to one third of the fundamental domain from the previous case, as cyclic permutations of the coordinates and momenta are now possible. We describe in more detail the fundamental domain in the case of equal masses.

Suppose we insist that $0 \leq \alpha_1 \leq \alpha_2 \leq \alpha_3$ and $\alpha_3 > 0$ (excluding triple collision). Then whenever a trajectory passes through a face or through an edge of this region, we apply an appropriate discrete symmetry to the trajectory to reflect it at that boundary. These boundaries are illustrated on the shape spheres in figures 3.4a and 3.4b.

The symbolic dynamics for equal masses, table 3.3, consists of the alphabet

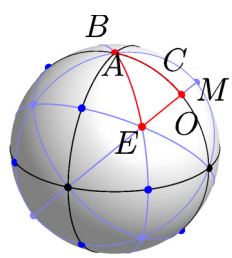
$$\{C, A, O, B, E, M, F\},$$

where each letter corresponds to passing through the corresponding boundary of the fundamental domain.

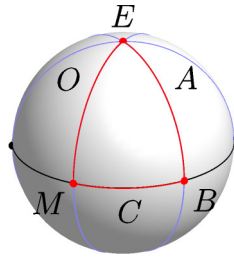
Trajectories that leave the fundamental domain are mapped back into it at each

Symbol	Boundary in regularised coordinates
C :	$\{0 = \alpha_1 < \alpha_2 < \alpha_3\}$
A :	$\{0 < \alpha_1 = \alpha_2 < \alpha_3\}$
O :	$\{0 < \alpha_1 < \alpha_2 = \alpha_3\}$
B :	$\{0 = \alpha_1 = \alpha_2 < \alpha_3\}$
E :	$\{0 < \alpha_1 = \alpha_2 = \alpha_3\}$
M :	$\{0 = \alpha_1 < \alpha_2 = \alpha_3\}$
F :	$\{\pi_1 = \pi_2 = \pi_3 = 0\}$

Table 3.3: Boundaries of the fundamental domain for equal masses.



(a) Regularised shape sphere.



(b) Classical shape sphere.

Figure 3.4: The fundamental domain on (a) the regularised shape sphere, and (b) the classical shape sphere, with $m_1 = m_2 = m_3$.

symbol by the following symmetries (figure 3.5):

$$\begin{array}{lll} C : \rho s_1, & A : \rho \sigma_3, & O : \rho \sigma_1, \\ B : s_3, & E : \rho \sigma_2, & M : \sigma_1 s_1. \end{array}$$

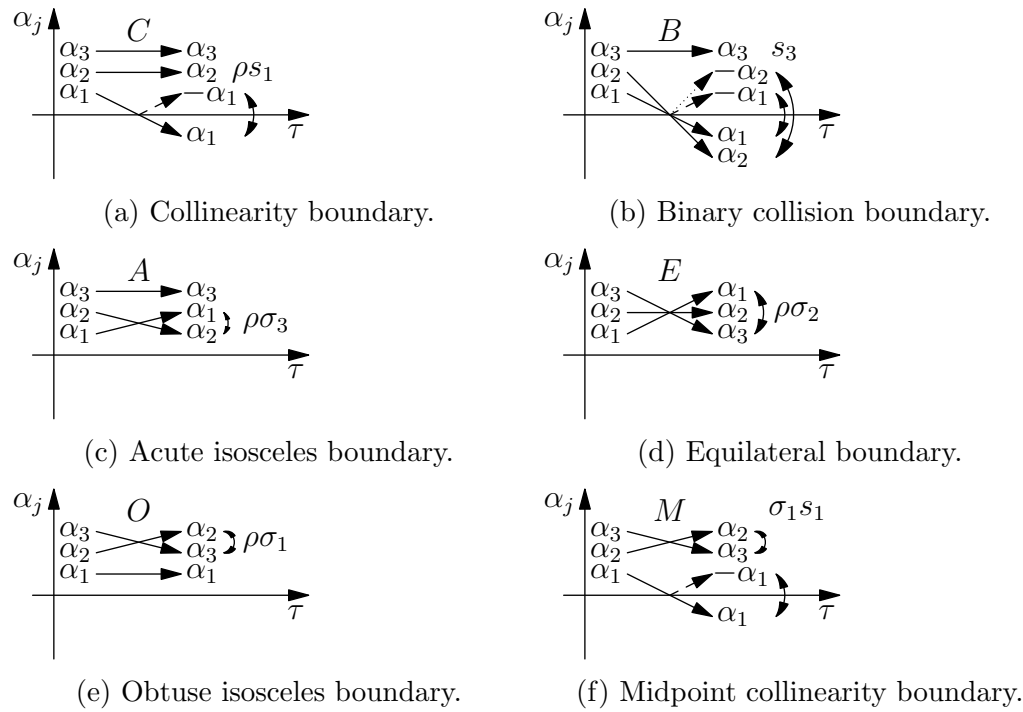


Figure 3.5: Actions mapping a trajectory back into the fundamental domain for equal masses.

3.3.2 Reduced symbolic dynamics in invariant subspaces

The reduced symbolic dynamics in each case has seven symbols, each associated with a discrete symmetry, and each with a reversing symmetry. If γ is a non-reversing symmetry of the regularised vector field with a meaningful fixed set $\text{Fix}(\gamma)$ (that is, the fixed set is not, for example, any of the symmetries in section 2.3.3 for the complete list of fixed sets and their meanings), then $\text{Fix}(\gamma)$ is an invariant subspace; any solution that begins exactly in such a space remains there for all time.

Two groups of fixed sets are too small to be interesting. They are $\text{Fix}(\sigma_j)$, $\text{Fix}(\sigma_j s_j)$ corresponding to isosceles collinear configurations with the central body at rest and the outer bodies' velocities radially oriented, and $\text{Fix}(c^i)$, $\text{Fix}(c^i s_j)$ corresponding to equilateral configurations with all velocities equal and radially oriented. Both fixed sets form invariant subspaces of dimension 2; too small for interesting dynamics to happen. After fixing the energy $h < 0$, only one parameter is free to vary: either fix the coordinates and the momenta are determined (up to sign), or fix the momenta and the coordinates are determined (up to sign).

In both cases, if the initial configuration is chosen to be small and the momenta are chosen such that the initial velocities are chosen pointing outward, the system evolves in the same configuration with momenta decreasing until zero. At this point the solution touches the free fall boundary and begins to reverse, leading back to the initial condition (with reversed signs of momenta) and ultimately to triple collision. With the time scaling due to regularisation, this is removed to $t = \pm\infty$.

More interesting dynamics are possible in the other invariant subspaces.

In the case of unequal masses, the only invariant subspaces are collinear configurations with all momenta in the line of the bodies. These fixed sets are of the form $\text{Fix}(\rho s_j)$ for each j (corresponding to the index of the body in the middle).

When exactly two of the masses are equal, say $m_k = m_l$, we add to the invariant subspaces the set $\text{Fix}(\rho\sigma_j)$ and $\text{Fix}(\rho\sigma_j s_j)$, for permanently isosceles orbits with m_j on the axis of symmetry.

When all masses are equal, we add the rest of the permutation symmetries, permitting two other isosceles invariant subspaces.

In all cases, invariant subspaces become the edge boundaries of the fundamental domain, and orbits living in these subspaces would record the given symbol continuously. Thus the symbolic dynamics should only include the relevant corner points of the domain.

Explicitly, this means that in the collinear subspaces $\text{Fix}(\rho s_1)$, $\text{Fix}(\rho s_2)$, and $\text{Fix}(\rho s_3)$

for unequal masses the alphabets respectively contains only $\{b, c, F\}$, $\{a, c, F\}$, and $\{a, b, F\}$.

When $m_2 = m_3$, the alphabet for $\text{Fix}(\rho s_1)$ becomes $\{M, c, F\}$, while the other two are mapped into one symbolic dynamics with alphabet $\{a, c, F\}$. The isosceles invariant subspace $\text{Fix}(\rho \sigma_1)$ is added, on which the alphabet is $\{a, M, F\}$.

Finally, when $m_1 = m_2 = m_3$ every collinear invariant subspace is dynamically equivalent, where all thus have alphabet $\{B, M, F\}$, and every isosceles invariant subspace is dynamically equivalent, where all have alphabet $\{B, M, E, F\}$.

3.4 Symmetry-reduced symbolic dynamics and the symmetries of periodic solutions

We now consider the relationship between the symmetries of a solution and its symbolic dynamics. The symbol sequence of a solution $z(t)$ corresponds to every point on the solution where $z(t)$ momentarily attains one of a given set of configurations, including brake points.

We found that two cases occur: first, when the symmetries of the solution are generated by a non-reversing element γ of order k ; second, then the symmetries of the solution are generated by two reversing elements $R_1 = \tau\gamma_1$ and $R_2 = \tau\gamma_2$ whose composition $\gamma_2\gamma_1$ is cyclic of order k . In both cases, the solution repeats itself with some non-reversing symmetry applied successively k times; as our symbolic dynamics are reduced with respect to discrete symmetries, this means that if Ω is the word corresponding to $\frac{1}{k}$ -th of the solution, the entire symbol sequence is just Ω^k , where k indicates the number of repetitions of Ω ; the symbolic dynamics are invariant under non-reversing symmetries.

In the first case, this is all that can be done. In the second case, we have not accounted for each of the reversing symmetries individually. We phase-shift the solution so that $\tau\gamma_1(z(t)) = \gamma z(-t)$, and $\tau\gamma_2(z(t)) = \gamma z(\frac{T}{k} - t)$, thus $z(0) \in \text{Fix}(\tau\gamma_1)$ and $z(\frac{T}{2k}) \in \text{Fix}(\tau\gamma_2)$. Observe that the $\frac{1}{k}$ -th word Ω must contain further structure. In particular, it must have an even number $2n$ of symbols, the first symbol X corresponds to the region of the boundary of the fundamental domain of which $z(0)$ is an element, and the n -th symbol Y corresponds to the region of the fundamental domain of which $z(\frac{T}{2k})$ is an element, and the behaviour of $z(t)$ before $t = \frac{T}{2k}$ and afterwards are identical up to a spatial symmetry and reflection in time about that point. This means that if $\tilde{\Omega}$ is the word corresponding to the $\frac{1}{k}$ -th of $z(t)$ for which $0 \leq t \leq \frac{T}{k}$, the entire symbol sequence of $z(t)$ is $\tilde{\Omega}^k$, and is palindromic about each symbol X and Y on which a

reversing symmetry occurs.

We can thus decompose $\tilde{\Omega}$ into two words Ω and its reverse Ω' punctuated by X and Y . That is, $\tilde{\Omega} = X\Omega Y\Omega'$, and $\tilde{\Omega}^k = (X\Omega Y\Omega')^k$. This motivates the following definition.

Definition 3.1. *The sequence class of a periodic orbit $z(t)$ is the decomposition of its symbol sequence according to the symmetries of $z(t)$. Two sequence classes occur: Ω^k , when the symmetry group of $z(\tau)$ is cyclic of order k after a quotient by the symmetry of an invariant subspace; and $(X\Omega Y\Omega')^k$, when the symmetry group of $z(t)$ is dihedral of degree k after quotient by the symmetry of an invariant subspace.*

The sequence class is defined so that the symmetry group (up to isomorphism) can be read off quickly and easily from the symbol sequence information, and the configuration at any reversing symmetry is immediately apparent.

Note that the smallest word guaranteed by the symmetries of $z(t)$ to repeat is always denoted Ω , but the symbol sequence of $z(t)$ may contain more symmetry than $z(t)$ itself. Several orbits are known whose symbol sequences are more symmetric than the orbits themselves; they are $t0(2,30)$, $t0(2,35)$, $t0(2,53)$, $t0(2,100)$, $t1(2,1)$, $t1(2,9)$, *isosceles*(4,1), and *rectilinear*(4,40). In each of these the word Ω is itself a palindrome, but the central symbol does not correspond to a reversing point of the orbit.

4 Geometric phase

4.1 Introduction

Geometric phase in physics first became of serious interest with Berry's paper [4]. Later, Wu [86] used the work of Berry [4], Guichardet [20], and Iwai [28] to develop a similar result for the classical 3-body problem, as earlier papers had largely been concerned with quantum mechanical systems.

Montgomery's formula [47] is

$$dG = -\frac{1}{2}w_3 d\theta, \quad (4.1)$$

where G is the geometric phase angle, $\theta = \arg(w_1 + iw_2)$ is an azimuthal angle on the shape sphere, and the w_i are coordinates on the shape sphere of half unit radius (c.f. equation (1.53)). Equation (4.1) computes an “area” on the shape sphere when evaluated over a closed loop. We apply the chain rule to obtain $d\theta$ in terms of regularised coordinates:

$$d\theta = \frac{1}{w_1^2 + w_2^2} \sum \left(w_1 \frac{\partial w_2}{\partial \alpha_j} - w_2 \frac{\partial w_1}{\partial \alpha_j} \right) \dot{\alpha}_j dt$$

and finally obtain

$$dG = \frac{m^3 A \sum F_j(z)}{\left(\sum M_j a_j^2 \right)^2 \left(\left(\sum M_j a_j^2 \right)^2 - 16MmA^2 \right)} dt =: U(z) dt \quad (4.2)$$

for $z = (\alpha_1, \alpha_2, \alpha_3, \pi_1, \pi_2, \pi_3)$, with

$$F_j(z) = f_j(z) \alpha_j \pi_j,$$

where

$$f_j(z) = M_j (a_k - a_l) a_j \alpha^2 - M_k (2\alpha_k^2 + a_k) a_k \alpha_l^2 + M_l (2\alpha_l^2 + a_l) a_l \alpha_k^2$$

and $M_j = m_k m_l$ and $M = m_1 m_2 m_3$.

Define the geometric phase of a T -periodic orbit $z(t)$ by $\Delta G = \int_0^T U(z(s)) ds$. It is also useful to define the function $G(t) := \int_0^t U(z(s)) ds$.

4.2 A criterion for vanishing geometric phase

Unlike the formula for $\dot{\phi}$, equation (1.39), which is singular at each of the binary collisions, the formula U is singular only at two points on the classical shape sphere (thus at eight points on the regularised shape sphere). They occur when the denominator is equal to zero, which is only possible when

$$(M_1 a_1^2 + M_2 a_2^2 + M_3 a_3^2)^2 = 16MmA^2.$$

In the case of equal masses, this reduces to

$$(a_1^2 + a_2^2 + a_3^2)^2 = 48A^2,$$

which only happens when $a_1 = a_2 = a_3$, the equilateral triangle.

When $m_2 = m_3$, we obtain

$$(m_2^2 a_1^2 + m_1 m_2 (a_2^2 + a_3^2))^2 = 16m_1 m_2^2 (m_1 + 2m_2) A^2,$$

which clearly may only happen at an isosceles configuration with $a_2 = a_3$. Simplifying gives

$$(m_2^2 a_1^2 + 2m_1 m_2 a_2^2)^2 = m_1 m_2^2 (m_1 + 2m_2) (a_1 + 2a_2) (2a_2 - a_1) a_1^2,$$

which means the singularity occurs when $a_1 = \sqrt{\frac{2m_1}{m_1 + m_2}} a_2$, a particular isosceles triangle.

The final case is that all three masses differ. Here the singularities do not correspond to any symmetry but require that for some positive parameter λ the side lengths are given by $a_j = \lambda \sqrt{m_j(m_k + m_l)}$. This triangle is special in the sense that it minimises the moment of inertia, given a scale factor λ . Its moment of inertia simplifies to $I = 2M\lambda^2$.

In all cases it is easily checked that the singular points correspond to shape sphere coordinates $(w_1, w_2, w_3) = (0, 0, \pm 1)$. These points are coordinate singularities only for this choice of gauge; the integral we compute is actually the area enclosed on the shape sphere.

The numerator vanishes at any collinearity or collision. The three collinear subspaces are thus automatically accounted for, but also each case such that $m_k = m_l$ with $\alpha_k = \pm \alpha_l$ and $\pi_k = \pm \pi_l$, the six possible isosceles invariant subspaces of the regularised system. That is, the geometric phase identically vanishes for periodic orbits in invariant subspaces. Given that the invariant subspaces map to arcs on the shape sphere, and thus enclose no area, this is natural.

One now asks the question: what symmetries may an orbit possess such that the geometric phase cancels over a whole period? Here we consider only symmetries that do not correspond to invariant subspaces.

Definition 4.3. A (possibly reversing) symmetry γ of the regularised vector field is a symmetry of U if

$$U(z) = U(\gamma(z)).$$

Similarly, γ is an antisymmetry of U if

$$U(z) = -U(\gamma(z)).$$

Lemma 4.4. The antisymmetries of U are exactly the symmetries $\gamma \in \tilde{\Gamma}$ whose projection onto the centre C_4 is either τ or ρ .

Proof. Recall that $\tilde{\Gamma} = C_4 \times S \rtimes F_4$, so that every $\gamma \in \tilde{\Gamma}$ can be uniquely written as a product of elements of C_4 , S , and F_4 . It suffices to show that every element $\gamma \in \tilde{S} = S \rtimes F_4$ is a symmetry of U , that ρ is an antisymmetry, and that τ is an antisymmetry.

The denominator of U is invariant under F_4 and invariant under any $\gamma \in S$, containing only positive constants and squares of phase space variables. So we only need consider the numerator $A \sum F_j$ (up to the constant factor involving the masses).

Consider first arbitrary masses. In this case, $\tilde{S} \cong F_4$, as no permutation of the bodies is a symmetry. In f_j there are only expressions involving masses and lengths (squares of the regularised coordinates), so each f_j is invariant under sign flip symmetries. As each sign flip symmetry flips both the coordinate and momenta simultaneously, the sign of each F_j is also invariant, due to the product $\alpha_j \pi_j$. Thus each $s_j \in F_4$ is a symmetry of U .

Next we consider exactly two equal masses: without loss of generality, $m_2 = m_3$. Here an extra element $\sigma_1 \in S$ is permitted. Recall that σ_j flips the signs of all coordinates and momenta, so the product $\alpha_j \pi_j$ is “safe” in each F_j , but the signed area A is negated. What occurs inside each f_j ? Recall $M_j = m_k m_l$. Thus $M_2 = M_3$. Then the permutation $2 \leftrightarrow 3$ simply swaps signs and values $f_1(\sigma_1(z)) = -f_1(z)$, $f_2(\sigma_1(z)) = -f_3(z)$, and $f_3(\sigma_1(z)) = -f_2(z)$. Thus the same happens to each F_j and $\sum F_j(\sigma_1(z)) = -\sum F_j(z)$. But as $A \rightarrow -A$ under σ_1 we have that pairwise permutations are symmetries of U .

Finally, with equal masses, cyclic permutations are allowed, in addition to all pairwise permutations. As the masses are equal, every M_j and every m_j is identical, and as the cyclic permutations are compositions of two pairwise permutations, they too are symmetries of U .

Now the symmetry ρ flips all signs simultaneously. This does not change the sign of any f_j or any product $\alpha_j \pi_j$, but does send $A \rightarrow -A$. Thus ρ is an antisymmetry of U , and thus any $\gamma \in \tilde{S}$ composed with ρ is an antisymmetry of U .

The time-reversing symmetry τ flips only the signs of the momenta, so while the signed area is preserved and each f_j is invariant, we have that $\tau(\alpha_j \pi_j) = -\alpha_j \pi_j$. Thus τ also is an antisymmetry of U . Note that $\tau\rho$ is a symmetry of U . \square

Now we give a criterion for when a relative periodic orbit is in fact absolutely periodic.

Theorem 4.5. *Suppose a T -periodic solution $z(t)$ of the regularised equations of motion has isotropy subgroup Σ_z . If Σ_z contains an element that is an antisymmetry of U , then the geometric phase of $z(t)$ vanishes.*

Proof. The idea of the proof boils down to three concepts: first, the structure of subgroups of $\tilde{\Gamma}$; second, the orbit of a point on a periodic solution under the action of its isotropy subgroup; and third, the evaluation of ΔG from the points generated by the action of the isotropy subgroup.

The first key idea is that any subgroup $G < \tilde{\Gamma}$ that projects to a nontrivial subgroup of the centre has even order and, if the projection is other than $\{I, \tau\rho\}$, half its elements are antisymmetries of U . If the projection is $\{I, r\}$, where r is any nontrivial element of C_4 , then half the elements of G are of the form $r\gamma$, with $\gamma \in \tilde{S}$. Thus if $r = \tau$ or if $r = \rho$, then exactly half the elements of G are antisymmetries of U ; if $r = \tau\rho$ then every element of G is a symmetry of U . If the projection of G is the whole centre, then exactly one quarter of elements of G are of the form $\rho\gamma$, one quarter are of the form $\tau\gamma$, one quarter are of the form $\tau\rho\gamma$, and the rest may be written as $\gamma \in \tilde{S}$; so half the elements of G are again antisymmetries of U .

The second key idea is that an isotropy subgroup of order k breaks a solution into k segments. A single point $z(t_0)$ on the solution is mapped to k points related by $\gamma \in \Sigma_z$. The value of U at each point is $U(\gamma(z(t_0))) = \pm U(z(t_0))$, with the sign depending on whether γ is a symmetry or an antisymmetry of U .

The third and final idea is that the value of ΔG is obtained by summing the integral of $U(z(t))$ over each fundamental segment as dictated by $\Sigma_z \cong G$. If Σ_z contains one antisymmetry of U , then, because antisymmetries of U comprise half the elements of G , each fundamental segment may be paired with another on which the integral of U has the opposite sign. \square

We now know that many of the possible isotropy subgroups will force the geometric phase to vanish over a periodic orbit. For the remaining cases the geometric phase will be generically non-zero.

Theorem 4.6. *Orbits with isotropy subgroups as described in Theorem 4.5 are the only ones for which the geometric phase necessarily vanishes.*

Proof. Extending the idea of the proof of Theorem 4.5, consider the two possible cases in which Σ_z contains no antisymmetry of U : either its projection onto the centre is trivial, or is $\{I, \tau\rho\}$. As all such subgroups contain only symmetries of U , there is no pairing of segments of periodic solution $z(t)$ with U having opposite sign in each. At best, it could be that the integral vanishes “by accident” in each segment for some solution $z(t)$ regardless of symmetry. \square

We now show examples of how Theorem 4.5 works out in two specific cases: first, when $\Sigma_z \cong \mathbb{Z}_{2k}$, where Σ_z is generated by an element of form $r\gamma$, with $r = \tau$ or ρ and $\gamma \in \tilde{S}$; and second, when $\Sigma_z \cong D_k$ generated by two reversing symmetries $\tau\gamma_1$ and $\tau\gamma_2$.

Case 1: a solution $z(t)$ whose isotropy subgroup is a cyclic subgroup (that is, containing no reversing elements $\tau\gamma$) of order $2k$ generated by the antisymmetry $\rho\gamma$, where $\gamma \in \tilde{S}$. Consider an interval of time $0 \leq t \leq \frac{T}{k}$, the time such that $z(t + \frac{T}{k}) = (\rho\gamma)^2(z(t)) = \gamma^2(z(t))$, and at the midpoint $z(t + \frac{T}{2k}) = \rho\gamma(z(t))$. We have

$$\begin{aligned} G\left(\frac{T}{k}\right) &= \int_0^{\frac{T}{k}} U(z(s))ds \\ &= \int_0^{\frac{T}{2k}} U(z(s))ds + \int_{\frac{T}{2k}}^{\frac{T}{k}} U(z(s))ds \\ &= G\left(\frac{T}{2k}\right) + \int_{\frac{T}{2k}}^{\frac{T}{k}} U(\rho\gamma(z(s + \frac{T}{2k})))ds \\ &= G\left(\frac{T}{2k}\right) + \int_0^{\frac{T}{2k}} U(\rho\gamma(z(s)))ds \\ &= G\left(\frac{T}{2k}\right) - \int_0^{\frac{T}{2k}} U(z(s))ds \\ &= G\left(\frac{T}{2k}\right) - G\left(\frac{T}{2k}\right) \\ &= 0. \end{aligned}$$

Thus every segment of length $\frac{T}{k}$ contributes nothing to the integral and the geometric phase vanishes, as illustrated in figure 4.1.

Case 2: a solution $z(t)$ whose isotropy subgroup is generated by two time reversing symmetries $\tau\gamma_1$ and $\tau\gamma_2$, where $\gamma_1 \in \tilde{G}$ is any spatial symmetry (be it a symmetry or antisymmetry of U) and $\gamma_2 \in \tilde{S}$ a symmetry of U , and the element $(\tau\gamma_1)(\tau\gamma_2) = \gamma_2\gamma_1$ has order k . Phase-shift the orbit such that $z(t) = \tau\gamma_1(z(-t)) = \tau\gamma_2(z(\frac{T}{k} - t))$.

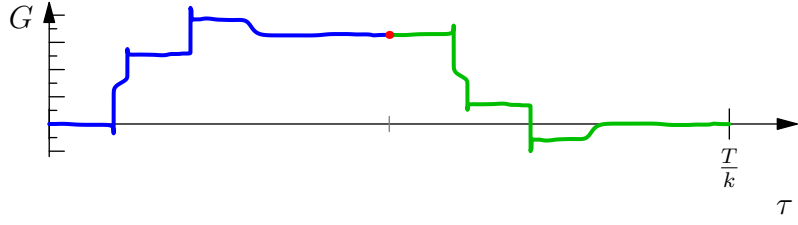


Figure 4.1: Integral of geometric phase formula over a fraction of one period in the non-reversing case, indicating by the red dot the point $\frac{T}{2k}$ at which the configuration $z(\frac{T}{2k}) = \rho\gamma z(0)$.

Consider an interval $0 \leq t \leq \frac{T}{k}$. Now

$$\begin{aligned}
 G\left(\frac{T}{k}\right) &= \int_0^{\frac{T}{k}} U(z(s))ds \\
 &= \int_0^{\frac{T}{2k}} U(z(s))ds + \int_{\frac{T}{2k}}^{\frac{T}{k}} U(z(s))ds \\
 &= G\left(\frac{T}{2k}\right) + \int_{\frac{T}{2k}}^{\frac{T}{k}} U(z(s))ds \\
 &= G\left(\frac{T}{2k}\right) + \int_{\frac{T}{2k}}^{\frac{T}{k}} U(\tau\gamma_2(z(\frac{T}{k} - s)))ds \\
 &= G\left(\frac{T}{2k}\right) - \int_{\frac{T}{2k}}^{\frac{T}{k}} U(z(\frac{T}{k} - s))ds \\
 &= G\left(\frac{T}{2k}\right) - \int_{-\frac{T}{2k}}^0 U(z(-s))ds \\
 &= G\left(\frac{T}{2k}\right) + \int_0^{-\frac{T}{2k}} U(z(-s))ds \\
 &= G\left(\frac{T}{2k}\right) - \int_0^{\frac{T}{2k}} U(z(s))ds \\
 &= G\left(\frac{T}{2k}\right) - G\left(\frac{T}{2k}\right) \\
 &= 0.
 \end{aligned}$$

As in case 1, every segment of length $\frac{T}{k}$ contributes nothing to the integral and the geometric phase vanishes, as illustrated in figure 4.2.

By way of contrast, if the cyclic symmetry is a symmetry of U or if both reversing symmetries are symmetries of U , then the step where the symmetry is eliminated from U inside the second integral does not change its sign. The rest proceeding as in the respective cases above we have $G\left(\frac{T}{k}\right) = 2G\left(\frac{T}{2k}\right)$, which is not, in general, zero.

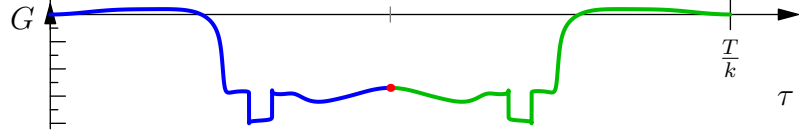


Figure 4.2: Integral of geometric phase formula over a fraction of one period in the reversing case, indicating by the red dot the point $\frac{T}{2k}$ at which the configuration is $z(\frac{T}{2k}) \in \text{Fix}(\tau\gamma_2)$.

Finally, recall table 2.1; it summarises the structure and properties of the symmetry group with regard to geometric phase and the relationship to the reduced symbolic dynamics. The result is simple: the geometric phase of an orbit necessarily vanishes if any element from columns 2 or 3 appear in its isotropy subgroup; if the isotropy subgroup contains no such element, in general we expect the orbit to have non-zero geometric phase. That is, we are now able to choose symmetries such that an orbit with vanishing angular momentum is absolutely or relatively periodic, although this does not allow us to choose the value of ΔG if it is non-vanishing. An orbit with reversing symmetries whose sequence class specifies reversing B , M , or F configurations is absolutely periodic, and generically relatively periodic otherwise.

5 Numerical methods

5.1 Introduction

Numerical methods are a key tool in modern analysis of complicated dynamical systems, as very rarely can explicit solutions be found. In this chapter we discuss the construction and use of numerical tools used in the body of work represented by this thesis.

At the heart of the numerical methods we employ is the numerical integrator, approximating solutions to Hamilton's equations of motion. It is well known that “traditional” methods, though highly accurate and efficient over short time scales, are unsuitable for long time integration of Hamiltonian systems. A “natural” integration scheme for a Hamiltonian system respects the symplectic structure of all Hamiltonian systems. We discuss the selection and construction of a scheme for approximating solutions to the reduced and regularised 3-body problem before examining its performance with several test cases.

Once an integration method for the system has been obtained we desire to find periodic orbits. This is done via an implementation of Newton-Raphson iteration on an appropriately chosen Poincaré section over a grid of points in the section.

Finally, results from such a broad search may turn up the same orbit more than once, so we must filter the results to pick out each orbit unique up to symmetry before further analysis can take place.

5.2 Symplectic integration of the reduced and regularised 3-body problem

The work in this section has been published as [60], which publication was a direct result of work towards this thesis.

5.2.1 Splitting methods

A Hamiltonian system $\dot{z} = J \nabla H z$ has a formal solution $z(t) = e^{\{\cdot, H\}t} z_0$, for some initial condition z_0 . The exponential is identified with the flow φ_H^t of H . If $H = H_1 + \dots + H_n$, the formal solution is equivalent to $e^{\{\{\cdot, H_1\} + \dots + \{\cdot, H_n\}\}t} z_0$. By the Baker-Campbell-Hausdorff formula, this may be written as a power series in t , which, if truncated, becomes an approximation of the flow comprising compositions of the H_i with various coefficients. If, furthermore, each H_i is exactly integrable, then the flows may be written explicitly, and the truncated power series represents an explicit integration scheme.

We see first of all that

$$\varphi_H^t = \varphi_{H_1+\dots+H_n}^t = \varphi_{H_1}^t \circ \dots \circ \varphi_{H_n}^t + \mathcal{O}(t^2) \quad (5.1)$$

gives an approximation accurate to first order in time. Any order of compositions will work, but given one ordering another is distinguished.

Define the *adjoint* of a flow as the inverse of the time-reversed flow. That is, $\varphi_H^t{}^* = (\varphi_H^{-t})^{-1}$. If a system is reversible, then $(\varphi_H^t)^{-1} = \varphi_H^{-t}$, and it is clearly self-adjoint. Reversibility is key to what follows.

If we define a first order composition $\varphi_{H,1}^t = \varphi_{H_1}^t \circ \dots \circ \varphi_{H_n}^t$, the adjoint is

$$\begin{aligned} \varphi_{H,1}^t{}^* &= (\varphi_{H,1}^{-t})^{-1} \\ &= (\varphi_{H_1}^{-t} \circ \dots \circ \varphi_{H_n}^{-t})^{-1} \\ &= (\varphi_{H_n}^{-t})^{-1} \circ \dots \circ ()^{-1} \quad = \varphi_{H_n}^t \circ \dots \circ \varphi_{H_1}^t \text{ by reversibility,} \end{aligned} \quad (5.2)$$

which, as we see, is merely composition in the reverse order.

Second, it is well known [11, 23, 40, 33] that the composition of a first order method with its adjoint (each following the flow for $\frac{t}{2}$) forms a second order scheme that takes a step t . Explicitly, this is

$$\begin{aligned} \varphi_{H,2}^t &= \varphi_{H,1}^{\frac{t}{2}} \circ \varphi_{H,1}^{\frac{t}{2}}{}^* + \mathcal{O}(t^3) \\ &= \varphi_{H_1}^{\frac{t}{2}} \circ \dots \circ \varphi_{H_n}^{\frac{t}{2}} \circ \varphi_{H_n}^{\frac{t}{2}} \circ \dots \circ \varphi_{H_1}^{\frac{t}{2}} + \mathcal{O}(t^3) \\ &= \varphi_{H_1}^{\frac{t}{2}} \circ \dots \circ \varphi_{H_n}^{\frac{t}{2}} \circ \dots \circ \varphi_{H_1}^{\frac{t}{2}} + \mathcal{O}(t^3). \end{aligned}$$

Thus a second order integrator $\varphi_{H,2}^t$ is produced from the composition of a first order scheme and its adjoint. Note that, based on the assumption that each H_i has a reversible flow, this integrator is reversible! In the case that $H = T(p) + V(q)$ this

process results in the symplectic leapfrog integrator by composing the first order symplectic Euler with its adjoint.

Different schemes, all second order, are produced by choosing different permutations of composition of the first order integrator, which may affect computational efficiency and accuracy at the point of implementation in a computer.

Higher (even) order, reversible symplectic integrators may be produced by compositions of a reversible even order integrator, as described by [87, 23], through the use of carefully chosen coefficients. If $\varphi_{H,2}^t$ represents a reversible second order scheme, a higher order scheme is obtained by $\varphi_{H,2}^{a_1 t} \circ \cdots \circ \varphi_{H,2}^{a_{n-1} t} \circ \varphi_{H,2}^{a_n t} \circ \varphi_{H,2}^{a_{n-1} t} \circ \cdots \circ \varphi_{H,2}^{a_1 t}$, where $2 \sum_{i=1}^n n - 1 a_i + a_n = 1$ and a_i satisfy an algebraic equation that guarantees that the composition approximates the true flow to the correct order.

5.2.2 Implementation

An integrable and separable Hamiltonian $H = H_1(q_1, p_1) + \cdots + H_n(q_n, p_n)$, being a sum of integrable Hamiltonians in disjoint degrees of freedom, gives the identity $\varphi_H^t = \varphi_{H_1}^t \circ \cdots \circ \varphi_{H_n}^t$. What happens if instead the Hamiltonian is a product $H = H_1(q_1, p_1) H_2(q_1, p_1) \dots$?

Lemma 5.3. *A Hamiltonian defined as a product of integrable autonomous Hamiltonians with disjoint degrees of freedom $H = H_1(q_1, p_1) H_2(q_2, p_2) \dots H_n(q_n, p_n)$ is integrable, with flow $\varphi_H^t = \varphi_{H_1}^{H_2 H_3 \dots H_n t} \circ \varphi_{H_2}^{H_1 H_3 \dots H_n t} \circ \cdots \circ \varphi_{H_n}^{H_1 H_2 \dots H_{n-1} t}$.*

Proof. Each H_i has a flow $\varphi_{H_i}^t$, and as each is autonomous, its value $h_i = H_i(q_{i,0}, p_{i,0})$ is constant along any solution with initial conditions $(q_{i,0}, p_{i,0})$. A constant multiple $H_i \rightarrow aH_i$ is equivalent to a rescaling of time by $t \rightarrow at$, as we have the equations of motion also multiplied by the same constant. As each H_i is integrable, we have a solution for the pair $(q_i(t), p_i(t))$. Thus we have $\varphi_{aH_i}^t = \varphi_{H_i}^{at}$.

The equations of motion for the i -th pair of canonical variables of H are

$$\begin{aligned}\dot{q}_i &= \left(\prod_{j \neq i} H_j \right) \frac{\partial H_i}{\partial p_i} \\ \dot{p}_i &= - \left(\prod_{j \neq i} H_j \right) \frac{\partial H_i}{\partial q_i}.\end{aligned}$$

As each H_j is a constant of motion, this is just a rescaling of time for the solution of H_i such that the flow of H in the $q_i p_i$ -plane of phase space is equivalent to $\varphi_{H_i}^{(\prod_{j \neq i} H_j)t}$.

This is the case for every $i = 1, \dots, n$, so the full flow of H must be the composition of the flows of each H_i up to time scaling by the value of the product $\prod_{j \neq i} H_j$. \square

Consider a monomial Hamiltonian $H_{mn} = q^m p^n$ in one degree of freedom. In the case that $m \neq n$ the flow is

$$\varphi_{mn}^t(q, p) = (q\beta^n, p\beta^{-m}), \text{ where } \beta = (1 + (n - m)q^{m-1}p^{n-1}t)^{\frac{1}{n-m}}, \quad (5.4)$$

while for $m = n$ it is

$$\varphi_{mn}^t(q, p) = (q\beta, p\beta^{-1}), \text{ where } \beta = \exp(m(qp)^{m-1}t). \quad (5.5)$$

A monomial in any number of degrees of freedom is a special case of the structure in lemma 5.3. Therefore any polynomial Hamiltonian is a sum of integrable monomial Hamiltonians and thus a splitting integrator can be constructed. Symplectic integration of polynomial Hamiltonians has been discussed in [67, 18, 11, 6, 58].

The cases that a Hamiltonian is a function of coordinates only or of momenta only result in explicit flows

$$\begin{aligned} \varphi_{T(p)}^t(q, p) &= (q + (\nabla_p T)t, p), \text{ and} \\ \varphi_{V(q)}^t(q, p) &= (q, p - (\nabla_q U)t). \end{aligned} \quad (5.6)$$

The fully reduced and regularised Hamiltonian equation (1.36) is polynomial of degree 6 in α_j, π_j , with 34 terms. Treating this naïvely as such, as per just using section 5.2.1 straight away, would lead to a second order method with $2 \times 34 - 1 = 67$ stages! It is therefore beneficial to note that 13 monomials are functions of the α_j only, and may thus be treated as a single stage with Hamiltonian $H_0(\alpha_1, \alpha_2, \alpha_3)$. Furthermore, other immediate optimisations are possible by grouping with appropriate disjoint degrees of freedom, making use of the cases discussed above.

We observe monomial terms $q^m p^n$ where $m = n = 1$, $m = n = 2$, and $m = 3, n = 1$. Now of the 21 terms that are mixed functions of coordinates and momenta, we may group them into 9 functions, making use of disjoint degrees of freedom, to obtain the following:

$$\begin{aligned} H_0 &= -\sum M_j \alpha_j^4 - (\sum M_j) (\sum \alpha_k^2 \alpha_l^2) - h a_1 a_2 a_3 = V_0 \\ H_j &= \frac{1}{8} \left(\frac{\alpha_k^2}{\mu_k} + \frac{\alpha_l^2}{\mu_l} \right) \alpha_j^2 \pi_j^2 = \frac{1}{8} V_j F_{j,22} \\ H_{j+3} &= \frac{1}{8} \left(\frac{\alpha_k^4}{\mu_k} + \frac{2}{m_j} \alpha_k^2 \alpha_l^2 + \frac{\alpha_l^4}{\mu_l} \right) \pi_j^2 = \frac{1}{8} V_{j+3} T_j \\ H_{j+6} &= -\frac{1}{4} \left(\frac{1}{m_l} \alpha_k \pi_k + \frac{1}{m_k} \alpha_l \pi_l \right) \alpha_j^3 \pi_j = -\frac{1}{4} G_j F_{j,31}, \end{aligned} \quad (5.7)$$

where $G_j = F_{k,11} + F_{l,11}$, $F_{j,mn} = \alpha_j^m \pi_j^n$, and $M_j = m_k m_l$ and $\frac{1}{\mu_j} = \frac{1}{m_k} + \frac{1}{m_l}$.

The structures of the flows of the nine terms with indices j , $j+3$, and $j+6$ are

$$\begin{aligned}\varphi_{H_j}^t &= \varphi_{V_j}^{\frac{1}{8}F_{j,22}t} \circ \varphi_{F_{j,22}}^{\frac{1}{8}V_j t} \\ \varphi_{H_{j+3}}^t &= \varphi_{V_{j+3}}^{\frac{1}{8}T_j t} \circ \varphi_{T_j}^{\frac{1}{8}V_{j+3} t} \\ \varphi_{H_{j+6}}^t &= \varphi_{G_j}^{-\frac{1}{8}F_{j,31}t} \circ \varphi_{F_{j+3,31}}^{-\frac{1}{8}G_j t} = \varphi_{F_{k,11}}^{-\frac{1}{8}F_{j,31}t} \circ \varphi_{F_{l,11}}^{-\frac{1}{8}F_{j,31}t} \circ \varphi_{F_{j+3,31}}^{-\frac{1}{8}G_j t}.\end{aligned}$$

All are integrable, with exact flows given explicitly in appendix C. Thus the flow of $K = H_0 + \dots + H_9$ is approximated to first order by any composition of the exact flows. The order of composition given in appendix C is the order used in our numerics to construct the second order method $\varphi_{K,2}^t$.

5.2.2.1 Higher order methods

Yoshida [87], along with others independently [17, 9], published methods the construct higher order symplectic maps. In particular, “Yoshida’s trick” generates reversible maps of arbitrary even order, though they are not very efficient, requiring many more evaluations of a base even order, reversible map than those provided in, say, [23], pp156-158.

The order conditions for symmetric composition methods are discussed in detail in [23], culminating in coefficients being provided for two methods of order 6 (with 7 and 9 stages), two methods of order 8 (with 15 and 17 stages), and one method of order 10 (with 35 stages).

All methods that we consider are of the form

$$\varphi_{H,r}^t = \varphi_{H,p}^{\gamma_s t} \circ \dots \circ \varphi_{H,p}^{\gamma_1 t}, \quad (5.8)$$

where the γ_i are coefficients chosen to adjust the step size of the base (symmetric) method $\varphi_{H,p}^t$ of order p , and s is the number of stages. By [23], Theorem II.4.1, as $\varphi_{H,p}^t$ is given to be symmetric of order p , then the composition (5.8) is of order at least $r = p + 1$ if the γ_i satisfy

$$\begin{aligned}\sum_{i=1}^s \gamma_i &= 1 \\ \sum_{i=1}^s \gamma_i^{p+1} &= 0.\end{aligned}$$

We may furthermore wish to impose the constraint $\gamma_i = \gamma_{s+1-i}$ so that $\varphi_{H,r}^t$ is itself symmetric, requiring odd s . Note that no real solutions for γ_i exist if p is odd.

Choosing $s = 3$ yields Yoshida's method with $\gamma_1 = \gamma_3 = \frac{1}{2 - 2^{\frac{1}{p+1}}}$, $\gamma_2 = -\frac{2^{\frac{1}{p+1}}}{2 - 2^{\frac{1}{p+1}}}$, yielding a method of order $r = p + 2$. More efficient methods can be found for a base method of order 2 and a choice of larger s . Rather than go over the theory of order considerations for such methods, we provide the coefficients directly in appendix D.

5.2.3 Performance

We construct several methods of orders 4 to 10 by the techniques described in section 5.2.2.1, using the second order symmetric method $\varphi_{K,2}^t$ built according to the splitting described in section 5.2.2. We test the integrators thus obtained for their average performance over an ensemble of points. In [60] we then demonstrated the integrator on three different orbits: the figure-8 choreography ($t0(12,1)$); the “Pythagorean orbit” (whose final motions were fully mapped out by [76]); and an unstable periodic collision orbit of type-1 ($t1(2,2)$).

5.2.3.1 Efficiency

Efficiency is determined by the work-precision diagram figure 5.1, with methods denoted as $O(r_s)$, where r denotes the order of the method and s is the number of evaluations of $\varphi_{K,2}^t$ per time step. We choose an ensemble of points in phase space, integrate forward in time for a fixed interval, then average the energy error to obtain the y -values of the points. Here the energy is not the physical energy h , a fixed parameter, but the value of the regularised Hamiltonian K , which on valid physical trajectories is identically 0. The x -values indicate the number of evaluations of the base method over the given interval with that integrator. Large time steps on the interval appear to the left, and small time steps to the right.

Each method clearly shows the correct order behaviour, but the methods constructed with Yoshida's coefficients clearly have larger error, with method $O(8_{27})$ clearly performing far worse than either $O(8_{15})$ or $O(8_{17})$. These, in turn, typically appear to perform better than $O(10_{35})$, as at the point where the latter would overtake the former roundoff error due to finite machine precision begins to dominate, resulting in the distinctive “elbow” for each method. The step size at the elbow is considered optimal for each method¹.

¹Note that $O(2_1)$ could go to smaller time steps before reaching the elbow, but an eyeball estimation puts the optimal time step at its elbow of $\delta t \approx 10^{-6}$. Its accuracy at that point would be no

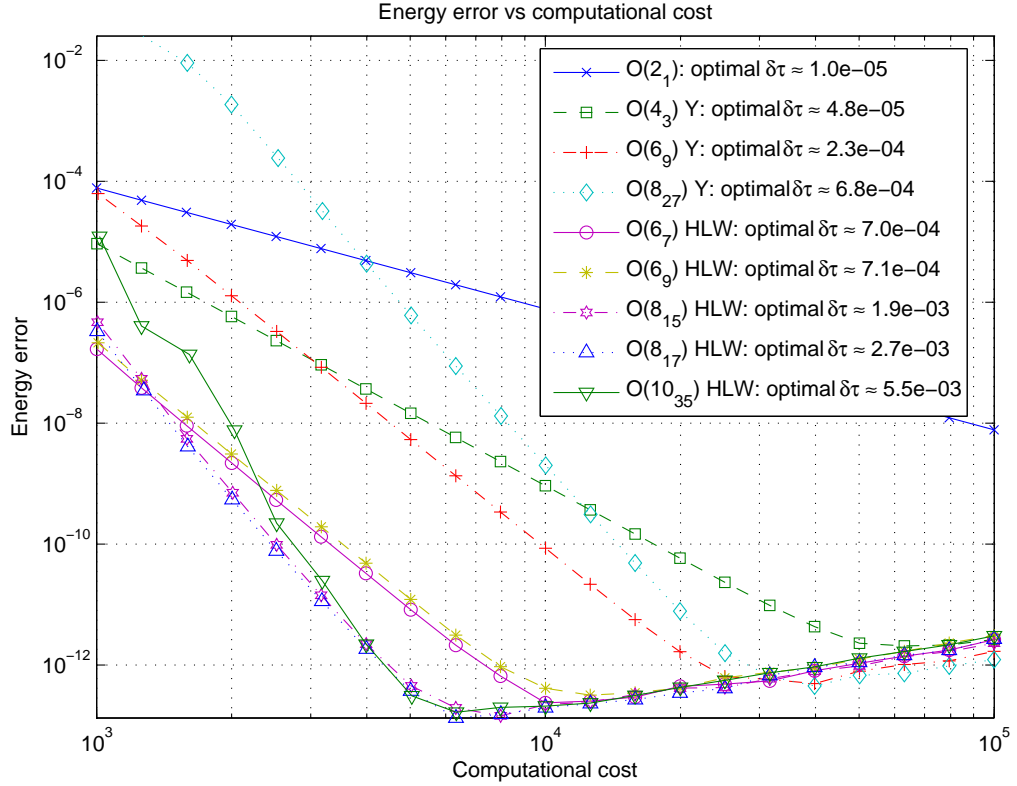


Figure 5.1: Work-precision diagram for methods $O(p_s)$ of order p with s stages, indicating source for coefficients, where appropriate ('Y' for [87], 'HLW' for [23]) and optimal time step δt .

Consequently, the obvious choice to use is $O(8_{17})$, which has slightly lower average error than does $O(8_{15})$ for little difference in cost, with a step size of $\delta t = 0.0027$.

5.2.3.2 Examples

Three specific orbits are chosen to illustrate and test the integrator. Each orbit is integrated forwards over a specified interval, and then at various points along the trajectory it is integrated “in reverse” (that is, with a negative δt) back to $t = 0$. This allows a measure of the accumulated error in the energy over the total integration time, as well as in the final coordinates upon return. The former provides a “kinder” test of the integrator, as we expect the energy to be approximately conserved by a

better than that of $O(8_{17})$ with a complexity cost nearly three orders of magnitude smaller and far from the latter’s own minimal error.

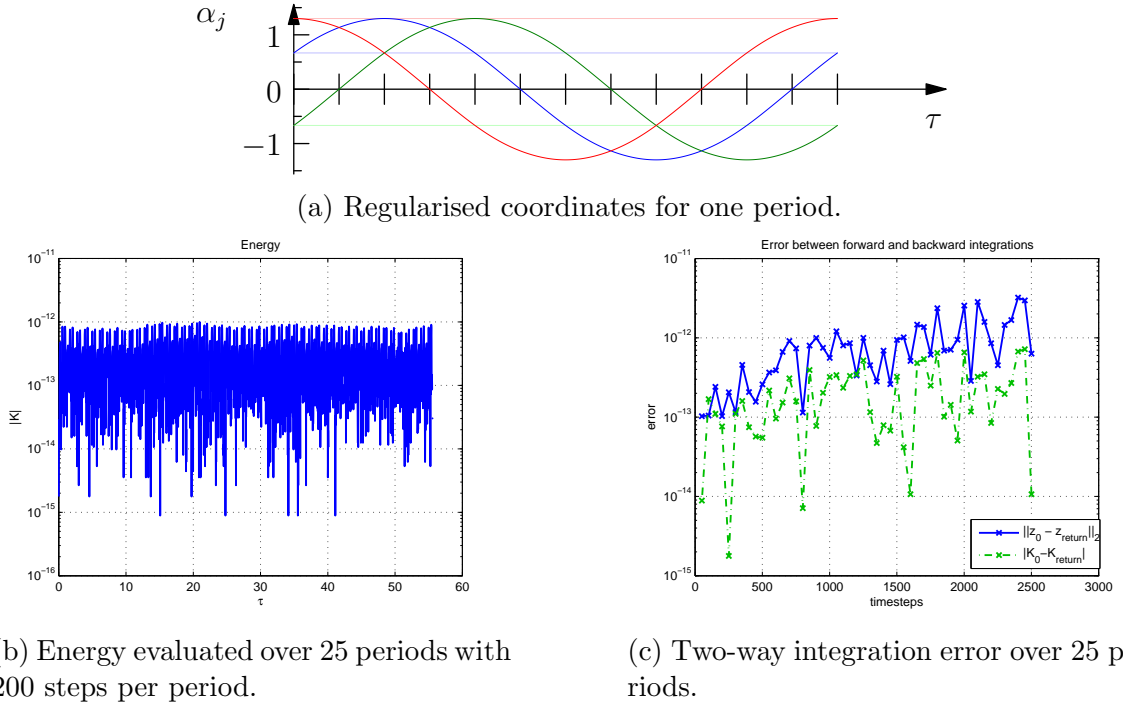


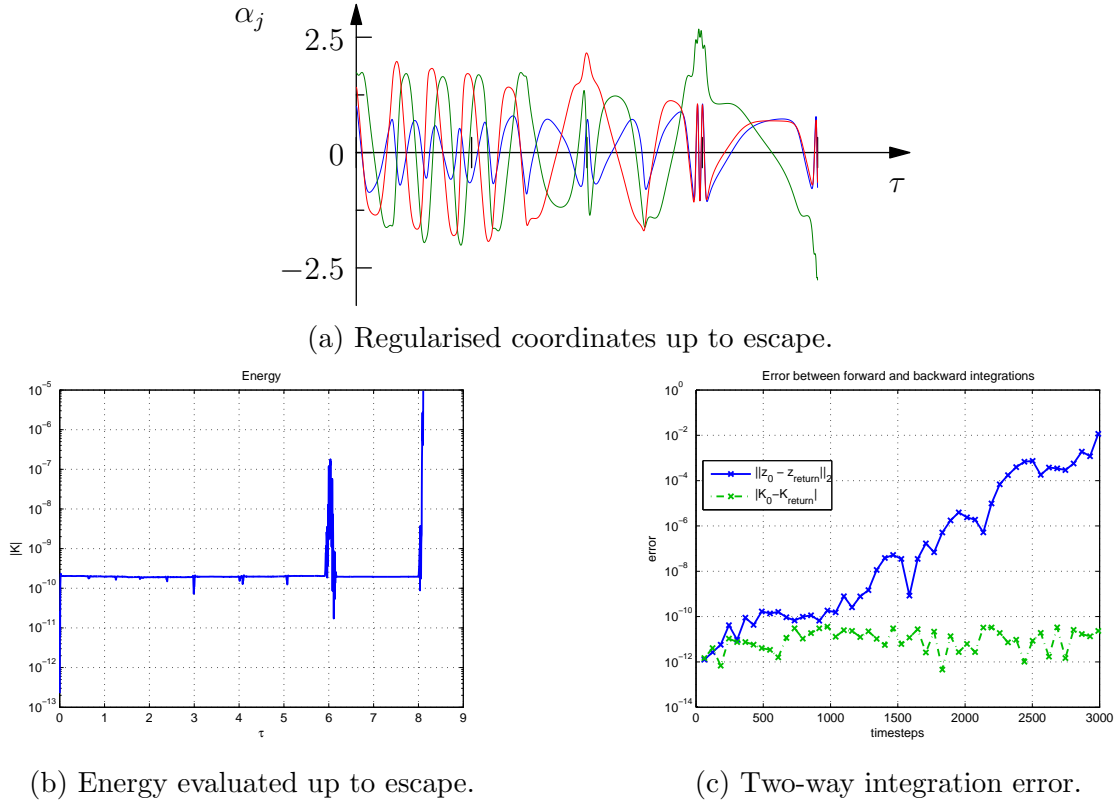
Figure 5.2: Figure-8 choreography with regularised period $T_r = 2.22181372$ and $h = -1$.

symplectic method, and a symmetric method should return to its original value (up to the accumulation of roundoff).

The first orbit, the figure-8 choreography, figure 5.2, is well known for its simplicity, its beauty and the sheer surprisingness of its existence. First discovered by [51], later proven to exist by [16], and explored in more detail by [71, 70], this orbit has three bodies of equal mass following the same path with a cyclic permutation symmetry at $\frac{T}{3}$.

The second is the “Pythagorean orbit”, figure 5.3, an orbit with masses in the ratio $m_1 : m_2 : m_3 = 5 : 3 : 4$, initially at rest, forming a triangle with sides proportional to the masses—that is, $a_1 : a_2 : a_3 = 5 : 3 : 4$, forming a Pythagorean triangle. This orbit is of note² because its final motions are known, due to [76], and it suffers a

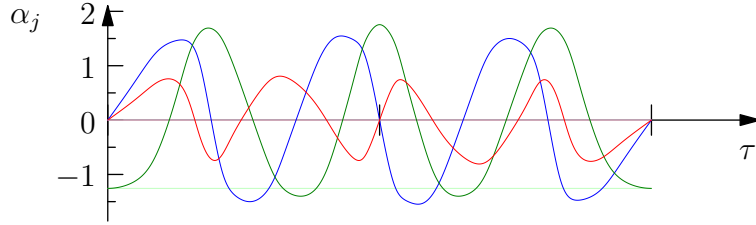
²A wonderful account of the story of this problem is given by [75]. In summary, Meissel in 1893 conjectured that the initial conditions of this problem lead to periodic motion. On what basis this conjecture was made we do not know. Burrau, in 1913, attempted to calculate the solution numerically—by hand. After several close encounters of the bodies he reached his limit. The solution was completed by [76], and while the solution is not periodic, it may be that Meissel was not totally wrong—it appears that the initial conditions of this problem may lie quite close to a true periodic solution.

Figure 5.3: Pythagorean orbit integrated up to $t = 8.105$.

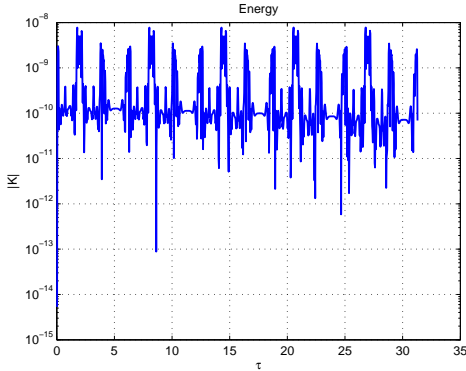
close encounter between bodies 1 and 3 at $t \approx 15.8$ ($t \approx 1.52$ in scaled time), where the mutual distance is $a_2 \approx 4.2 \times 10^{-4}$. The final motion is known to be the escape to $+\infty$ of body 2, while bodies 1 and 3 as a “hard binary” go to $-\infty$. While this does not happen in finite time in the physical problem, the time scaling monitor function $\frac{d\tilde{t}}{dt} = a_1 a_2 a_3$ results in disproportionately larger steps of the physical time \tilde{t} compared to the fixed scaled time step δt as any of the distances gets large; if any one body should be ejected to infinity, this is compounded. We halt the computation at scaled time $t = 8.105$, when the exploding regularised distances and momenta cause the energy to explode rapidly as well.

The results that we obtain with our integrator are indistinguishable from those published by Szebehely and Peters [76], and by Gruntz and Waldvogel [19] in their exposition on numerical integration of three-body orbits.

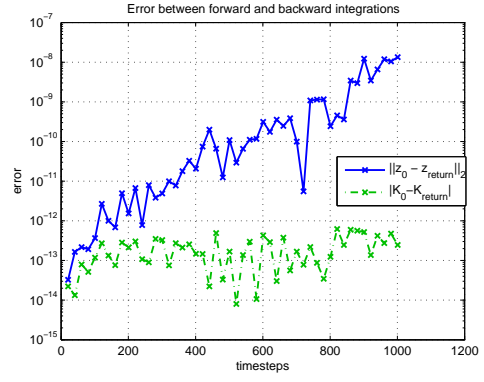
The final orbit is periodic collision orbit $t1(2, 2)$, figure 5.4, discovered by the methods described in section 5.3 and chosen for its relatively short length and simplicity. Its stability and precise symmetry were not known at the time of selection, but we now



(a) Regularised coordinates for one period.



(b) Energy evaluated over 5 periods with 200 steps per period.



(c) Two-way integration error over 5 periods.

Figure 5.4: Collision orbit with regularised period $T_r = 6.25205150$ and $h = -1$.

know its largest eigenvalue to have absolute magnitude 7.29425400, and its isotropy subgroup is $\{(I, 0), (\tau s_2, 0)\}$, indicating that the only non-trivial symmetry is a pair of brake-collisions at $\frac{T}{2}$ apart.

In all cases, observe that energy is well conserved, both across an orbit and in the return to $t = 0$. Both the Pythagorean and collision orbits exhibit exponential divergence in phase space from the initial condition with distance integrated forwards in time. This is to be expected due to the accumulation of small errors during integration if the trajectory lives in a chaotic region of the phase space or is an unstable periodic orbit (as is the collision orbit). The figure-8, however, a stable orbit, has a very close return, even after 25 periods with large step size.

While it is arguable that ultimately our integrator is not very efficient, it is suitable for our purposes, as periodic orbits remain bounded for all time (though it appears we must, by necessity, risk excluding periodic orbits with particularly large excursions as a consequence of the time scaling). Due to its symplecticity it may be able to find unstable orbits that would otherwise be lost.

5.3 Finding periodic orbits

5.3.1 Poincaré sections

Montgomery [48, 49] demonstrates that for $p_\phi = 0$ there will always be syzygies along a solution curve $z(t)$, except in the case of homothetic collapse. As we have equal masses, it is sufficient to pick just one syzygy condition, say the Poincaré surface of section $S(z) = \alpha_1 = 0$ with $\pi_1 \geq 0$ and seek periodic motions on this section; any solution we find will have “sister” solutions related by discrete symmetries, including permutation of indices. If we impose no symmetry on our initial conditions beyond this, however, the search space is large.

There are three coordinates α_j and canonical momenta π_j . Fixing $\alpha_1 = 0$, we have five values left to choose; but as the Hamiltonian is autonomous, its value is conserved along solution curves, reducing the dimension by one more. Indeed, the energy is fixed (we choose $h = -1$ as a parameter), so if we choose four out of $\alpha_2, \alpha_3, \pi_1, \pi_2, \pi_3$, then the remaining value is determined (possibly up to the value of one sign in the momenta) by the Hamiltonian and the other parameters themselves. We wish a one-sided section condition, which means that the direction in which the section is pierced is important.

At $\alpha_1 = 0$ syzygy we have $\dot{\alpha}_1 = \frac{1}{4} \left(\frac{\alpha_1^2}{m_1} + \frac{\alpha_2^2}{m_3} + \frac{\alpha_3^2}{m_2} \right) \pi_1$, so the direction through the section is determined by the sign of π_1 . We choose α_2, α_3 inside the Hill region and π_2, π_3 on the momentum ellipsoid and calculate $\pi_1 > 0$. Note that $\alpha_1 = \pi_1 = 0$ puts all solutions in the invariant subspace $\text{Fix}(\rho s_1)$, which would result in solutions with no points off the Poincaré section.

Define $\Omega \subset \mathbb{R}^4$ the set of permissible points in the phase space of K such that $\alpha_1 = 0$, $\pi_1 \geq 0$, and $h = -1$, and define $P: \Omega \rightarrow \Omega$ the Poincaré map generated by the reduced, regularised system.

The Poincaré map is obtained by integrating numerically (using the method constructed in section 5.2) the initial condition $z(0)$ determined from the section point z_0 until the section condition is met again, determining z_1 and so on. As the numerical method is discrete, it is hardly to be expected that the numerical solution should land on the section perfectly. Hénon [24] provides an elegant method of stepping directly onto the section itself, with little extra machinery than is already at our disposal, up to the accuracy of a numerical integrator. We summarise the result here.

Suppose a dynamical system is governed by the differential equations

$$\frac{dz}{dt} = F(z), \quad (5.9)$$

$F: \mathbb{R}^n \rightarrow \mathbb{R}^n$. Given the surface of section $S(z) = 0$ and a numerical method of approximating solutions $z(t)$, how do we find points on $S(z) = 0$ without resorting to interpolation, bisection, or other inefficient and possibly inaccurate methods?

By extending the equations of motion to include $\frac{dt}{dt} = 1$, we can make another variable the independent variable and use that to step directly onto the surface of section! Suppose the section is $S(z) = z_1 = 0$, and we expand the extended equation (5.9) to get

$$\begin{aligned} \frac{dz_1}{dt} &= F_1(z_1, \dots, z_n) \\ &\vdots \\ \frac{dz_n}{dt} &= F_n(z_1, \dots, z_n) \\ \frac{dt}{dt} &= 1. \end{aligned}$$

We can now make z_1 the independent variable by the chain rule, dividing the entire system by $\frac{dz_1}{dt} = F_1(z_1, \dots, z_n)$ to obtain

$$\begin{aligned} \frac{dz_1}{dz_1} &= 1 \\ &\vdots \\ \frac{dz_n}{dz_1} &= \frac{F_n(z_1, \dots, z_n)}{F_1(z_1, \dots, z_n)} \\ \frac{dt}{dz_1} &= \frac{1}{F_1(z_1, \dots, z_n)}. \end{aligned} \quad (5.10)$$

This can be integrated by a standard method, though it cannot be used to go from one section point to the next, because in between any two there must be a point on the solution curve where $\frac{dz_1}{dt} = 0$.

What we can do is integrate equation (5.9) numerically until we have two points straddling the section $S(z) = 0$. That is, we detect a change of sign of $S(z)$. At this point it is a simple matter to determine which point is closest and use the distance in the independent variable from the section to integrate one step in the modified system equation (5.10) onto the surface of section directly (up to the precision of our integrator).

We constructed an implicit *symplectic* Runge-Kutta scheme of order 6 to do this step, using the implicit symplectic midpoint method as our base.

5.3.2 Newton-Raphson method on the Poincaré section

If for some $z_0 \in \Omega$ and $i > 0$ we say that z_0 is *i-periodic* if we have $z_i = P^i(z_0) = z_0$. In order to find such points, define the function

$$F_i(z) = P^i(z) - z \quad (5.11)$$

so that z is *i-periodic* implies $F_i(z) = 0$. The Jacobian of F_i is

$$DF_i(z) = DP^i(z) - I,$$

where I is the 4×4 identity matrix (as $z \in \mathbb{R}^4$).

With this we may iteratively approach fixed points of P^i , using the Newton-Raphson method to approximate zeros of F_i . To find z_{n+1} we solve the linear system

$$DF_i(z_{n+1} - z_n) = -F_i(z_n), \quad (5.12)$$

in which the unknown is $z_{n+1} - z_n$.

In addition to the well known caveats of Newton-Raphson iteration, some further complications must be considered.

The Jacobian DP^i of the Poincaré map is not known explicitly, which means we must resort to possibly crude methods to approximate DP^i , and thus DF . Without going to great lengths to build a symplectic variational integrator for the problem, we use a numerical derivative $D(z) = (D_j(z)) \in \mathbb{R}^4 \times \mathbb{R}^4$ obtained by the double-sided approximation

$$D_j(z) = \frac{1}{\|\delta z_j\|} \left(F_i(z + \frac{\delta z_j}{2}) - F_i(z - \frac{\delta z_j}{2}) \right).$$

Each $\delta z_j \in \mathbb{R}^4$ has the value $\|z\| \sqrt{\epsilon_{mac}}$ in the j -th entry and is zero elsewhere, where ϵ_{mac} is the machine epsilon. The machine epsilon is also known as the unit roundoff, the smallest number that can be added to unity in floating point representation that does not round down to unity. In standard double precision arithmetic its value is $\epsilon_{mac} = 2^{-52} \approx 2.22 \times 10^{-16}$.

This method takes twice as long to evaluate as the single-sided approximation, but is marginally more accurate.

It is possible that the point $P^i(z)$ lies sufficiently close to the free fall boundary in the surface of section that $z \pm \delta z_j$ lies outside Ω for one choice of sign and some j . In such

a case we halt the iterations, as we must do when the Jacobian is not invertible. This does not preclude us from finding collinear brake orbits altogether, however; merely those which are collinear with body 1 in syzygy. The reason is that we may pick up such solutions lying in either invariant subspace $\text{Fix}(\rho s_2)$ or $\text{Fix}(\rho s_3)$, which intersect the surface of section at the collisions $\alpha_1 = \alpha_2 = 0$ or $\alpha_1 = \alpha_3$ respectively, and due to the symmetry $m_1 = m_2 = m_3$ we know that a sister solution lies in the invariant subspace $\text{Fix}(\rho s_1)$.

Finally, it is possible that the point we have chosen is on a trajectory that will come arbitrarily close to triple collision or otherwise take an arbitrarily long time to reach its next intersection with the surface of section. Due to the regularisation procedure, triple collision is moved to $\pm\infty$ in regularised time t . Such cases we exclude by choosing a (rather large!) cutoff time of $t = 50$ after which integration is halted.

5.3.3 Searching phase space

We consider two approaches to finding periodic orbits and choose one.

Method 1: construct a grid of points $\Omega_0 \subset \Omega$, then fix i and run the Newton-Raphson method with each element of Ω_0 as candidates to find i -periodic orbits or k -th repetitions of $\frac{i}{k}$ -periodic orbits, if k divides i . This method must be repeated for each length i , up to an appropriate choice of i_{max} .

Method 2: construct a grid of points as in method 1 and obtain all section points for each initial condition up to some maximum times t_{max} . For each initial condition consider the set $\{x_i\}$ of section points. If for some $\epsilon > 0$ and $j > i$ we have $\|x_j - x_i\| < \epsilon$, we consider x_i a candidate initial condition for a $(j-i)$ -periodic solution. If we later find some j' such that $j' - i = k(j - i)$, for $k > 1$, such that $\|x_{j'} - x_i\| < \epsilon$ we ignore x_i as a candidate for a $(j'-i)$ -periodic solution, as it will most likely return a solution that is just k repetitions of whatever solution may be near x_i with period $(j-i)$.

Both methods are bound to be computationally expensive, as we only restrict to initial conditions in the section $0 \leq \alpha_2 \leq \alpha_3 \leq 4$ (under the assumption that most solutions will have at least some crossing of the section in this region³), and full freedom of π_2, π_3 such that $x = (\alpha_2, \alpha_3, \pi_2, \pi_3) \in \Omega$. Noting that $\alpha_2 = 0$ implies collision, π_2 can have arbitrary values when this is the case, so we restricted to $|\pi_2| < 4$. Assuming a uniform grid in Ω , the number of points to consider in Ω_0 scales as the fourth power of the linear density of the grid.

³We justify this by virtue of the fact that this already extends into the arms of the Hill region, so should capture many orbits anyway

If the linear density is n , method 1 entails $\mathcal{O}(i_{max}n^4)$ calls to the Newton-Raphson routine, which entails 8 calls of the Poincaré map routine per iteration while computing the numeric derivative. Even with a large pool of parallel computational resources, this becomes unacceptable for large n , especially as we must consider each i separately. Because of the sheer daunting size of this method for $n \sim 100$ we did not attempt it.

Method 2 offers a compromise in that all $\mathcal{O}(n^4)$ points must be evaluated with the Poincaré map routine once, and it is cheap to compare distances between section points and obtain candidate orbits of many lengths all at once. While periodic orbits are dense in chaotic regions, “many” of these are expected to be extremely long; only a comparatively short list candidate orbits need be considered, on which to run the Newton-Raphson routine. We choose a grid spacing of 0.05, giving $n = 80$, and $t_{max} = 150$.

5.3.4 Determining unique orbits

We do not expect either method to return a list of periodic points unique up to symmetry (or phase-shift), or even with their minimal periods⁴. As we only consider the surface of section $\alpha_1 = 0$, $\pi_1 \geq 0$, it is possible that two seemingly different results belong to orbits related by $z_1(t) = \gamma(z_2(t+t_0))$, where $z_1(t)$ and $z_2(t)$ are two solutions in our list and $\gamma \in \tilde{\Gamma}$ is any reversing or non-reversing discrete symmetry and t_0 is a phase difference between the solutions. It is also possible that the period in the Poincaré map ($j - i$) is an integer multiple of the true period after converging to the nearby periodic point.

To account for both of these we define a list $Z_i = \{z_i(t_j)\}$ of syzygies and collisions in orbit i (occurring at times t_j , with $t_0 = 0$ and $t_n = T_i$ the period of $z_i(t)$ as it was returned from the search). That is, rather than just the one-sided $\alpha_1 = 0$ section condition we now use all three double-sided surfaces of section; or if a solution lies in a collinear invariant subspace we record only collisions.

In case the solution has been returned “too long”, we test whether or not

$$\|z(t_j) - z(0)\| < \delta \approx \sqrt{\epsilon_{mac}}$$

for each divisor j of n . If this happens to be the case, the smallest j is chosen and the true period is $\frac{jT_i}{n}$.

⁴Nor, indeed, a complete list for any given maximal period to consider. While the Newton-Raphson method can capture unstable orbits, we do not expect our initial search for candidates to return enough candidate points to capture everything.

Once every solution has been reduced to its shortest period we compute

$$d_l = \|z_i(0) - \gamma_l(z_j(t_k))\|$$

for every symmetry $\gamma_l \in \tilde{\Gamma}$ and pair of returned solutions $z_i(t)$ and $z_j(t)$, and phase shift $z_j(t)$ to each syzygy or collision in turn. If $d < \delta \approx \sqrt{\epsilon_{mac}}$ we have that $z_i(t)$ and $z_j(t)$ are the same up to discrete symmetry. We discard one and keep the other.

6 “Experimental” Results and Discussion

6.1 Introduction

In Chapter 5 we discussed numerical methods, and in section 5.3 in particular we described an “experimental” set up with which to search for periodic orbits, and in section 3.4 the classification scheme used in the presentation of the “Bestiary” (appendix F). Up to discrete symmetries and time shifts, 363 periodic orbits were discovered, ranging, among those of type-0 (without collisions), from the well known stable figure-8 choreography ($t_0(12, 1)$) to a heretofore unknown unstable choreography with isotropy subgroup also of order 12 ($t_0(12, 2)$), to a less symmetric but still stable “extended 8” choreography ($t_0(6, 1)$), with its sister, an unstable relative choreography ($t_0(6, 2)$), to various relative partial choreographies (such as $t_0(8, 1)$, $t_0(4, 13)$, and $t_0(4, 21)$), to orbits with no symmetry at all ($t_0(1, 36)$, clearly related to $t_0(8, 1)$). Orbits of type-1 (passing through only one collision axis) were found, with symmetry groups of orders 4 (F2.1) and 2 (F2.2), as well as orbits of type-2 (passing through two collision axes, F3). Some isosceles orbits were found (F4), as were many rectilinear orbits (F5).

The purpose of this chapter is to explore key observations coming out of the Bestiary. It is recommended that, if at all possible, this chapter be read in a PDF viewer supporting JavaScript (modern versions of Adobe® Reader do so nicely), with the Bestiary document “A_bestiary.pdf” in the same directory. Links within this chapter lead to the Bestiary, and 3D images in both documents may be double-clicked to bring up a window allowing interaction with (rotation, panning, zooming of) the 3D figure, while 2D images may be enlarged in a separate window.

Before delving into our results, we review some recent work and discoveries regarding periodic orbits in the 3-body problem.

6.2 Known periodic orbits

A remarkable publication, [73], describes a substantial number of previously unknown collisionless (type-0) periodic orbits of the 3-body problem for equal masses and van-

Name in [73]	Example in Bestiary
“Butterfly”	$t0(4, 8)$
“Bumblebee”	$t0(4, 6)$
“Dragonfly”	$t0(4, 41)$
“Goggles”	$t0(4, 42)$
“Moth”	$t0(8, 2)$
“Yarn”	$t0(4, 25)$
“Yin-Yang”	$t2(8, 2)$

Table 6.1: Examples from the Bestiary of orbits similar to those from [73].

ishing angular momentum. These results were obtained by a similar method of search to our own, albeit on a smaller (and admittedly more manageable, 2-dimensional) set of initial conditions in the fixed set of reversing symmetries on the collinear isosceles configuration. Being constructed to have such a symmetry, all their orbits are absolutely periodic. Among their orbits are what they call “butterfly”, “bumblebee”, “dragonfly”, “moth”, “goggles”, “yarn”, and “yin-yang” orbits, some the same as and some similar to many that appear in our search. The classification of these orbits is topological in nature, making use of the topology of the shape sphere as a thrice-punctured sphere.

In table 6.1 we show examples related to each of the named classes of orbits in [73].

A very recent paper [74] presents work on choreographic motions, where their own numerical survey has turned up choreographies including our $t0(12, 2)$ and $t0(6, 1)$.

Very different orbits are presented in [12], where the goal (quite successfully achieved) was to find periodic brake orbits in the isosceles 3-body problem. Several of these orbits appeared in our search, as *isosceles*(8, 2), *isosceles*(8, 3), and *isosceles*(8, 4). Indeed, these three orbits can easily be identified with orbits of type 3 with the number n of binary collisions per half-period respectively for each being 1, 2, and 3.

Even more recently, [82] has performed investigations into the case of vanishing angular momentum, focusing on the cases of the figure-8, and the free-fall problem. In this paper the figure-8 is modified by continuation of one of the masses into a “split figure-eight”, where one mass is decreased and an isosceles reversing symmetry is imposed on the initial condition. A free-fall orbit for equal masses is presented as well—particularly of interest as our search unfortunately turned up no such orbits.

The most remarkable string of papers, arguably adding a great deal of momentum to the search for periodic orbits, is [16], followed closely by [71, 70], where the figure-8 choreography was presented and explored (along with other choreographic solutions by Simó in [70]).

Our work stands separately from much of that presented here because we do not use symmetry to restrict ourselves to a particular type of orbit. We have thus discovered many orbits possessing minimal symmetry through to the maximum possible for each of the common modes of behaviour that we observe. It is our hope that what we present will go a long way towards understanding what kinds of orbits are possible and the construction of particular desired patterns of solutions.

6.2.1 Classification

Having reduced the results of sections 5.3.3 and 5.3.4 to only those orbits that are unique up to symmetries, we wish to classify orbits by their symmetry type. In the regularised setting it may seem artificial to separate collision orbits from collisionless orbits, but we do so on the grounds that elastic collision orbits are artificial, at least from an astronomical perspective¹. Each invariant subspace is also considered distinct. We consider invariant subspaces and collision class to be the top level classification, dividing orbits into type-0, type-1, type-2, isosceles and rectilinear groups. Recall that a type-1 orbit contains collisions only between one particular pair of masses, while a type-2 has one body that collides with each of the others, but those two do not collide with each other, and type-0 orbits are without any collisions at all.

Within each class of orbit we classify further by the structure of the isotropy subgroup. The isotropy subgroup is computed similarly to the determination of unique orbits, except here we compute the points of the orbit every time it crosses a boundary of a copy of the fundamental domain on the shape sphere. This produces a list of points $\Lambda = \{z(t_j)\}$, where $z(t_j)$ is the unique point on the orbit in a small neighbourhood of t_j that corresponds to a symbol of its reduced symbolic dynamics. All discrete symmetries are applied to Λ , and its elements are cycled in each case until the distance between Λ and $\gamma(\Lambda)$ vanishes, thus determining both the symmetries in the isotropy subgroup of $z(t)$ and the shifts such that $\gamma(z(t)) = z(t + \frac{nT}{k})$, for some positive $n < k$, where k is the order of γ .

This classification allows us to write the sequence type of the orbit, which we recall from definition 3.1. It is Ω^k if the orbit is generated by one non-reversing symmetry γ whose order is k , or $(s_1\Omega s_2\Omega')^k$, where s_1 and s_2 are letters of the reduced symbolic dynamics corresponding to points in the fixed sets of reversing symmetries R_1 and R_2 (possibly the same) and k is the order of $R_1 R_2$.

Ordering within the full list of results is as follows:

¹In space no bodies bounce, you see. See [1, 55, 25].

- a) Collision class or invariant subspace;
- b) Order of isotropy subgroup;
- c) Stability;
- d) Sequence type; and then
- e) Physical period.

6.3 Common modes of behaviour

6.3.1 An observation and subsequent classification

Recall that the invariant subspaces correspond to planes in the space of regularised variables, projecting to great circles on the regularised shape sphere. Collinear subspaces correspond to $\alpha_j = \pi_j = 0$, of which there are three (one case for each different body in the middle). Isosceles subspaces correspond to $\alpha_k = \pm\alpha_l, \pi_k = \pm\alpha_l$, for each permutation of k, l , and each permutation of signs, leading to six such spaces. This number reduces to three when mapping back to the classical shape sphere, as the regularised coordinates are squared during this process.

Remarkably, most orbits can be classified easily by how “spread out” they are when projected onto special planes in regularised shape space, or by their localisation near these planes. In the regularised shape space there are three collinear subspaces, which are planar, and orthogonal to each through the origin is one of the coordinate axes, where the other two collinear subspaces and two of the isosceles subspaces intersect. There are six isosceles subspaces. Through the origin are lines corresponding to isosceles collinear configurations, orthogonal to each of the isosceles subspaces. That is, these isosceles collinear lines are at the intersections of *different* isosceles subspaces with a collinear subspace. Further, there are four planes through the origin which are orthogonal to the lines of equilateral configurations (which are at the centre of each octant).

The equations of the planes of collinearity are $\alpha_j = 0$ for each j . The equations of the six isosceles subspaces are given by the relations $\alpha_k^2 = \alpha_l^2$. The equations for the four planes orthogonal to the equilateral configurations are $\alpha_1 \pm \alpha_2 \pm \alpha_3 = 0$, where the \pm signs may be chosen independent of one another.

The regularised variables straighten out most orbits such that they remain close to such planes, even if they appear much more complicated in the un-regularised shape

space. This localisation we refer to as the *mode* of an orbit. The mode is names after the axis of symmetry that is orthogonal to the plane of localisation. That is, if a solution lies near a plane of collinearity it is classified as being in *B-mode*, as the orthogonal axis is a binary collision axis. Similarly, if a solution lies near the plane of an isosceles subspace we classify it as being in *M-mode*, as orthogonal to the isosceles subspace is an axis of isosceles collinear configurations. Finally, solutions near the plane through the origin orthogonal to a line of equilateral configurations is classified as *E-mode*, though the corresponding plane is not an invariant subspace.

Planes through the origin of regularised shape space reduce to great circles on the regularised shape sphere. The corresponding orthogonal lines reduce to a pair of antipodal points. Figure 6.1 illustrates the projections of the characterising planes and axes onto the regularised shape sphere: figure 6.1a illustrates one of the *M*-modes; figure 6.1b illustrates one of the *B*-modes; and figure 6.1c illustrates one of the *E*-modes. Orbits in *M*-mode, *B*-mode, and *E*-mode can be characterised respectively as isosceles-like (one body in the middle avoids close interactions with the other two), collinear-like (one body in the middle exchanges between the other two), and choreography-like (each body tends to chase one other and be chased by the the other).

The placement of such solutions in the regularised shape space also relates closely to the symmetries they have. Orbits in *M*-mode can have no more than rectangular symmetry (Figure 6.2a), as

Table 6.2 lists all non-isosceles and non-rectilinear orbits in the Bestiary by mode as calculated by finding the plane P_X about which the orbit is localised, corresponding also to the plane within which its projection is most spread out.

The localisation is measured by the variance of the projection of $\alpha(t)$ onto L_X , the axis corresponding to P_X . We compute $l_X(t) = \alpha(t) \cdot \hat{n}_X$, where \hat{n}_X is the unit normal to P_X and compute the variance of $l_x(t)$ by

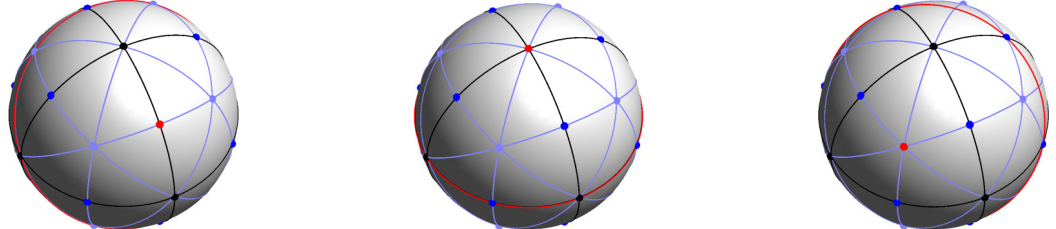
$$\sigma_X^2 = \frac{1}{T} \int_0^T (l_X(t) - \mu_X)^2 dt,$$

where $\mu_X = \frac{1}{T} \int_0^T l_X dt$ is the mean of the projection of $\alpha(t)$ onto L_X . The axis L_X for which σ_X^2 is minimal determines the mode.

The projection of $\alpha(t)$ onto P_X is computed by $\alpha_X(t) = \alpha(t) - (\alpha(t) \cdot \hat{n}_X) \hat{n}_X$, and the distance from the origin of P_X is $d_X(t) = |\alpha_X(t)|$. The spread in the projection onto P_X is the mean

$$\bar{d}_X = \frac{1}{T} \int_0^T d_X(t) dt.$$

The plane P_X on which \bar{d}_X is maximal corresponds in practise (for our set of orbits)

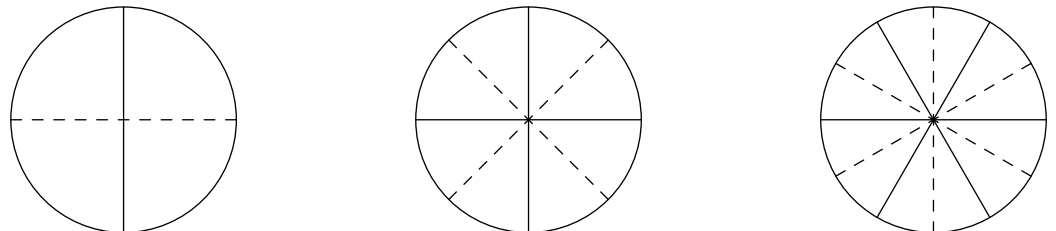


(a) Isosceles, or M -mode. Great circle highlighted in red is an isosceles invariant subspace. Dots highlighted in red correspond to antipodal isosceles collinear configuration.

(b) Collinear, or B -mode. Great circle highlighted in red is a collinear invariant subspace. Dots highlighted in red correspond to antipodal collinear collision configurations.

(c) Choreographic, or E -mode. Great circle highlighted in red corresponds to no invariant subspaces and avoids all collisions and equilateral configurations. Dots highlighted in red correspond to antipodal equilateral configurations.

Figure 6.1: The three observed modes by which most periodic orbits can be characterised. The points of symmetry and corresponding great circles on the shape sphere are highlighted in red in each case.



(a) Rectangular symmetry of M -mode.

(b) Square symmetry of B -mode.

(c) Hexagonal symmetry of E -mode.

Figure 6.2: Maximal symmetry of each mode. Dashed lines represent lines of reflection about isosceles configurations; solid lines represent lines of reflection about collinear configurations.

to the axis L_X for which σ_X^2 is minimal.

There are three B -axes to be checked, for which $\hat{\mathbf{n}}_B = (1, 0, 0)$, $(0, 1, 0)$, or $(0, 0, 1)$. There are six M -axes, for which $\hat{\mathbf{n}}_B = \frac{1}{\sqrt{2}}(0, 1, 1)$, $\frac{1}{\sqrt{2}}(0, 1, -1)$, $\frac{1}{\sqrt{2}}(1, 0, 1)$, $\frac{1}{\sqrt{2}}(1, 0, -1)$, $\frac{1}{\sqrt{2}}(1, 1, 0)$, or $\frac{1}{\sqrt{2}}(1, -1, 0)$. Finally, there are four E -axes, for which $\hat{\mathbf{n}}_B = \frac{1}{\sqrt{3}}(1, 1, 1)$, $\frac{1}{\sqrt{3}}(1, 1, -1)$, $\frac{1}{\sqrt{3}}(1, -1, 1)$, or $\frac{1}{\sqrt{3}}(1, -1, -1)$.

Type-0					M -mode	E -mode		
B -mode	$t0(8, 1)$	$t0(4, 47)$	$t0(2, 30)$	$t0(1, 4)$	$t0(2, 49)$	$t0(4, 1)$	$t0(2, 25)$	$t0(12, 1)$
$t0(8, 2)$	$t0(4, 48)$	$t0(2, 31)$	$t0(1, 5)$	$t0(2, 51)$	$t0(4, 2)$	$t0(2, 26)$	$t0(12, 2)$	
$t0(8, 3)$	$t0(4, 49)$	$t0(2, 32)$	$t0(1, 6)$	$t0(2, 52)$	$t0(4, 3)$	$t0(2, 27)$	$t0(6, 1)$	
$t0(8, 4)$	$t0(4, 50)$	$t0(2, 33)$	$t0(1, 7)$	$t0(2, 54)$	$t0(4, 5)$	$t0(2, 47)$	$t0(6, 2)$	
$t0(8, 5)$	$t0(4, 51)$	$t0(2, 34)$	$t0(1, 8)$	$t0(2, 55)$	$t0(4, 6)$	$t0(2, 50)$	$t0(4, 23)$	
$t0(8, 6)$	$t0(4, 52)$	$t0(2, 35)$	$t0(1, 9)$	$t0(2, 56)$	$t0(4, 7)$	$t0(2, 53)$	$t0(4, 35)$	
$t0(8, 7)$	$t0(4, 53)$	$t0(2, 36)$	$t0(1, 10)$	$t0(2, 57)$	$t0(4, 15)$	$t0(2, 58)$	$t0(2, 5)$	
$t0(8, 8)$	$t0(4, 54)$	$t0(2, 37)$	$t0(1, 11)$	$t0(2, 59)$	$t0(4, 16)$	$t0(2, 61)$	$t0(2, 15)$	
$t0(4, 4)$	$t0(4, 55)$	$t0(2, 38)$	$t0(1, 12)$	$t0(2, 60)$	$t0(4, 17)$	$t0(2, 63)$	$t0(2, 16)$	
$t0(4, 8)$	$t0(4, 56)$	$t0(2, 39)$	$t0(1, 13)$	$t0(2, 62)$	$t0(4, 18)$	$t0(2, 71)$	$t0(2, 17)$	
$t0(4, 9)$	$t0(4, 57)$	$t0(2, 40)$	$t0(1, 14)$	$t0(2, 64)$	$t0(4, 19)$	$t0(2, 73)$	$t0(2, 18)$	
$t0(4, 10)$	$t0(4, 58)$	$t0(2, 41)$	$t0(1, 16)$	$t0(2, 67)$	$t0(4, 20)$	$t0(2, 82)$	$t0(2, 24)$	
$t0(4, 11)$	$t0(4, 59)$	$t0(2, 42)$	$t0(1, 17)$	$t0(2, 68)$	$t0(4, 21)$	$t0(2, 87)$	$t0(2, 65)$	
$t0(4, 12)$	$t0(4, 60)$	$t0(2, 43)$	$t0(1, 18)$	$t0(2, 69)$	$t0(4, 22)$	$t0(2, 91)$	$t0(2, 66)$	
$t0(4, 13)$	$t0(4, 61)$	$t0(2, 101)$	$t0(1, 19)$	$t0(2, 70)$	$t0(4, 27)$	$t0(2, 92)$	$t0(2, 72)$	
$t0(4, 14)$	$t0(2, 1)$	$t0(2, 102)$	$t0(1, 20)$	$t0(2, 74)$	$t0(4, 30)$	$t0(2, 93)$	$t0(2, 77)$	
$t0(4, 24)$	$t0(2, 2)$	$t0(2, 103)$	$t0(1, 27)$	$t0(2, 75)$	$t0(4, 33)$	$t0(2, 94)$	$t0(2, 78)$	
$t0(4, 25)$	$t0(2, 4)$	$t0(2, 104)$	$t0(1, 28)$	$t0(2, 76)$	$t0(4, 34)$	$t0(2, 98)$	$t0(2, 83)$	
$t0(4, 26)$	$t0(2, 6)$	$t0(2, 105)$	$t0(1, 30)$	$t0(2, 79)$	$t0(4, 41)$	$t0(2, 99)$	$t0(2, 84)$	
$t0(4, 28)$	$t0(2, 7)$	$t0(2, 106)$	$t0(1, 31)$	$t0(2, 80)$	$t0(4, 43)$	$t0(1, 15)$	$t0(2, 85)$	
$t0(4, 29)$	$t0(2, 8)$	$t0(2, 107)$	$t0(1, 32)$	$t0(2, 81)$	$t0(4, 44)$	$t0(1, 21)$	$t0(2, 88)$	
$t0(4, 31)$	$t0(2, 9)$	$t0(2, 108)$	$t0(1, 33)$	$t0(2, 86)$	$t0(4, 45)$	$t0(1, 22)$	$t0(1, 26)$	
$t0(4, 32)$	$t0(2, 10)$	$t0(2, 109)$	$t0(1, 34)$	$t0(2, 89)$	$t0(4, 46)$	$t0(1, 23)$		
$t0(4, 36)$	$t0(2, 11)$	$t0(2, 110)$	$t0(1, 35)$	$t0(2, 90)$	$t0(2, 3)$	$t0(1, 24)$		
$t0(4, 37)$	$t0(2, 12)$	$t0(2, 111)$	$t0(1, 36)$	$t0(2, 95)$	$t0(2, 13)$	$t0(1, 25)$		
$t0(4, 38)$	$t0(2, 19)$	$t0(2, 112)$	$t0(2, 44)$	$t0(2, 96)$	$t0(2, 14)$	$t0(1, 29)$		
$t0(4, 39)$	$t0(2, 21)$	$t0(1, 1)$	$t0(2, 45)$	$t0(2, 97)$	$t0(2, 20)$			
$t0(4, 40)$	$t0(2, 28)$	$t0(1, 2)$	$t0(2, 46)$	$t0(2, 100)$	$t0(2, 22)$			
$t0(4, 42)$	$t0(2, 29)$	$t0(1, 3)$	$t0(2, 48)$		$t0(2, 23)$			

Type-1					M -mode	E -mode
B -mode	$t1(4, 3)$	$t1(4, 30)$	$t1(2, 12)$	$t1(2, 28)$	$t1(4, 1)$	$t1(4, 29)$
$t1(4, 4)$	$t1(4, 31)$	$t1(2, 13)$	$t1(2, 29)$		$t1(4, 2)$	$t1(4, 33)$
$t1(4, 6)$	$t1(4, 32)$	$t1(2, 14)$	$t1(2, 31)$		$t1(4, 5)$	$t1(4, 35)$
$t1(4, 8)$	$t1(4, 34)$	$t1(2, 15)$	$t1(2, 32)$		$t1(4, 7)$	$t1(4, 36)$
$t1(4, 11)$	$t1(2, 2)$	$t1(2, 17)$	$t1(2, 33)$		$t1(4, 9)$	$t1(4, 37)$
$t1(4, 12)$	$t1(2, 3)$	$t1(2, 18)$			$t1(4, 10)$	$t1(4, 38)$
$t1(4, 13)$	$t1(2, 4)$	$t1(2, 19)$			$t1(4, 14)$	$t1(4, 39)$
$t1(4, 21)$	$t1(2, 5)$	$t1(2, 20)$			$t1(4, 15)$	$t1(4, 40)$
$t1(4, 22)$	$t1(2, 6)$	$t1(2, 21)$			$t1(4, 16)$	$t1(4, 41)$
$t1(4, 23)$	$t1(2, 7)$	$t1(2, 23)$			$t1(4, 17)$	$t1(2, 1)$
$t1(4, 24)$	$t1(2, 8)$	$t1(2, 24)$			$t1(4, 18)$	$t1(2, 16)$
$t1(4, 25)$	$t1(2, 9)$	$t1(2, 25)$			$t1(4, 19)$	$t1(2, 22)$
$t1(4, 26)$	$t1(2, 10)$	$t1(2, 26)$			$t1(4, 20)$	$t1(2, 30)$
$t1(4, 27)$	$t1(2, 11)$	$t1(2, 27)$			$t1(4, 28)$	$t1(2, 34)$

Type-2					M -mode	E -mode	
B -mode	$t2(8, 1)$	$t2(8, 2)$	$t2(8, 3)$	$t2(8, 4)$	$t2(8, 5)$	$t2(8, 6)$	$t2(8, 7)$
$t2(8, 1)$							
$t2(8, 2)$							
$t2(8, 3)$							
$t2(8, 4)$							
$t2(8, 5)$							
$t2(8, 6)$							
$t2(8, 7)$							

Table 6.2: Non-collinear, non-isosceles orbits by mode.

6.3.2 Observations on each mode

6.3.2.1 M -mode

Orbits in the M -mode are typically similar to isosceles orbits. In physical space (in a fixed or rotating frame) this may be characterised by an outer pair of bodies that move in opposing “horseshoe” shapes, with the third body sweeping transverse to the “horseshoes” to be far away whenever the outer pair have a close encounter.

The isosceles orbits themselves (F4) display two types of behaviour: winding and non-winding, with the non-winding orbits therefore touching the free fall boundary at brake points out in the arms of the Hill region. Figure 6.3 shows the two types of behaviour for isosceles orbits: figure 6.3a shows *isosceles*(8, 1), closely matched by $t0(4, 1)$ (and all other M -mode orbits not in an isosceles invariant subspace), shown projected onto the plane $\alpha_1 = -\alpha_2$ in figure 6.3b. The second type, mimicking the free-fall isosceles orbit *isosceles*(8, 2) or members of its family, have not been observed with close analogues outside the invariant subspace. This absence may simply be a shortcoming of our search.

Winding isosceles behaviour is all variation of orbit *isosceles*(8, 1) (Figure 6.3a), which is stable in the planar problem, but their realisations in physical space can be quite varied. A particularly striking group of results are the stable orbits $t0(4, 1)$, $t0(4, 2)$, and unstable orbits $t0(4, 15)$ to $t0(4, 22)$, which are all relative partial choreographies, when viewed in a rotating frame with angular velocity given by $\frac{\Delta G}{T}$.

The similarity of all non-isosceles M -mode orbits to *isosceles*(8, 1) means we could generate reduced symbol sequences for orbits by making specific perturbations. The symbol sequence for *isosceles*(8, 1) is

$$(BEME)^2 = BEMEBEME.$$

Each of the symbols can be replaced by a short word of edge symbols, depending on the symmetries we wish to preserve. Suppose we pentuple the period but wish to preserve the repetition number 2 and reversing symmetries on B and M symbols. Then we may write the pentupled sequence

$$(B^*\Omega M^*\Omega')^2, \quad \Omega = EMEBEMEBE$$

where the superscript * indicates a symbol we wish to preserve. Then all the unmarked “corner” symbols $\{M, E, B\}$ in Ω must be replaced by short words of “edge” symbols $\{A, O, C\}$. The exact word formed depends on the perturbation near the old symbol: we may have $E \rightarrow AO$ or OA ; $M \rightarrow C$, OC or CO ; $B \rightarrow CAC$.

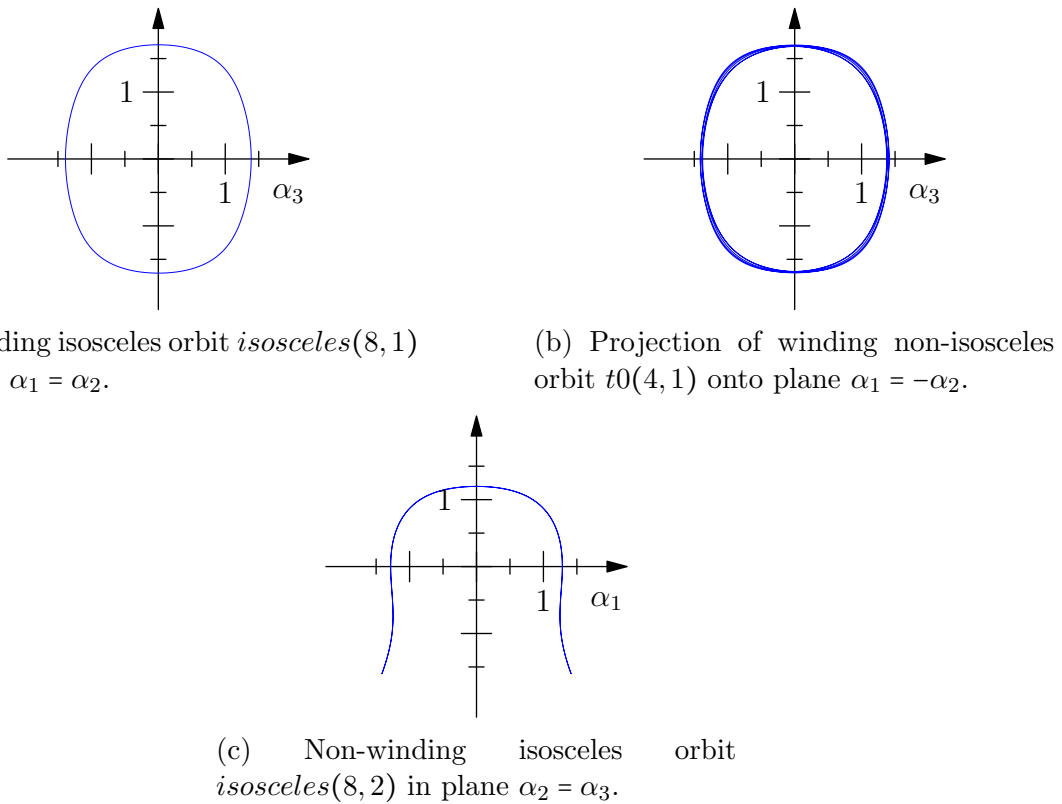


Figure 6.3: Two distinct types of purely isosceles motion (a), (c), and the projection onto the appropriate isosceles subspace of a non-isosceles M -mode orbit (b).

An example of such a period multiplication and perturbation is $t1(4, 34)$, whose symbol sequence is

$$(B\Omega M\Omega')^2, \quad \Omega = OACAOCACOAOCAOCACOACOA.$$

Compare Ω here to that from which we wished to perturb above:

$$\begin{array}{cccccccccc} OA & C & AO & CAC & OA & OC & AO & CAC & OA \\ E & M & E & B & E & M & E & B & E \end{array}.$$

The reverse process allows us to recover the more symmetric “base” symbol sequence.

Looking more generally at the isosceles invariant subspace, because the plane corresponding to this mode intersects only one collision axis, we expect that orbits in this mode and not in the corresponding invariant subspace will also only approach the one type of collision. We found no M -mode orbits of type-2 in the Bestiary, and this observation explains why we should not expect to.

6.3.2.2 B -mode

Orbits in the B -mode typically have character somewhat similar to rectilinear orbits. Two types of such motion occur: first, monotonic winding around the B -axis; second, non-winding behaviour that reaches into the “arms” of the Hill region. This is characterised in physical space (in a rotating or non-rotating frame) by two bodies that never have a close encounter, while the third exchanges between them, with possible excursions forming a temporary binary pair before another exchange.

Winding orbits are in some sense related to the Schubart orbit [65], which appears in the Bestiary as *rectilinear*(16, 1). The reduced symbol sequence of this orbit is simply

$$(BM)^4$$

(in one period of the regularised coordinates it is twice periodic on the classical shape sphere and in physical space), whereas its collision sequence for one physical period is

$$ac.$$

Body 2 (green) exchanges between bodies 1 and 3 with collisions. In the regularised shape space it forms a simple closed loop in the plane $\alpha_2 = 0$, winding around the α_2 -axis in one direction.

For comparison, consider $t0(8, 2)$. This orbit, similarly, winds around the α_2 -axis and lies closest to the plane $\alpha_2 = 0$. Similar to the Schubart orbit, it is twice-periodic in physical space during one period in regularised space. Its reduced symbol sequence is

$$(MACAOACACOACAOCAOCACAOACA)^4$$

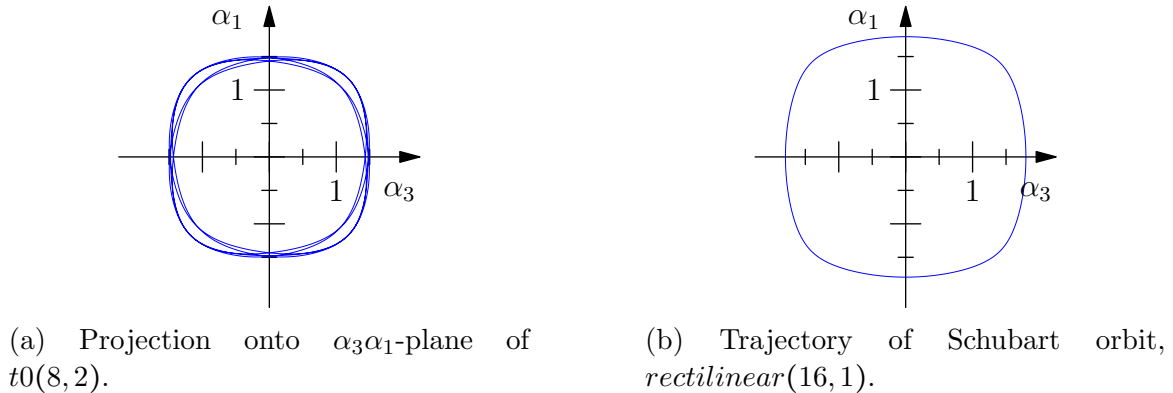


Figure 6.4: Comparison of two winding orbits in the B -mode.

(regularised), with syzygy sequence $(1231232132132123)^2$ (physical). Projecting this onto the collinear plane $\alpha_2 = 0$ we eliminate every 2 in its syzygy sequence and replace 1 by c and 3 by a to obtain

$$(cacacacaca)^2,$$

the same as the Schubart, with extended period. The analogous procedure for the reduced symbol sequence requires following the regularised trajectory to remove every C corresponding to passing through the plane $\alpha_2 = 0$, removing every A , and projecting every O to M and every remaining C to B .

Note that if $\Sigma_{t0(8,2)}$ is the isotropy subgroup of $t0(8, 2)$, the isotropy subgroup of the Schubart orbit can be obtained by the direct product $\{I, \rho s_2\} \times \Sigma_{t0(8,2)}$, as this particular instance of the Schubart orbit lives in the invariant collinear subspace $\alpha_2 = \pi_2 = 0$. A direct comparison of the orbits is given in figure 6.4, with figure 6.4a illustrating the projection of $t0(8, 2)$ onto the $\alpha_3\alpha_1$ -plane, and figure 6.4b showing $rectilinear(16, 1)$ in the plane in which it lives. Note that while the former is symmetric when projected onto the plane, it is asymmetric with respect to the reflection $\alpha_2 \rightarrow -\alpha_2$.

Non-winding types of orbits, extending into the arms of the Hill region, may have a non-zero winding number around their respective B -axes during one half period, which is cancelled during the second half of the orbit. These orbits characteristically spend time winding around at least one of the other collision axes (if not both, forming an ‘L’ shape in the plane characterised by the noted B -axis in the case of long binary excursions).

Two orbits illustrating this behaviour are the type-0 orbit $t0(4, 47)$ and the rectilinear orbit $rectilinear(8, 1)$, which have relatively similar behaviour and symmetry group structure (up to quotient by $\{I, \rho s_2\}$, corresponding to the collinear invariant subspace of the latter). Both orbits possess the reversing symmetry $\tau \rho s_2$, which gives time



(a) Projection onto $\alpha_3\alpha_1$ -plane of $t0(4, 47)$.

(b) Trajectory of *rectilinear*(8, 1).

Figure 6.5: Comparison of two ‘L’-shaped orbits in the *B*-mode.



(a) Projection onto $\alpha_3\alpha_1$ -plane of $t0(4, 42)$.

(b) Trajectory of *rectilinear*(8, 5).

Figure 6.6: Comparison of two ‘L’-shaped orbits winding fully around the *B* axis in any half period (and unwinding in the other half).

reflection on the collinear plane $\alpha_2 = 0$. For the non-collinear orbit this is a collinear reversing configuration, but for the collinear orbit this is a brake point (also given the symmetry τ).

Figure 6.5 illustrates the projections of both orbits onto the $\alpha_3\alpha_1$ -plane. Note that they are almost identical, but $t0(4, 47)$ (Figure 6.5a) is slightly smaller, as it does not reach up to touch the free fall boundary at its reversing points in this projection, whereas *rectilinear*(8, 1) (Figure 6.5b) does.

A pair of related orbits illustrating both non-zero winding (at least over each half-period) and ‘L’-shape extension into the arms are $t0(4, 42)$ (type-0) and *rectilinear*(8, 5), shown projected onto the $\alpha_2\alpha_3$ - and $\alpha_3\alpha_1$ -planes respectively.

Because of the mode being characteristically close to a plane of collinearity in the

regularised space (thus approaching closely two collision axes), and the exchange type motion of one body between the other two, both type-2 and type-1 orbits can exist in this mode.

6.3.2.3 *E*-mode

Orbits in the *E*-mode lie near a plane orthogonal to the axis through antipodal *E* points on the regularised shape space. These planes do not correspond to any invariant subspace. An important family of orbits live near such planes, however: the figure-8 ($t_0(12, 1)$) and other choreographies ($t_0(12, 2)$, $t_0(6, 1)$, and the relative choreography $t_0(6, 2)$), and others that are not choreographic but have lower symmetry (see the corresponding column of table 6.2). Interestingly, every such plane avoids all collision axes and equilateral configurations.

6.3.3 Connection to isotropy subgroups

As discussed in section 6.3.1, the least symmetric mode is the *M*-mode, for which P_M is one of the isosceles subspaces. All combinations of reversing symmetries observed in the search are listed with examples in table 6.3, with schematics of the combinations in figures 6.7 and 6.8. In these figures the plane P_M (respectively P_B for figures 6.9 and 6.10 and P_E for figure 6.11) is represented by a disk (coloured yellow in figures 6.7 and 6.9 for the case of orbits in the respective invariant subspace), while other planes of symmetry for the mode are shaded in grey, and the axes of symmetry drawn as black lines. If a particular sequence class has a reversing symmetry on a given plane or axis, it is highlighted in red. Recall that the sequence class is defined by the generators of the isotropy subgroup of an orbit: if the generators are $R_{1,2}$, the sequence class is of the form $(X_1\Omega X_2\Omega')^n$, where $X_{1,2}$ are the symbols corresponding to the points in the fundamental domain on which the symmetry occurs and n is the order of the cyclic element (R_2R_1) .

Reversing symmetries on planes correspond to reflections about those planes with time reversal. Similarly, reversing symmetries on lines act like rotations by π about those lines with time reversal.

Here the most symmetric orbits in the *M*-mode live in P_M itself, with symmetry of order 8, and have reversing symmetries on both the isosceles and collinear subspaces intersecting orthogonally to P_M (Figure 6.7a), or on one of these subspaces and the free fall boundary (Figure 6.7b). The isotropy subgroups corresponding to these symmetries are isomorphic to $\mathbb{Z}_2 \times D_2$. No examples turned up of isosceles orbits with sequence class $(B\Omega F\Omega')^2$.

Group (Order)	C	O	A	M	B	F	Fix	Example	Visualisation
$\mathbb{Z}_2 \times D_2 (8)$				✓	✓		✓	$\text{isosceles}(8, 1)$	Figure 6.7a
$\mathbb{Z}_2 \times D_2 (8)$					✓	✓	✓	$\text{isosceles}(8, 2)$	Figure 6.7b
$D_2 (4)$	✓		✓					$t0(4, 1)$	Figure 6.8a
$D_2 (4)$			✓	✓				$t0(4, 3)$	Figure 6.8b
$D_2 (4)$	✓				✓			$t0(4, 6)$	Figure 6.8c
$D_2 (4)$			✓			✓		$t1(4, 1)$	Figure 6.8d
$D_2 (4)$	✓					✓		$t1(4, 5)$	Figure 6.8e
$D_2 (4)$					✓	✓		$t1(4, 34)$	Figure 6.8f
$\mathbb{Z}_2 \times \mathbb{Z}_2 (4)$					✓✓		✓	$\text{isosceles}(4, 1)$	Figure 6.7c
$\mathbb{Z}_2 (2)$	✓✓							$t0(2, 3)$	Figure 6.8g
$\mathbb{Z}_2 (2)$			✓✓					$t0(2, 20)$	Figure 6.8h
$\mathbb{Z}_2 (2)$	✓	✓			✓✓			$t0(2, 26)$	Figure 6.8h
$\mathbb{Z}_2 (2)$						✓✓		$t0(2, 63)$	Figure 6.8i
$\mathbb{Z}_2 (2)$								$t1(2, 1)$	Figure 6.8j

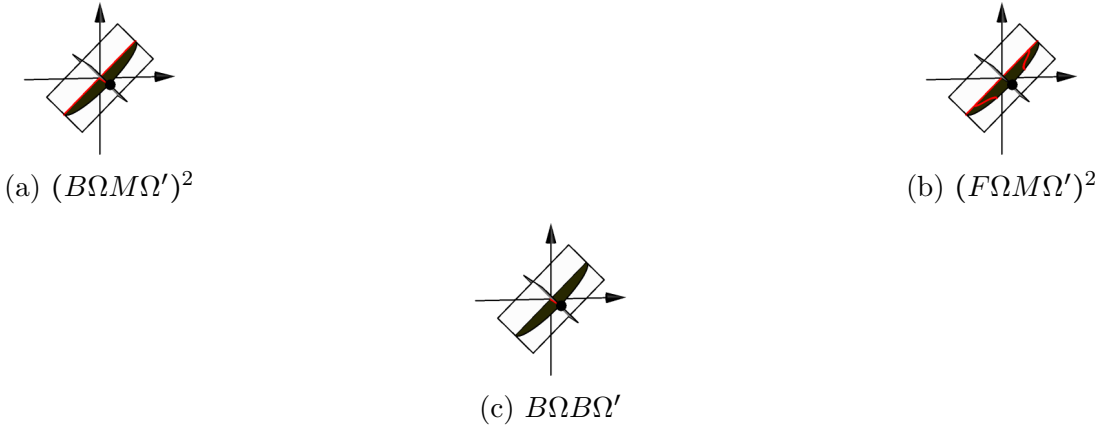
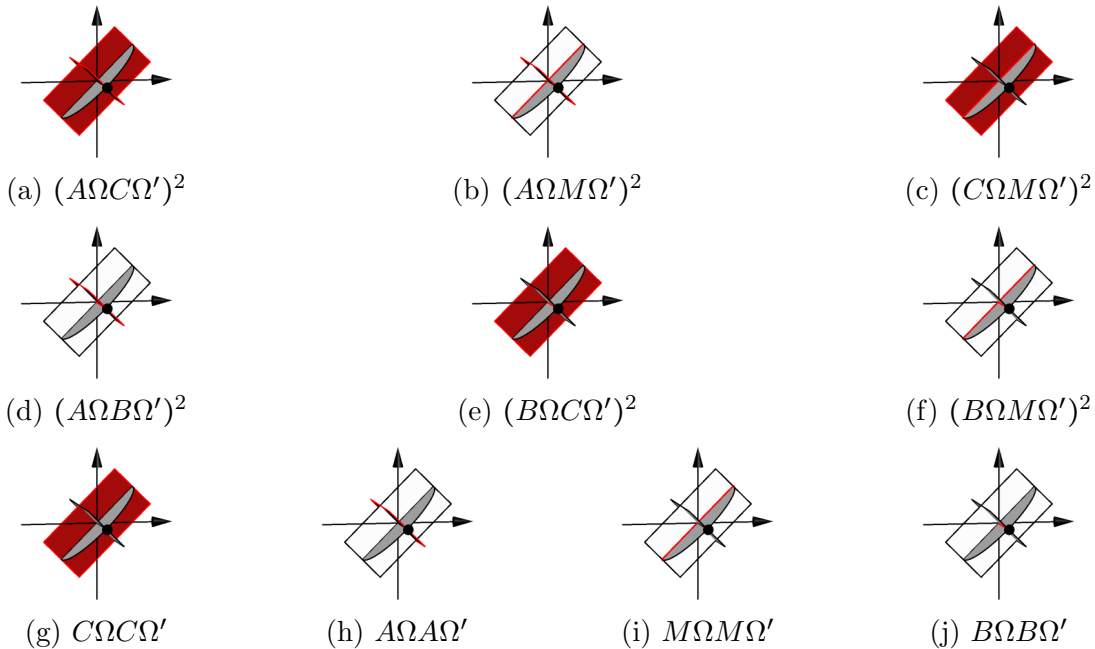
Table 6.3: Reversing symmetries in the M -mode appearing in the Bestiary.

Figure 6.7: Isosceles reversing symmetries present in the Bestiary.

By moving off the isosceles subspace, the order of the isotropy subgroup is reduced to 4, isomorphic to D_2 . Reversing symmetries can occur on any non-identical pairs from $\{A, B, C, M\}$, with six possibilities, all realised in the Bestiary, as illustrated in table 6.3 and figures 6.8a–6.8f.

Breaking one symmetry means that both reversing symmetries are on the same line or plane of symmetry, generating groups isomorphic to \mathbb{Z}_2 , and therefore there are four possibilities, realised in the Bestiary and illustrated in table 6.3 and figures 6.8g, 6.8j, 6.11e and 6.11f. Only one isosceles orbit with symmetry order 4 (thus with only one reversor), isomorphic to $\mathbb{Z}_2 \times \mathbb{Z}_2$, appeared in the search, but many more have been shown to exist in [12], particularly orbits of types 5 and 6 of [12].

The next most symmetric mode is the B -mode, where P_B coincides with one of the planes of collinearity $\alpha_j = 0$. Examples of each collection of reversing symmetries found in the Bestiary are given in table 6.4, and figures 6.9 and 6.10 show schematics for each of the combinations of reversing symmetries that occur.

Figure 6.8: M -mode reversing symmetries present in the Bestiary.

Possible reversing symmetries for orbits living in the collinear subspace may be chosen from $\{B, F, M\}$, determining the number of repetitions of the fundamental sequence of the sequence class. As the B and M reversing symmetries in P_B are aligned with an angular separation of $\frac{\pi}{4}$, this choice generates D_4 , so a corresponding rectilinear orbit's isotropy subgroup will be isomorphic to $\mathbb{Z}_2 \times D_4$, order 16. This symmetry is illustrated in figure 6.9a, with one representative, the Schubart orbit *rectilinear*(16,1). If its generators are $R_1 = \tau s_k$ (brake collision) and $R_2 = \tau \sigma_l s_l$ (isosceles collinear reversor), the composition $(R_1 R_2)^2 = (\tau s_k \tau \sigma_l s_l)^2 = s_k \sigma_l s_l s_k \sigma_l s_l = s_k s_j \sigma_l^2 s_j s_l = s_k s_j^2 s_l = s_k s_l = s_j$, a symmetry induced by regularisation which forces the physical trajectory to complete twice in one period of the regularised trajectory.

Interestingly, the only sequence class found in the collinear subspace with a repetition number of 2 is $(FΩMΩ')^2$. Its symmetry is illustrated in figure 6.9b. We do not presently know whether orbits expressing the other two possible combinations, $(BΩFΩ')^2$ and $(BΩMΩ')^2$, of symmetry with this repetition number are impossible for some reason, or if they were simply missed in our search. All such orbits would have isotropy subgroups isomorphic to $\mathbb{Z}_2 \times D_2$.

Finally, all three possible collinear sequence types with only one repetition are represented in the Bestiary, and their reversing symmetries are illustrated in figures 6.9c–6.9e.

Group (Order)	C	O	A	M	B	F	Fix	Example	Visualisation
$\mathbb{Z}_2 \times D_4$ (16)				✓	✓		✓	$\text{rectilinear}(16, 1)$	Figure 6.9a
D_4 (8)	✓				✓			$t0(8, 2)$	Figure 6.10a
D_4 (8)	✓		✓					$t0(8, 1)$	Figure 6.10b
D_4 (8)	✓	✓						$t0(8, 7)$	Figure 6.10b
D_4 (8)			✓		✓			$t2(8, 1)$	Figure 6.10c
D_4 (8)			✓		✓			$t2(8, 5)$	Figure 6.10c
D_4 (8)	✓			✓	✓			$t2(8, 2)$	Figure 6.10d
$\mathbb{Z}_2 \times D_2$ (8)					✓	✓	✓	$\text{rectilinear}(8, 1)$	Figure 6.9b
D_2 (4)			✓	✓				$t0(4, 4)$	Figure 6.10e
D_2 (4)		✓		✓				$t0(4, 8)$	Figure 6.10e
D_2 (4)	✓		✓					$t0(4, 14)$	Figure 6.10f
D_2 (4)	✓	✓						$t0(4, 47)$	Figure 6.10f
D_2 (4)	✓			✓				$t0(4, 42)$	Figure 6.10g
D_2 (4)	✓✓							$t0(4, 39)$	Figure 6.10h
D_2 (4)	✓	✓✓			✓			$t0(4, 61)$	Figure 6.10i
D_2 (4)	✓				✓			$t1(4, 3)$	Figure 6.10j
D_2 (4)	✓				✓			$t1(4, 11)$	Figure 6.10k
$\mathbb{Z}_2 \times \mathbb{Z}_2$ (4)					✓✓		✓	$\text{rectilinear}(4, 1)$	Figure 6.9c
$\mathbb{Z}_2 \times \mathbb{Z}_2$ (4)						✓✓	✓	$\text{rectilinear}(4, 13)$	Figure 6.9d
$\mathbb{Z}_2 \times \mathbb{Z}_2$ (4)				✓✓			✓	$\text{rectilinear}(4, 40)$	Figure 6.9e
\mathbb{Z}_2 (2)			✓✓					$t0(2, 1)$	Figure 6.10l
\mathbb{Z}_2 (2)		✓✓						$t0(2, 6)$	Figure 6.10l
\mathbb{Z}_2 (2)		✓						$t0(2, 28)$	Figure 6.10l
\mathbb{Z}_2 (2)	✓✓							$t0(2, 2)$	Figure 6.10m
\mathbb{Z}_2 (2)	✓✓							$t0(2, 37)$	Figure 6.10n
\mathbb{Z}_2 (2)			✓✓					$t0(2, 64)$	Figure 6.10o
\mathbb{Z}_2 (2)				✓✓		✓✓		$t1(2, 2)$	Figure 6.10p

Table 6.4: Symmetry types in the B -mode appearing in the Bestiary.

Off the collinear subspace, order 8 isotropy subgroups isomorphic to D_4 were found with reversing symmetries taken one each from $\{A, M\}$ and $\{B, C\}$. Each of these is represented in the Bestiary, and their reversing symmetries are represented in figures 6.10b–6.10d. These orbits, similar to the Schubart orbit, must also possess a period-doubling symmetry s_j (the difference is that the reversing symmetries R_1, R_2 may lie on collinear or isosceles configurations that do not also intersect P_B).

In the next lower order of symmetry, isotropy subgroups are isomorphic to D_2 , order 4. The reversing symmetries become richer, with eight possibilities (six distinct), depicted in figures 6.10e–6.10j. Of note are those with one reversing symmetry on a C symbol, but that C corresponds to P_B itself! In all such cases (depicted in figures 6.10e and 6.10g), the other reversor occurs on an isosceles (or isosceles collinear) configuration, and the orbit as a result extends down two “arms” of the Hill region in a symmetric ‘L’ shape. No orbit has appeared where both reversing symmetries are on different planes of collinearity such that the orbit returns up the same arm or extends down the opposite one. The two cases where symmetry points lie on orthogonal subspaces, figures 6.10h and 6.10i, also must possess a period-doubling symmetry s_j . If $R_1 = \tau\rho s_k$ and $R_2 = \tau\rho s_l$, the composition $R_1R_2 = \tau\rho s_k\tau\rho s_l = s_j$. Similarly, if $R_1 = \tau\rho\sigma_j$ and $R_2 = \tau\rho\sigma_js_j$, we have $R_1R_2 = \tau\rho\sigma_j\tau\rho\sigma_js_j = s_j$.

The final case has symmetry of order 2, isotropy subgroups isomorphic to \mathbb{Z}_2 , with reversing symmetries chosen on the same line or plane of symmetry. There are six possibilities, four distinct, illustrated in figures 6.10l, 6.10m, 6.10o and 6.10p.

The final mode observed is the E -mode, characterised by the L_E , the intersection

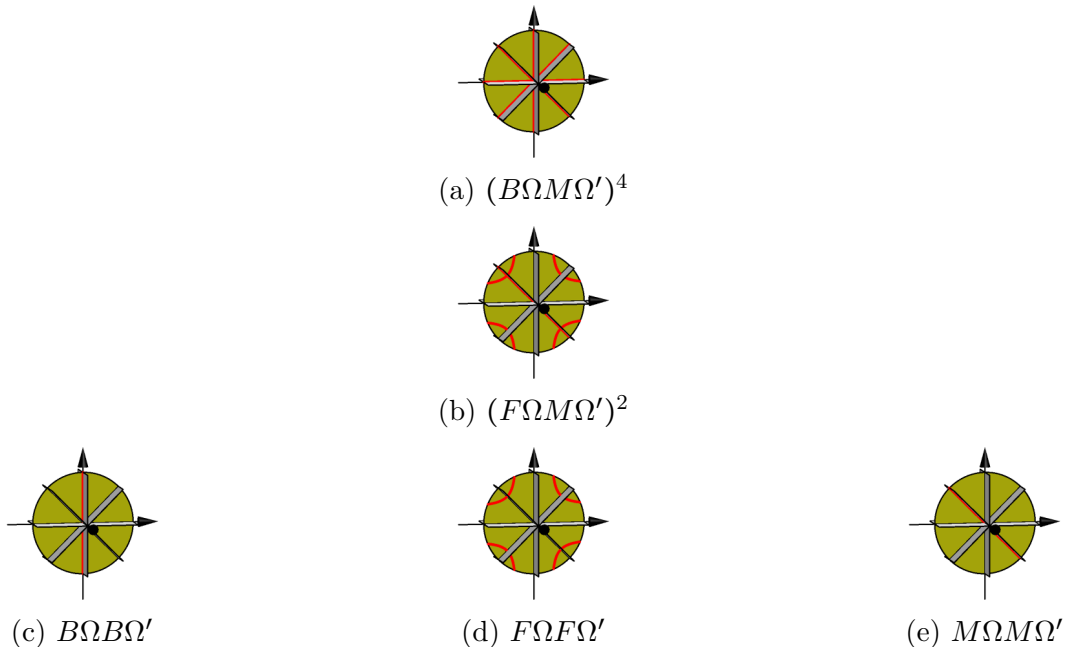


Figure 6.9: Rectilinear reversing symmetries found in the Bestiary.

of three isosceles subspaces: equilateral configurations. The corresponding plane P_E corresponds to no invariant subspace. The types of reversing symmetries appearing in the Bestiary in the E -mode are listed with examples in table 6.5, and the corresponding schematics are shown in figure 6.11. All possible reversing symmetries in this mode are the isosceles subspaces intersecting P_E orthogonally, or the points of intersection of P_E with the planes of collinearity at their intersection points with the remaining isosceles subspaces at isosceles collinear configurations.

The most symmetric orbits in the E -mode have reversing symmetries in all possible locations, with isotropy subgroups isomorphic to D_6 , order 12. The reversing symmetries for this symmetry are illustrated in figure 6.11a, with a reversor on each isosceles configuration orthogonal to P_E and each collinear isosceles configuration on P_E .

By removing either class or reversing symmetries from the symmetry group of order 12 we obtain two possible order 6 isotropy subgroups isomorphic to D_3 , illustrated in figures 6.11b and 6.11c.

If exactly one isosceles collinear line is chose for a reversor with its orthogonal isosceles plane, we have one order 4 isotropy subgroup isomorphic to D_2 , illustrated in figure 6.11d.

Finally, at order 2, there are two possibilities again, isomorphic to \mathbb{Z}_2 , illustrated in

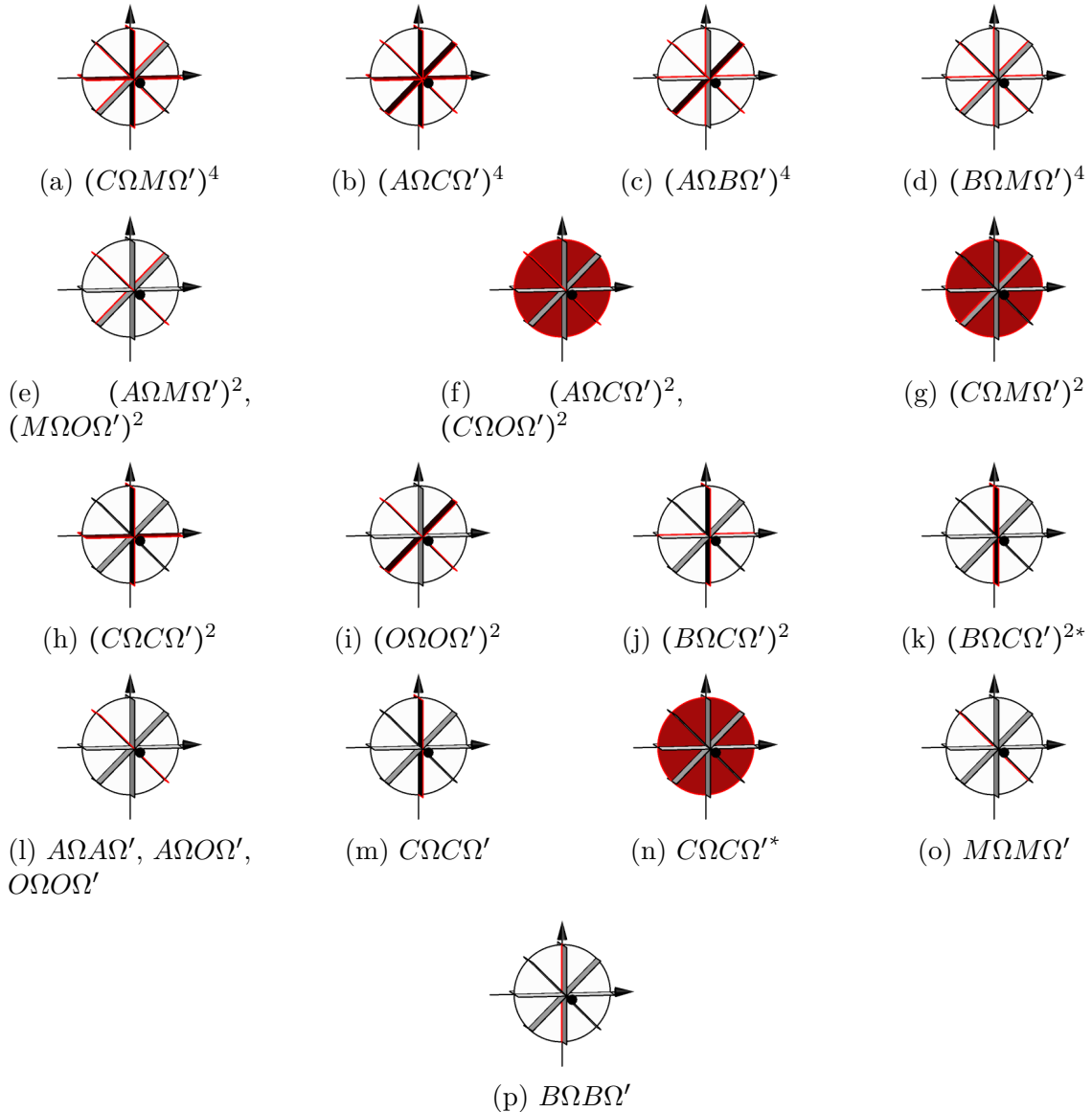
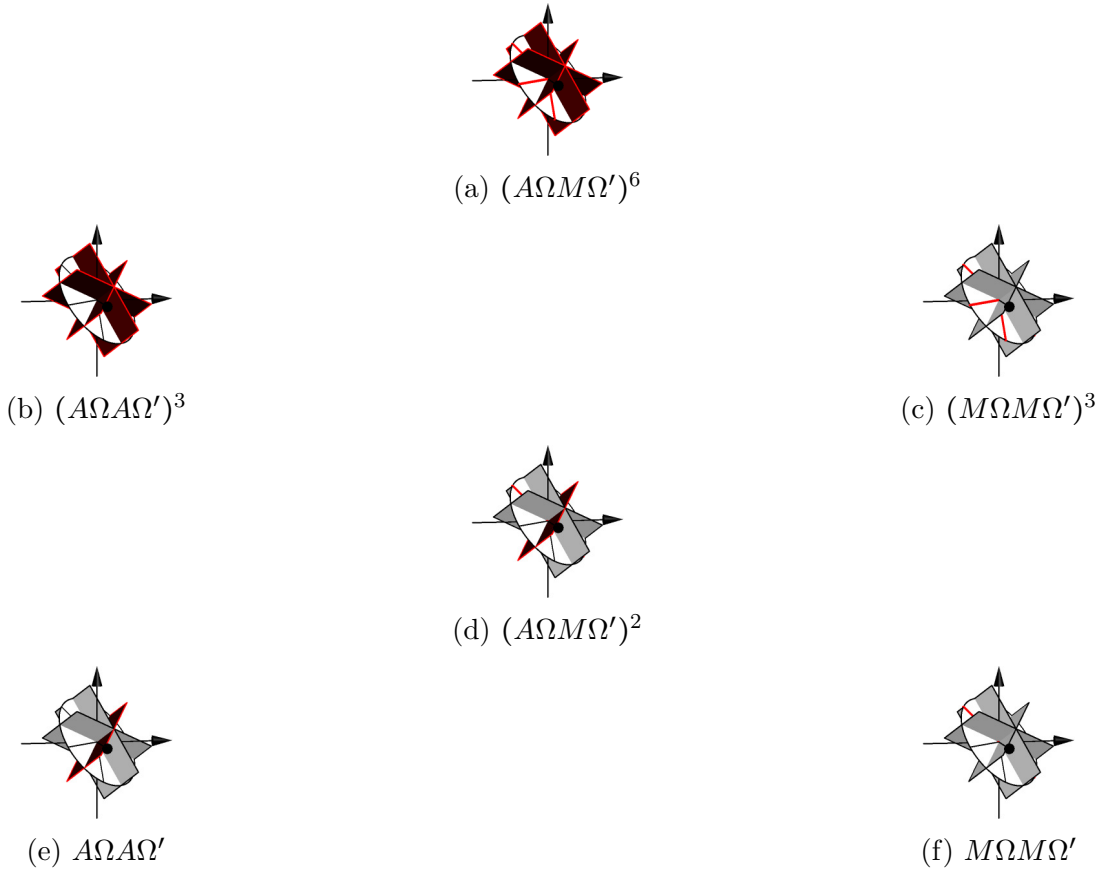


Figure 6.10: *B*-mode reversing symmetries found in the Bestiary. Asterisk * indicates same sequence type, but different realisation via isotropy subgroup.

Figure 6.11: Reversing symmetries in the E -mode found in the Bestiary.

figures 6.11e and 6.11f.

Conspicuously absent in at least the B - and M -mode orbits away from the invariant subspaces are those with sequence classes $(F\Omega X\Omega')^n$, for some (possibly the same) reversor X and repetition number n . Their absence is quite possibly a failure of our search, as orbits with sequence class $(C\Omega F\Omega')^2$ (by visual inspection) in the M -mode are known for unequal masses ([13]) near known isosceles free-fall orbits, and one free-fall orbit for equal masses is presented in [82].

Group (Order)	A	M	Example	Visualisation
D_6 (12)	✓	✓	$t_0(12, 1)$	Figure 6.11a
D_3 (6)	✓✓		$t_0(6, 2)$	Figure 6.11b
D_3 (6)		✓✓	$t_0(6, 1)$	Figure 6.11c
D_2 (4)	✓	✓	$t_0(4, 23)$	Figure 6.11d
\mathbb{Z}_2 (2)	✓✓		$t_0(2, 15)$	Figure 6.11e
\mathbb{Z}_2 (2)		✓✓	$t_0(2, 5)$	Figure 6.11f

Table 6.5: Symmetry types in the E -mode.

6.4 Stability

The stability of periodic solutions is of interest to understand the behaviour of nearby orbits under perturbations. Such perturbations are with respect to the symmetry-reduced, regularised variables (α_j, π_j) , and thus in configuration space are planar and conserve angular momentum. Table 6.6 lists by their arrangement in the Bestiary all orbits that are stable.

We make several observations on these results: first and most interesting is the existence of stable periodic collision orbits. More than half of the highly symmetric type-2 collision orbits are indeed stable, and a great many of the more symmetric type-1 orbits of order 4 are also stable. However, only one order 2 orbit of type-1 appears stable, $t1(2, 1)$, in the M -mode, fairly long (physical period approximately 184.06, regularised period approximately 44.44), and *nearly* symmetric under a symmetry operation like $(\rho\sigma_3, \frac{1}{2})$ or $(\rho\sigma_3s_3, \frac{1}{2})$. Two related stable and more symmetric, shorter orbits are $t1(4, 1)$ and $t1(4, 2)$, both in the M -mode.

The second observation is the stability of orbits in the invariant subspaces. Only one orbit of each subspace in the Bestiary is stable, but each is clearly related to many, many other orbits. We discussed briefly in sections 6.3.2.1 and 6.3.2.2 a relationship between the winding orbits of the M -mode and B -mode, and (respectively) *isosceles*(8, 1) and *rectilinear*(16, 1), that by extending the “base” orbit in either invariant subspace by a multiple of its period and perturbing the resulting orbit we can realise certain sequences of the reduced symbolic dynamics.

It may be that there exists a stable non-winding rectilinear orbit which serves as a similar “basis” for the non-winding non-collinear B -mode orbits, but the simplest such orbit, *rectilinear*(8, 1), appears as simple as such orbits could be, and it is not stable.

Other relatively short (stable) orbits, such as $t2(8, 2)$, appear to serve as “base” orbits for families with lower symmetry. Related orbits include $t1(2, 2)$, $t0(2, 64)$, and $t0(1, 30)$. Another example, the figure-8 serves as a base for all other E -mode orbits.

6.5 Choreographies

Choreographies are special periodic solutions of the n -body problem, wherein more than one body traces over the same path. *Simple choreographies* are choreographies in which all bodies trace over the same path, and *partial choreographies* are those in which the number of paths is greater than 1 and less than n (the latter just being a

Type-0						
Order 16	Order 12	Order 8	Order 6	Order 4	Order 2	Order 1
N/A	$t0(12, 1)$	$t0(8, 1)$ $t0(8, 2)$ $t0(8, 3)$ $t0(8, 4)$	$t0(6, 1)$	$t0(4, 1)$ $t0(4, 2)$ $t0(4, 3)$ $t0(4, 4)$ $t0(4, 5)$ $t0(4, 6)$ $t0(4, 7)$	$t0(4, 8)$ $t0(4, 9)$ $t0(4, 10)$ $t0(4, 11)$ $t0(4, 12)$	$t0(2, 1)$ $t0(2, 2)$ $t0(2, 3)$ $t0(2, 4)$ $t0(2, 5)$ $t0(2, 6)$ $t0(2, 7)$

Type-1						
Order 16	Order 12	Order 8	Order 6	Order 4	Order 2	Order 1
N/A	N/A	N/A	N/A	$t1(4, 1)$ $t1(4, 2)$ $t1(4, 3)$ $t1(4, 4)$ $t1(4, 5)$ $t1(4, 6)$ $t1(4, 7)$	$t1(4, 8)$ $t1(4, 9)$ $t1(4, 10)$ $t1(4, 11)$ $t1(4, 12)$ $t1(4, 13)$	$t1(2, 1)$ N/A

Type-2						
Order 16	Order 12	Order 8	Order 6	Order 4	Order 2	Order 1
N/A	N/A	$t2(8, 1)$ $t2(8, 2)$ $t2(8, 3)$ $t2(8, 4)$	N/A	N/A	N/A	N/A

Isosceles						
Order 16	Order 12	Order 8	Order 6	Order 4	Order 2	Order 1
N/A	N/A	<i>isosceles</i> (8, 1)	N/A		N/A	N/A

Rectilinear						
Order 16	Order 12	Order 8	Order 6	Order 4	Order 2	Order 1
<i>rectilinear</i> (8, 1)	N/A		N/A		N/A	N/A

Table 6.6: Stable orbits arranged by type and order of symmetry group.

“typical” periodic orbit). Due to this remarkable nature, since the discovery of the figure-8 choreography by Moore in 1993 [51], and its re-discovery and proof of existence by Chenciner and Montgomery nearly a decade later [16], there has been an intense interest in these special orbits. Simó investigated the figure-8 in more detail [71], and then he and others continued to look at the n -body problem in general [70, 72, 15, 8, 81]. A recent publication by Šuvakov and Shibayama [74] has discovered several more interesting 3-body choreographies with vanishing angular momentum. Comprehensive work has been done by Montaldi and Steckles to classify the symmetries of n -body choreographies [45].

The basic properties of n -body choreographies are equal masses and a cyclic permutation of the bodies associated with a time shift of $\frac{T}{n}$. That is, after $\frac{T}{n}$ the second body is in the original position of the first, the third is in the original position of the second, and so on. It is not known whether choreographic motions exist for the 3-body problem with unequal masses if the requirement of equal time spacing is removed [14]; however, it is known that for n up to 5 there are no unequal-mass choreographies with equal time spacing.

Simple choreographies may be absolute or relative. Theorem 4.5 gives us a symmetry criterion by which to construct absolute simple choreographies or (generically) relative simple choreographies. From our observations in section 6.3.3 (in particular figure 6.11

and table 6.5) we could in principle find more simple choreographies of either type with dihedral symmetry. We do not have a proof of the non-existence of choreographies whose isotropy subgroup is isomorphic to \mathbb{Z}_3 (generated by $(c, \frac{1}{3})$) or \mathbb{Z}_6 (generated by $(\rho c, \frac{1}{6})$), but we know that almost all of the former must be relatively periodic, and the latter absolutely periodic. Orbits with such isotropy subgroups were not found, but may simply be elusive.

Partial choreographies have been discussed with numerically discovered examples in [8], for $n = 4$ and 5. The symmetry conditions for partial choreographies with $n > 3$ may become complicated if the number of curves exceeds 2, but for $n = 3$ the only possible number of curves is exactly 2, and we require that at $\frac{T}{2}$ two of the bodies exchange roles via a pairwise permutation, while the other body covers the same path twice in a single period. Thus $(\sigma_j, \frac{1}{2})$ is the symmetry requirement for a partial choreography for the 3-body problem.

6.5.1 Simple absolute choreographies

Three simple choreographies appeared in our search: the well known figure-8 choreography $t0(12, 1)$; another highly symmetric choreography $t0(12, 2)$ (only recently published in [74]); and a less symmetric choreography $t0(6, 1)$, similar to the figure-8, but approximately seven times its period. Because their symmetry groups contain symmetries from columns 2 and 3 of table 2.1 (with sequence classes of the form $(M\Omega X\Omega')^n$, for an allowable X and corresponding n), they satisfy Theorem 4.5, and are absolutely periodic.

6.5.2 Simple relative choreographies

A relative choreography appeared as well, $t0(6, 2)$, whose reversing symmetries are on acute isosceles lines of the shape sphere. Accordingly, its symmetries only come from columns 1 and 4 of table 2.1, and thus its geometric phase is non-vanishing. Transforming to a rotating frame with angular velocity $\omega = \frac{\Delta G}{T}$, using the geometric phase $\Delta G \approx 0.146$ computed over the orbit, we see the orbit becomes choreographic. The only known example of this type of orbit has sequence class $(A\Omega A\Omega')^3$.

6.5.3 Partial relative choreographies

An interesting class of periodic orbits are relatively periodic, and partially choreographic when viewed in the frame rotating with angular velocity $\omega = \frac{\Delta G}{T}$.

The following is a list of relative partial choreographies we have found:

- Order 8, *B*-mode: $t0(8,1)$, $t0(8,5)$.
- Order 4, *B*-mode: $t0(4,13)$, $t0(4,14)$.
- Order 4, *M*-mode: $t0(4,1)$, $t0(4,2)$, $t0(4,15)$, $t0(4,16)$, $t0(4,17)$, $t0(4,18)$, $t0(4,19)$, $t0(4,20)$, $t0(4,21)$, $t0(4,22)$.

These are not the only relative partial choreographies, however! There are a number of orbits which can be turned into relative partial choreographies by adding or subtracting extra turns to the rotating frame over one period. For example, $t0(2,8)$ is a relative periodic orbit in the *B*-mode, with the cyclic symmetry $(\sigma_2, \frac{1}{2})$. Its geometric phase is $\Delta G \approx 0.454$. Yet by choosing a rotating frame with $\omega = \frac{\Delta G - 2\pi}{T}$, it becomes a relative partial choreography, which is illustrated in figure 6.12d.

If choosing $\omega = \frac{\Delta G}{T}$ is sufficient to make a solution periodic, we can always choose to add an arbitrary number of extra turns per period. That is, $\omega = \frac{\Delta G + 2k\pi}{T}$ is another frame in which an orbit is periodic. We observe that the orbits listed above are partially choreographic if we choose rotating frames with $\omega = \frac{\Delta G + 8k\pi}{T}$ for any integer k , and we observe that the projections of their isotropy subgroups onto the un-regularised symmetry group all contain a subgroup $\{(I, 0), (\sigma_j, \frac{1}{2})\}$. But these are not the only orbits with such a subgroup of its isotropy subgroup. By choosing an appropriate number of extra rotations, all solutions with such a subgroup—even those which are absolutely periodic—can be made relatively choreographic.

This is perhaps to be expected, precisely because the permutation symmetry σ_j at $\frac{T}{2}$ swaps the roles of bodies k and l for the second half of the period. The number of extra turns to reveal the relative partial choreography (or to preserve it in the case of orbits listed above) is detailed in table 6.7.

Orbits which are partially choreographic with extra rotation are

- Order 16, *B*-mode: *rectilinear*(16,1) (Figure E.4a).
- Order 8, *B*-mode: $t0(8,7)$ (Figure 6.12a), $t0(8,8)$ (Figure 6.12b), $t2(8,2)$ (Figure E.2a), $t2(8,3)$ (Figure E.2b), $t2(8,4)$ (Figure E.2c), *rectilinear*(8,1) (Figure E.4b), *rectilinear*(8,2) (Figure E.4c), *rectilinear*(8,3) (Figure E.4d), *rectilinear*(8,4) (Figure E.4e), *rectilinear*(8,5) (Figure E.4f), *rectilinear*(8,6) (Figure E.4g).
- Order 8, *E*-mode: *isosceles*(8,1) (Figure E.3a), *isosceles*(8,2) (Figure E.3b), *isosceles*(8,3) (Figure E.3c), *isosceles*(8,4) (Figure E.3d).

Orbit classification	Sequence type	Extra turns per period	Choreography type
type-0	$(A\Omega M\Omega')^6$	$3k$	absolute simple
	$(A\Omega C\Omega')^4$	$4k$	relative partial
	$(O\Omega C\Omega')^4$	$2(2k+1)$	relative partial
	$(M\Omega M\Omega')^3$	$3k$	absolute simple
	$(A\Omega A\Omega')^3$	$3k$	relative simple
	$(A\Omega C\Omega')^2$	$2k$	relative partial
	$(O\Omega C\Omega')^2$	$(2k+1)$	relative partial
	Ω^4	$2k$	relative partial
	Ω^2	$(2k+1)$	relative partial
	$(B\Omega M\Omega')^2$	$(2k+1)$	relative partial
type-1	$(B\Omega M\Omega')^4$	$2(2k+1)$	relative partial
<i>isosceles</i>	$(B\Omega M\Omega')^2$	$(2k+1)$	relative partial
	$(F\Omega M\Omega')^2$	$(2k+1)$	relative partial
<i>rectilinear</i>	$(B\Omega M\Omega')^4$	$2(2k+1)$	relative partial
	$(F\Omega M\Omega')^2$	$(2k+1)$	relative partial

Table 6.7: Sequence types corresponding to choreographic or partially choreographic motion, and the number of extra turns per period to add to the rotating frame such that the choreography is preserved (or revealed, $k = 0$ yields a non-zero number), with $k \in \mathbb{Z}$.

- Order 4, B -mode: $t0(4, 47)$ (Figure 6.12c).
- Order 4, M -mode: $t1(4, 34)$ (Figure E.1a), $t1(4, 35)$ (Figure E.1b), $t1(4, 36)$ (Figure E.1c), $t1(4, 37)$ (Figure E.1d), $t1(4, 38)$ (Figure E.1e), $t1(4, 39)$ (Figure E.1f), $t1(4, 40)$ (Figure E.1g), $t1(4, 41)$ (Figure E.1h).
- Order 2, B -mode: $t0(2, 8)$ (Figure 6.12d), $t0(2, 9)$ (Figure 6.12e), $t0(2, 10)$ (Figure 6.12f).

Relative periodic orbits that become relative partial choreographies under extra rotation are shown in figure 6.12 in the frame with minimal angular velocity such that they become relative partial choreographies. Colour choice is automatic and “random”, due to the particular initial conditions from the numerical search, and is insignificant except to distinguish curves.

The absolutely periodic orbits which are relatively partially choreographic under extra rotation are illustrated in appendix E.

6.5.4 Absolute partial choreographies

No absolute partial choreographies appeared as a result of our search. The following theorem explains why not.

Theorem 6.1. *Partial choreographies of the equal-mass planar 3-body problem with vanishing angular momentum, with isotropy subgroups generated either by a cyclic symmetry or two reversing symmetries, are generically not absolutely periodic.*

Proof. For an orbit to be partially choreographic its physical symmetry group must contain $(\sigma_j, \frac{1}{2})$. In the regularised symmetry group, this means we may have involutions $(\sigma_j, \frac{1}{2})$, $(\sigma_j s_j, \frac{1}{2})$, or an order-4 cyclic element $(\sigma_j s_l, \frac{1}{4})$.

By Theorems 4.5 and 4.6, the geometric phase of an orbit is generically non-zero unless it has a reversing symmetry on either an isosceles collinear M configuration, a brake-collision B configuration, a brake point or a cyclic element $(\rho\gamma, \frac{1}{k})$, where $\gamma \in \tilde{S} = S \rtimes F_4$ and $\rho\gamma$ is of order k .

In the cyclic case, there is no $\gamma \in \tilde{S}$ such that there exists some integer i for which $(\rho\gamma)^i$ is equal to any of the partial choreography symmetries.

In the remaining case, the only possible choices of reversing symmetries R_1, R_2 that produce any of the required symmetries is R_1 a reversing isosceles collinear configuration (reversing M) and R_2 a brake-collision (reversing B) or a brake-point (F). While

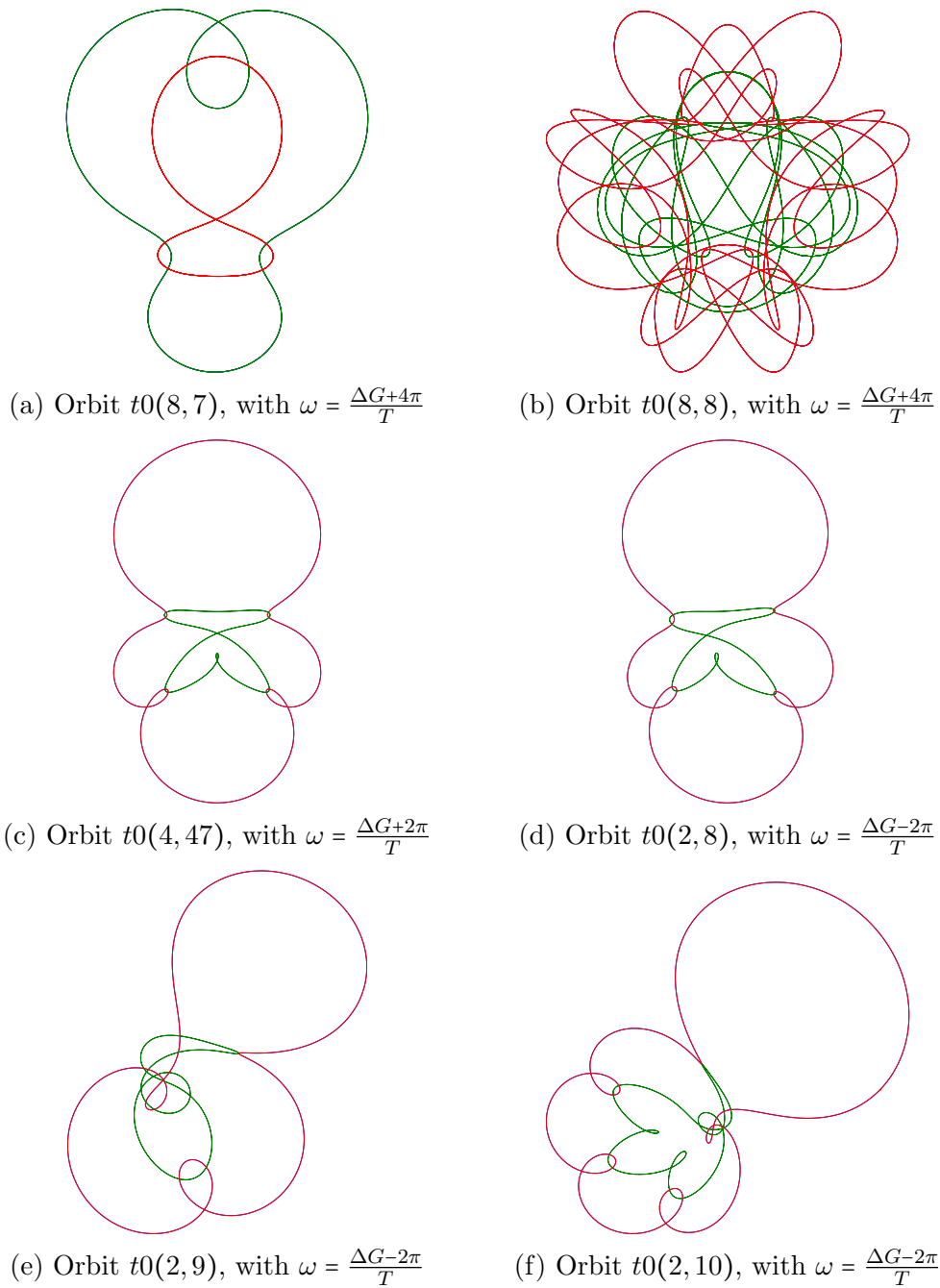


Figure 6.12: Type-0 , sequence types $(O\Omega C\Omega')^k$, $k = 4$ (a-b), $k = 2$ (c), and Ω^2 (d-f).

such a solution is absolutely periodic, orbits with brake-points or brake-collisions retrace themselves directly in configuration space. Thus if the orbit $z(t)$ begins with $z(0) \in \text{Fix}(R_1)$ with $z(\frac{t_1}{2}) \in \text{Fix}(R_2)$, where $t_1 = \frac{1}{2}$ or $\frac{1}{4}$ (where the denominator is the order of $R_2 R_1$), we must have that the physical configuration at $t = t_1$ is exactly the configuration at $t = 0$ with the momenta reversed. Thus the two bodies that would be interchanged by the permutation σ_j are not tracing over the same path in the inertial frame but are back in their original positions, rather than interchanged. \square

This explains the results observed in section 6.5.3 and appendix E, whereby choosing a particular rotating frame makes absolutely periodic orbits with the partial choreography symmetry into relative partial choreographies.

6.6 Geometric phase

An early question in our research was “*what relative periodic orbits’ geometric phase maximises the angular velocity of the rotating frame in which it is periodic?*” The production of the Bestiary was initially an attempt to gain insight to answer that question, leading to Theorem 4.5, instead instructing us how to ensure a periodic orbit has vanishing geometric phase and is absolutely periodic. We remain interested, however, in orbits with large geometric phase, and in this section we examine some.

Due to the symmetries occurring in all type-1 and type-2 orbits, and that of orbits in all invariant subspaces, the only group of orbits of interest in this section are those of type-0 (F1), and of those, we pay attention to orbits with reversing symmetries only on A , O or C points, or with only non-reversing symmetries from column 1 of table 2.1.

A number of relative partial choreographies have large values of ΔG (close to or exceeding 2π). Those for which $\Delta G > 2\pi$ can be reconstructed in a rotating frame with $\omega = \frac{\Delta G - 2\pi}{T}$, in which they look similar to orbits with smaller geometric phase. Figure 6.13 illustrates $t0(4, 16)$ drawn in the frame with the smallest ω required for it to close.

The geometric phase of an orbit can perhaps be increased arbitrarily for orbits with arbitrarily long excursions into the arms of the Hill region, as in the L-shaped B -mode orbits, with one binary pair rotating in one direction, while the third body orbits retrograde with respect to the common centre of mass of the pair at a much greater distance. Numerical evidence suggests that in the case of equal masses and vanishing angular momentum no periodic orbit exists which remains in such a configuration. An example of an orbit that spends a long time in one arm (and not so much time

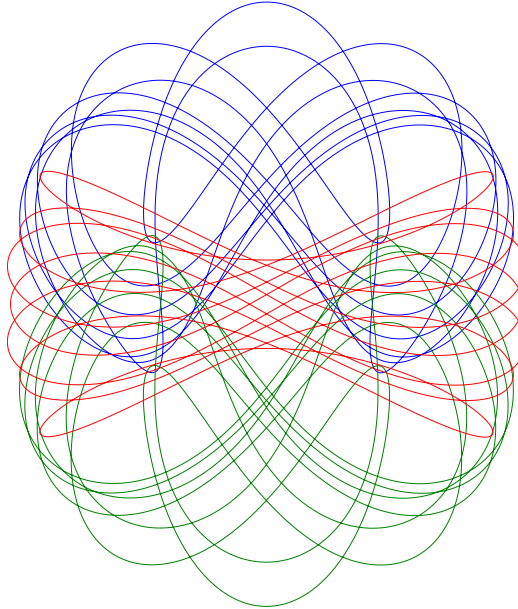


Figure 6.13: $t0(4, 16)$ drawn in the frame with minimal ω such that it is periodic.

in another) is $t0(2, 37)$, which has a substantial $\Delta G \approx 2.919$ but relatively small $\omega \approx 0.0729$.

The orbit with the largest $|\omega|$ is $t0(8, 5)$, with $\omega = \frac{\Delta G}{T} \approx 0.1845$. Figure 6.14 illustrates this orbit in the inertial frame. This orbit happens to be one of the few which is a relative partial choreography when reconstructed in a frame which rotates extra times per period, illustrated as such in figure 6.12a in the frame with the least $|\omega|$ with such that it is partially choreographic. The angular velocity of this frame is $\omega = \frac{\Delta G + 4\pi}{T} \approx -0.41275$.

Further work to find maximisers of geometric phase would use the knowledge gained from this body of work to build families of periodic orbits for each class of symmetry, with the aim of finding a maximiser (should it exist) in each class that permits geometric phase.

6.6.1 A remark on reconstructing in the rotating frame

Throughout the Bestiary, where an orbit is relatively periodic only, it is reconstructed in a frame rotating with constant angular velocity $\omega = \frac{\Delta G}{T}$. If the winding number W of the trajectory on the classical shape sphere is even, then we choose $\omega_e = \frac{\Delta G}{T_p}$ and the orbit closes. If the winding number is odd, we must choose $\omega_o = \frac{\Delta G + \text{sgn}(W)\pi}{T_p}$

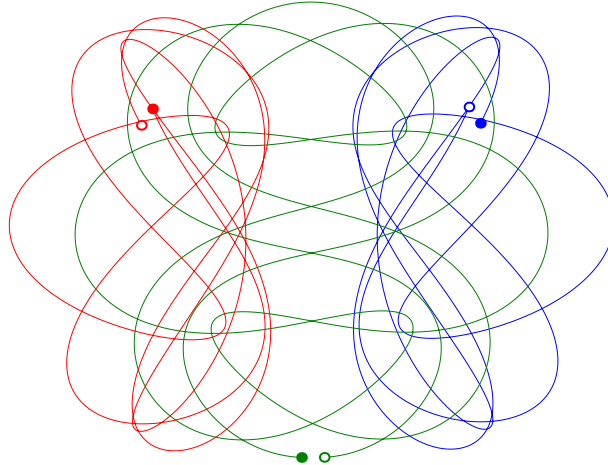


Figure 6.14: $t0(8, 5)$ drawn in the inertial frame. Hollow dots indicate initial positions; solid final.

in order for the physical curves to close. We observe that odd winding numbers only occur for all orbits with sequence class $(A\Omega O\Omega')^2$, and some with sequence class Ω .

6.6.2 A remark on ΔG and $\Delta \phi$

Recall that reconstruction of the original coordinates requires the angle ϕ , whose evolution is governed by equation (1.39). While $\dot{\phi}$ is defined differently from U , both have the same symmetries and antisymmetries. It is interesting to note that for every orbit the geometric phase ΔG and $\Delta \phi$ always differ by some integer multiple of $\frac{2\pi}{3}$. The integer multiple is zero when $\Delta G = \Delta \phi = 0$ (as Theorem 4.5 can be trivially reformulated in terms of $\dot{\phi}$), but also in a few other cases: $t0(6, 2)$ (E -mode, sequence class $(A\Omega A\Omega')^3$); $t0(4, 40)$ (B -mode, sequence class $(C\Omega C\Omega')^2$); $t0(4, 47)$ (B -mode, sequence class $(A\Omega O\Omega')^2$); $t0(2, 4)$ (B -mode, sequence class $C\Omega C\Omega'$); $t0(2, 8)$, $t0(2, 9)$ and $t0(2, 12)$ (B -mode, sequence class Ω^2); $t0(2, 15)$ to $t0(2, 18)$, $t0(2, 24)$ (E -mode, sequence class $A\Omega A\Omega'$); $t0(2, 30)$, $t0(2, 35)$, $t0(2, 36)$, $t0(2, 48)$, $t0(2, 50)$, $t0(2, 57)$ and $t0(2, 59)$ (sequence class $C\Omega C\Omega'$, B -mode, except $t0(2, 50)$ in M -mode); $t0(2, 101)$, $t0(2, 103)$ to $t0(2, 105)$, $t0(2, 109)$ and $t0(2, 112)$ (B -mode, sequence class $O\Omega O\Omega'$); $t0(1, 4)$, $t0(1, 5)$, $t0(1, 7)$, $t0(1, 10)$, $t0(1, 15)$, $t0(1, 19)$, $t0(1, 21)$, $t0(1, 22)$, $t0(1, 25)$ to $t0(1, 27)$, $t0(1, 30)$ to $t0(1, 33)$, $t0(1, 35)$ (sequence class Ω , B -mode, except $t0(1, 15)$, $t0(1, 21)$ $t0(1, 25)$ in M -mode, and $t0(1, 26)$ in E -mode).

No clear pattern emerges immediately to suggest when ΔG and $\Delta \phi$ should agree, although we note that for every E -mode orbit this is the case, and it is relatively rarely the case for any M -mode orbit for which $\Delta G \neq 0$ (and consequently $\Delta \phi \neq 0$).

We suppose that the connection is most likely related to the topology of the solutions—that is, their syzygy sequences.

7 Conclusion

In this thesis we examined the 3-body problem with vanishing angular momentum in symmetry-reduced coordinates that simultaneously regularise all binary collisions, as used by Waldvogel [85]. The square-root coordinates induce a four-fold cover of the shape sphere, and Poincaré’s trick to scale time slows down the binary collisions so that in these new coordinates all binary collision singularities are removed.

In Chapter 2 we examined the discrete symmetry group. For unequal masses the regularised symmetry group is of order 16, comprising spatial reflection, “sign flip” symmetries induced by regularisation, and time reversal. When exactly two masses are equal the group expands to include pairwise permutation of those two bodies, and is of order 32. The most symmetry occurs when all three masses are equal, the group is of order 96, when all three pairwise permutations, and cyclic permutations are possible. We determine the fixed sets of all symmetries and those that are of physical interest, including invariant subspaces and reversing involutions. The isotropy subgroups of periodic orbits are isomorphic to subgroups of the symmetry group, which we decompose into direct or semidirect products of normal and central factors, and we consider cases generated by one non-reversing symmetry, or by two reversing involutions.

Chapter 3 used our knowledge of the symmetry group to develop symmetry-reduced symbolic dynamics of the 3-body problem with vanishing angular momentum. Given the values of the masses, we determined the relevant fundamental domain (always a region of shape space mapping to a triangle in no more than one octant of the regularised shape sphere), and a symbolic dynamics for each case. The fixed sets of non-reversing involutions divide the shape space into a number of dynamically equivalent regions; one is chosen as the fundamental domain. The fundamental domain is bounded by the fixed sets of certain non-reversing involutions and the free fall boundary, though it is unbounded along the collision axes. A symbol is assigned to each distinct region of the boundary: one for each face; one for each edge where two faces meet; and one for the free fall boundary. Whenever a solution passes through a section of the boundary that symbol is recorded, and the solution is reflected back into the fundamental domain by an appropriate symmetry. By taking note of which symbols coincide with points in the fixed sets of reversing involutions we constructed the sequence class, which serves as a classification scheme for periodic orbits, and

allows us to determine the isotropy subgroup up to isomorphism.

We then moved on to the geometric phase of the 3-body problem, where the formula by Montgomery [47], equation (4.1), was written in regularised coordinates, equation (4.2), so that we could calculate the geometric phase of periodic orbits in the regularised variables. Certain symmetries—namely those which project onto the generators of the centre of the symmetry group, ρ and τ —reverse the sign of the integrand of the geometric phase. We used this fact, along with the structure of subgroups containing such elements, to prove our main result, Theorem 4.5, which gives us a very simple criterion to determine if a periodic orbit in the symmetry-reduced and regularised variables is absolutely periodic in configuration space. This result is especially nice in that if a periodic orbit is generated by two reversing symmetries, its sequence class immediately tells us if it is absolutely periodic in configuration space: if the sequence class contains either M or B , this is the case; otherwise the geometric phase is generically non-zero. No such simple test using the symbol sequence exists for orbits with purely cyclic symmetry, but to use the isotropy subgroups of such orbits is not difficult.

We changed setting in Chapter 5 to discuss the numerical tools and algorithms used in the remainder of the thesis. The most important result was the development of a novel explicit symplectic integrator for the regularised system, which we published in [60]. This integrator forms the backbone of our method to find periodic orbits of the regularised system. This search was not directed by symmetry constraints, with the goal of capturing as many relative periodic orbits as possible (unique up to discrete symmetries), yielding 363 relative periodic orbits, both with and without collisions, many of which were previously unknown, including many orbits in both the isosceles and rectilinear invariant subspaces.

The results of our numerical search were presented in Chapter 6 and appendix F. A number of the orbits we presented are known in the literature, but many are new. In summary, 25 collisionless orbits, 14 type-1 orbits, 4 type-2 orbits, and one each of the isosceles and rectilinear orbits are linearly stable. We also observed that most periodic orbits in the regularised variables are “straightened out” in such a way that they lie very near one or another of three sets of planes in the regularised shape space, orthogonal to the axes where planes of symmetry intersect. These behaviours we called “modes”, and they are characterised by behaviour similar to rectilinear (B -mode, very common), isosceles (M -mode, less common), or choreographic (E -mode, least common) motion, and there is a close relationship to the symmetry classification of periodic orbits.

We also found a number of relative partial choreographies, and proved that there can be no absolutely periodic partial choreographies for vanishing angular momentum,

although there are a number of absolutely periodic orbits with symmetry such that they can, with the choice of the correct rotating frame, be turned into relative partial choreographies. The orbit with the largest rate of rotation per period is $t0(8,5)$, a relative partial choreography.

It appears from our numerical survey that relative periodic orbits are more common than absolute periodic orbits of the 3-body problem with vanishing angular momentum even for equal masses. As a consequence of Theorem 4.5 it turns out that only brake orbits and brake-collision orbits are absolutely periodic in the case of unequal masses.

The work presented in this thesis contributes a large amount of data to the body of knowledge on the equal-mass 3-body problem with vanishing angular momentum, in the form of many new relative periodic orbits, a novel explicit symplectic integrator for the regularised and symmetry reduced 3-body problem with vanishing angular momentum, and in a simple symmetry criterion with a direct relationship to the symmetry reduced symbolic dynamics that allows us to distinguish absolute periodic orbits from the rest.

References

- [1] 20th Century Fox. Alien. Film, 1979.
- [2] Jan Awrejcewicz. *Classical mechanics: dynamics*. Springer, Dordrecht, 2012;1; edition, 2012.
- [3] Robert W Batterman. Falling cats, parallel parking, and polarized light. *Studies in History and Philosophy of Science Part B: Studies in History and Philosophy of Modern Physics*, 34(4):527–557, 2003.
- [4] Michael V Berry. Quantal phase factors accompanying adiabatic changes. In *Proceedings of the Royal Society of London A: Mathematical, Physical and Engineering Sciences*, volume 392, pages 45–57. The Royal Society, 1984.
- [5] George D. Birkhoff. *Dynamical systems*, volume 9. American Mathematical Society, Providence, R.I, rev. edition, 1966.
- [6] Sergio Blanes. Symplectic maps for approximating polynomial hamiltonian systems. *Phys Rev E Stat Nonlin Soft Matter Phys*, 65(5 Pt 2):056703, 2002.
- [7] R Broucke and D Boggs. Periodic orbits in the planar general three-body problem. *Celestial mechanics*, 11(1):13–38, 1975.
- [8] Roger A Broucke. Classification of periodic orbits in the four-and five-body problems. *Annals of the New York Academy of Sciences*, 1017(1):408–421, 2004.
- [9] J. Candy and W Rozmus. A symplectic integration algorithm for separable hamiltonian functions. *Journal of Computational Physics*, 92(1):230 – 256, 1991.
- [10] Alessandra Celletti and Sylvio Ferraz-Mello. *Periodic, Quasi-Periodic and Chaotic Motions in Celestial Mechanics: Theory and Applications: Theory and Applications: Selected Papers from the Fourth Meeting on Celestial Mechanics, CELMEC IV, San Martino Al Cimino, Italy, 11-16 September 2005*. Springer Science & Business Media, 2007.
- [11] Paul J. Channell and Filippo R. Neri. *An Introduction to Symplectic Integrators*, volume 10, pages 45–58. Fields Institute Communications, 1996.
- [12] Nai-Chia Chen. Periodic brake orbits in the planar isosceles three-body problem. *Nonlinearity*, 26(10):2875, 2013.
- [13] Nai-Chia Chen and Richard Montgomery. More periodic orbits. <http://www.tc.umn.edu/~chen1945/NoncollisionBrake.html>, 2014.
- [14] Alain Chenciner. Are there perverse choreographies? In *New Advances in Celestial Mechanics and Hamiltonian Systems*, pages 63–76. Springer, 2004.
- [15] Alain Chenciner, Joseph Gerver, Richard Montgomery, and Carles Simó. Simple choreographic motions of n bodies: a preliminary study. In *Geometry, mechanics,*

- and dynamics*, pages 287–308. Springer, 2002.
- [16] Alain Chenciner and Richard Montgomery. A remarkable periodic solution of the three body problem in the case of equal masses. *Annals of Mathematics*, 152:881–901, 2000.
 - [17] Étienne Forest and Ronald D. Ruth. Fourth-order symplectic integration. *Physica D: Nonlinear Phenomena*, 43(1):105 – 117, 1990.
 - [18] Ivan Gjaja. Monomial factorization of symplectic maps. *Particle Accelerators*, 43(3):133–144, 1994.
 - [19] D. Gruntz and J. Waldvogel. *Orbits in the Planar Three-Body Problem*, chapter 4, pages 51–72. Springer, 4 edition, 2004.
 - [20] Alain Guichardet. On rotation and vibration motions of molecules. In *Annales de l'IHP Physique théorique*, volume 40, pages 329–342, 1984.
 - [21] Jacques Hadamard. Les surfaces à courbures opposées et leurs lignes géodésique. *J. Math. pures appl.*, 4:27–73, 1898.
 - [22] John D Hadjidemetriou. The stability of periodic orbits in the three-body problem. *Celestial mechanics*, 12(3):255–276, 1975.
 - [23] E. Hairer, C. Lubich, and G. Wanner. *Geometric numerical integration*. Springer, Berlin, 2002.
 - [24] Michele Hénon. On the numerical computation of poincaré maps. *Physica 5D*, pages 412–414, 1982.
 - [25] JG Hills and CA Day. Stellar collisions in globular clusters. *Astrophysical Letters*, 17:87, 1976.
 - [26] Heinz Hopf. ber die abbildungen der dreidimensionalen sphre auf die kugelflche. *Mathematische Annalen*, 104(1):637–665, 1931.
 - [27] Takashi Ito and Kiyotaka Tanikawa. Long-term integrations and stability of planetary orbits in our solar system. *Monthly Notices of the Royal Astronomical Society*, 336(2):483–500, 2002.
 - [28] Toshihiro Iwai. A gauge theory for the quantum planar three-body problem. *Journal of mathematical physics*, 28(4):964–974, 1987.
 - [29] David G Kendall. Shape manifolds, procrustean metrics, and complex projective spaces. *Bulletin of the London Mathematical Society*, 16(2):81–121, 1984.
 - [30] Jeroen Steven Willibrord Lamb and GRW Quispel. Reversing k-symmetries in dynamical systems. *Physica D: Nonlinear Phenomena*, 73(4):277–304, 1994.
 - [31] Jacques Laskar. Is the solar system stable? In Bertrand Duplantier, Stphane Nonnenmacher, and Vincent Rivasseau, editors, *Chaos*, volume 66 of *Progress in Mathematical Physics*, pages 239–270. Springer Basel, 2013.
 - [32] Jacques Laskar. Numerical challenges in long term integrations of the solar system. In *Computer Arithmetic (ARITH), 2015 IEEE 22nd Symposium on*, pages 104–104. IEEE, 2015.
 - [33] Benedict Leimkuhler and Sebastian Reich. *Simulating Hamiltonian dynamics*.

- Cambridge University Press, 2004.
- [34] C.G. Lemaître. The three body problem. Technical report, NASA CR-110, <http://ntrs.nasa.gov/>, 1964.
 - [35] Christian Marchal. *The three-body problem*. Elsevier, 2012.
 - [36] Christian Marchal. *The three-body problem*, chapter 4. Elsevier, 2012.
 - [37] Christian Marchal. *The three-body problem*, chapter 8. Elsevier, 2012.
 - [38] Christian Marchal. *The three-body problem*, chapter 11. Elsevier, 2012.
 - [39] EJ Marey. Photographs of a tumbling cat. *Nature (Lond.)*, 51:80–81, 1894.
 - [40] Robert I. McLachlan and G. Reinout W. Quispel. Splitting methods. *Acta Numerica*, 11:341–434, 0 2002.
 - [41] Kenneth R. Meyer, Glen R. Hall, and Daniel C. Offin. *Introduction to Hamiltonian dynamical systems and the N-body problem*, volume 90. Springer Science+Business Media, New York, 2nd edition, 2009.
 - [42] Richard Moeckel. Chaotic dynamics near triple collision. *Archive for Rational Mechanics and Analysis*, 107(1):37–69, 1989.
 - [43] Richard Moeckel. Symbolic dynamics in the planar three-body problem. *Regular and Chaotic Dynamics*, 12(5):449–475, 2007.
 - [44] Richard Moeckel and Richard Montgomery. Symmetric regularization, reduction and blow-up of the planar three-body problem. *Pacific Journal of Mathematics*, 262(1):129–189, 2013.
 - [45] James Montaldi and Katrina Steckles. Classification of symmetry groups for planar-body choreographies. In *Forum of Mathematics, Sigma*, volume 1, page e5. Cambridge Univ Press, 2013.
 - [46] Richard Montgomery. Gauge theory of the falling cat. *Fields Inst. Commun.*, 1:193–218, 1993.
 - [47] Richard Montgomery. The geometric phase of the three-body problem. *Nonlinearity*, 9:1341–1360, 1996.
 - [48] Richard Montgomery. Infinitely many syzygies. *Archive for rational mechanics and analysis*, 164(4):311–340, 2002.
 - [49] Richard Montgomery. The zero angular momentum, three-body problem: All but one solution has syzygies. *Ergodic Theory and Dynamical Systems*, 27:1933–1946, 2007.
 - [50] Richard Montgomery. The three-body problem and the shape sphere. *The American Mathematical Monthly*, 122(04):299–321, 2015.
 - [51] Christopher Moore. Braids in classical dynamics. *Physical Review Letters*, 70:3675–3679, 1993.
 - [52] Marston Morse and Gustav A Hedlund. Symbolic dynamics. *American Journal of Mathematics*, pages 815–866, 1938.
 - [53] FD Murnaghan. A symmetric reduction of the planar three-body problem. *American Journal of Mathematics*, pages 829–832, 1936.

- [54] Isaac Newton. The mathematical principles of natural philosophy (1846) — wikisource,, 2014. [Online; Translation into English by Andrew Motte, American revised and corrected edition by N. W. Chittenden].
- [55] EJ Oplk. On the catastrophic effect of collisions with celestial bodies. *Irish Astronomical Journal*, 5:34, 1958.
- [56] H. Poincaré and R. Magini. Les méthodes nouvelles de la mécanique céleste. *Il Nuovo Cimento (1895-1900)*, 10(1):128–130, 1899.
- [57] Henri Poincaré. Les méthodes nouvelles de la méchanique céleste. *Paris: Gauthier-Villars, 1892, 1893,— c1899, 1, 1899.* Quote translated by Alain Chenciner.
- [58] G. Reinout W. Quispel and Robert I. McLachlan. Explicit geometric integration of polynomial vector fields. *BIT Numerical Mathematics*, 44:515–538, 2004.
- [59] John AG Roberts and Gilles Reinout W Quispel. Chaos and time-reversal symmetry. order and chaos in reversible dynamical systems. *Physics Reports*, 216(2):63–177, 1992.
- [60] Danya Rose and Holger R. Dullin. A symplectic integrator for the symmetry reduced and regularised planar 3-body problem with vanishing angular momentum. *Celestial Mechanics and Dynamical Astronomy*, 117(2):169–185, 2013.
- [61] AE Roy and MW Ovenden. On the occurrence of commensurable mean motions in the solar system: The mirror theorem. *Monthly Notices of the Royal Astronomical Society*, 115(3):296–309, 1955.
- [62] Archie E Roy. *Orbital motion*. CRC Press, 2004.
- [63] Masaya Masayoshi Saito and Kiyotaka Tanikawa. The rectilinear three-body problem using symbol sequence i. role of triple collision. *Celestial Mechanics and Dynamical Astronomy*, 98(2):95–120, 2007.
- [64] Masaya Masayoshi Saito and Kiyotaka Tanikawa. The rectilinear three-body problem using symbol sequence ii: role of the periodic orbits. *Celestial Mechanics and Dynamical Astronomy*, 103(3):191–207, 2009.
- [65] J v Schubart. Numerische aufsuchung periodischer lösungen im dreikörperproblem. *Astronomische Nachrichten*, 283(1):17–22, 1956.
- [66] TH Seligman and HA Weidenmüller. Semi-classical periodic-orbit theory for chaotic hamiltonians with discrete symmetries. *Journal of Physics A: Mathematical and General*, 27(23):7915, 1994.
- [67] Jicong Shi and Yitong T. Yan. Explicitly integrable polynomial hamiltonians and evaluation of lie transformations. *Physical Review E*, 48(5):3943, 1993.
- [68] Carl L Siegel and Jürgen K Moser. *Lectures on Celestial Mechanics: Reprint of the 1971 Edition*. Springer Science & Business Media, 2012.
- [69] Carl Ludwig Siegel. On the integrals of canonical systems. *Annals of Mathematics*, pages 806–822, 1941.
- [70] C. Simó. Periodic orbits of the planar N-body problem with equal masses and

- all bodies on the same path. In B. A. Steves and A. J. Maciejewski, editors, *The Restless Universe*, pages 265–284, 2001.
- [71] C. Simó. Dynamical properties of the figure eight solution of the three-body problem. In A. Chenciner, R. Cushman, C. Robinson, and Z. J. Xia, editors, *Celestial Mechanics, Dedicated to Donald Saari for his 60th Birthday*, pages 209–228, 2002.
 - [72] Carles Simó. New families of solutions in N -body problems. In *European Congress of Mathematics*, pages 101–115. Springer, 2001.
 - [73] Milovan Šuvakov and V Dmitrašinović. Three classes of newtonian three-body planar periodic orbits. *Physical review letters*, 110(11):114301, 2013.
 - [74] Milovan Šuvakov and Mitsuru Shibayama. Three topologically nontrivial choreographic motions of three bodies. *Celestial Mechanics and Dynamical Astronomy*, pages 1–8, 2015.
 - [75] Victor Szebehely. Burrau’s problem of three bodies. *Proceedings of the National Academy of Sciences of the United States of America*, 58(1):60, 1967.
 - [76] Victor Szebehely and C. Frederick Peters. Complete solution of a general problem of three bodies. *Astronomical Journal*, 72:876–883, September 1967.
 - [77] Kiyotaka Tanikawa and Seppo Mikkola. One-dimensional three-body problem via symbolic dynamics. *Chaos: An Interdisciplinary Journal of Nonlinear Science*, 10(3):649–657, 2000.
 - [78] Kiyotaka Tanikawa and Seppo Mikkola. Triple collisions in the one-dimensional three-body problem. *Celestial Mechanics and Dynamical Astronomy*, 76(1):23–34, 2000.
 - [79] Kiyotaka Tanikawa and Seppo Mikkola. A trial symbolic dynamics of the planar three-body problem. *arXiv preprint arXiv:0802.2465s*, 2008.
 - [80] Kiyotaka Tanikawa and Seppo Mikkola. Symbol sequences and orbits of the free-fall three-body problem. *Publications of the Astronomical Society of Japan*, page psv087, 2015.
 - [81] Susanna Terracini. n-body problem and choreographies. In Robert A. Meyers, editor, *Mathematics of Complexity and Dynamical Systems*, pages 1043–1069. Springer New York, 2011.
 - [82] V Titov. Three-body problem periodic orbits with vanishing angular momentum. *Astronomische Nachrichten*, 336(3):271–275, 2015.
 - [83] Jörg Waldvogel. The close triple approach. *Celestial mechanics*, 11(4):429–432, 1975.
 - [84] Jörg Waldvogel. The three-body problem near triple collision. *Celestial mechanics*, 14(3):287–300, 1976.
 - [85] Jörg Waldvogel. Symmetric and regularized coordinates on the plane triple collision manifold. *Celestial Mechanics*, 28:69–82, 1982.
 - [86] Yihren Wu. Berry’s phase and the planar three-body problem. *Journal of Physics*

- A: Mathematical and General*, 22(4):L117, 1989.
- [87] Haruo Yoshida. Construction of higher order symplectic integrators. *Physics Letters A*, 150(57):262 – 268, 1990.

A Reconstruction from regularised coordinates

Reconstruction formulæ for the regularised coordinates are given in [85]. However, the formulæ for the momenta given in [85] are singular at collinearity, and, applied directly, result in undesirable spurious rotations at collinearities. Here we are going to derive formulæ that are smooth everywhere except at triple collision. We begin the reconstruction with known quantities: $\alpha_1, \alpha_k, \alpha_l, \pi_j, \pi_k, \pi_l, \phi, p_\phi \in \mathbb{R}$ and $m_j, m_k, m_l \in \mathbb{R}^+$. The goal is to find the relative exterior angles θ_j and the absolute angles of the sides ϕ_j .

A1 Exterior angles and side angles

The exterior angles are related to the regularised coordinates by

$$\cos \theta_j = \frac{\alpha_k^2 \alpha_l^2 - \alpha_j^2 \alpha^2}{a_k a_l} \quad (\text{A.1})$$

$$\sin \theta_j = \frac{2A}{a_k a_l} \quad (\text{A.2})$$

$$\tan \theta_j = \frac{2A}{\alpha_k^2 \alpha_l^2 - \alpha_j^2 \alpha^2}, \quad (\text{A.3})$$

with half angle formulæ

$$\cos \frac{\theta_j}{2} = \frac{\alpha_k \alpha_l}{\sqrt{a_k a_l}}, \quad (\text{A.4})$$

$$\sin \frac{\theta_j}{2} = \frac{\alpha_j \alpha}{\sqrt{a_k a_l}} \quad (\text{A.5})$$

$$\tan \frac{\theta_j}{2} = \frac{\alpha_j \alpha}{\alpha_k \alpha_l}, \quad (\text{A.6})$$

where the side lengths $a_j = \alpha_k^2 + \alpha_l^2$ and semiperimeter $\alpha^2 = \sum \alpha_j^2$.

Using the inverse transformations as given in [85] to reconstruct a computed trajectory leads to surprising errors, which we describe and understand first, then solve. The

absolute side angles are given by $\phi_j = \phi + \frac{1}{3}(\theta_k - \theta_l)$. If we compute the relative exterior angles θ_j from equation (A.3), at each collinearity the signed area A changes sign as one of the regularised coordinates α_j does. At each change of sign the sum of the exterior angles changes from $\pm 2\pi$ to $\mp 2\pi$, coincident with one of the computed exterior angles jumping from $\pm\pi$ to $\mp\pi$, which can potentially result in a difference of $\pm\frac{2\pi}{3}$ in each ϕ_j .

We can fix the problem simply and automatically by making use of the observation that sum of exterior angles is identically 0 mod 2π and then a) lifting two of the exterior angles to \mathbb{R} , and b) setting the third angle to the negative of the sum of the other two.

Correct angles are found by computing θ_2 and θ_3 from equation (A.3) and lifting them to \mathbb{R} , then setting $\theta_1 = -(\theta_2 + \theta_3)$. The side angles become

$$\begin{aligned}\phi_1 &= \phi + \frac{1}{3}(\theta_2 - \theta_3) \\ \phi_2 &= \phi + \frac{1}{3}(2\theta_3 + \theta_2) \\ \phi_3 &= \phi - \frac{1}{3}(\theta_3 + 2\theta_2).\end{aligned}$$

This (or any such) choice trivially satisfies $\theta_1 + \theta_2 + \theta_3 \equiv 0$ mod 2π , and, furthermore, because any jumps of $\pm 2\pi$ in the exterior angles have been removed, so have any jumps in the absolute side angles.

At or near any kl -collision we use the fact that $\frac{\alpha_k}{\alpha_l} \sim \frac{\pi_k}{\pi_l}$ as $\alpha_k, \alpha_l \rightarrow 0$ to reduce numerical error in the calculation of θ_2, θ_3 .

A2 Positions and momenta

With correct computation of the absolute side angles, we can now perform the reconstruction of the physical positions X_j and momenta P_j in the centre of mass frame.

Positions relative to the centre of mass are obtained by

$$X_j = \frac{1}{m} (m_l a_k e^{i\phi_k} - m_k a_l e^{i\phi_l}). \quad (\text{A.7})$$

Denote the incentre of triangle $X_1 X_2 X_3$ by $C = \frac{1}{2\alpha^2} \sum a_j X_j$ and *incentre-relative* co-ordinates for the vertices $\tilde{X}_j = X_j - C$. The angle of \tilde{X}_j relative to the reference angle of our inertial frame we denote by ψ_j . We may then also write $\tilde{X}_j = r_j e^{i\psi_j}$, for $r_j = \frac{\alpha_j}{\alpha} \sqrt{a_k a_l}$.

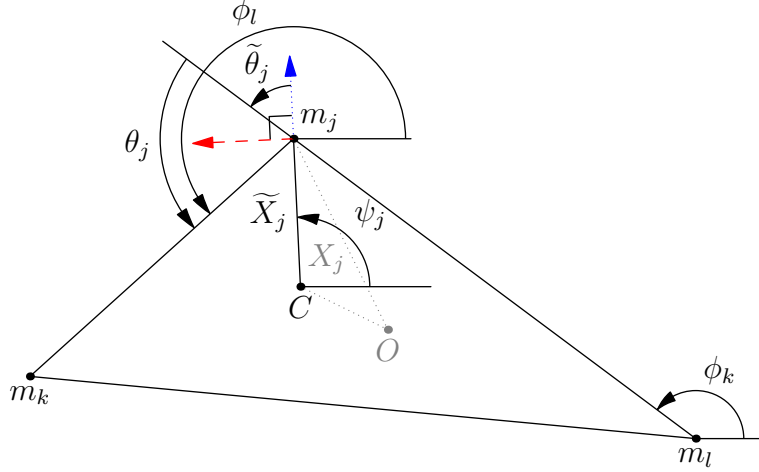


Figure A.1: Geometry of the relationship between ψ_j and ϕ_k, ϕ_l . In blue the extension of $\widetilde{X}_j = X_j - C$ connecting the incentre to m_j and in red its perpendicular. The length and direction of the blue/dotted and, respectively, red/dashed lines are given by $e^{i\phi_k} - e^{i\phi_l}$ and $e^{i\phi_k} + e^{i\phi_l}$. As defined in the proof of lemma A.10, $\widetilde{\theta}_j = \frac{1}{2}(\pi - \theta_j)$.

Momenta are obtained by

$$P_j = p_k e^{i\phi_k} - p_l e^{i\phi_l} + \frac{ip_\phi}{3} \left(\frac{e^{i\phi_k}}{a_k} - \frac{e^{i\phi_l}}{a_l} \right) \quad (\text{A.8})$$

with

$$p_j = \frac{1}{4} \left(\frac{\pi_k}{\alpha_k} + \frac{\pi_l}{\alpha_l} - \frac{\pi_j}{\alpha_l} \right), \quad (\text{A.9})$$

the latter of which contains singularities at every syzygy (whereas it is known that the only true singularities of the 3-body problem are collisions). Clearly calculation of each p_j and substitution into equation (A.8) is undesirable.

Substitution and rearrangement gives the still singular

$$P_j = \frac{1}{4} \left((e^{i\phi_k} - e^{i\phi_l}) \frac{\pi_j}{\alpha_j} + (e^{i\phi_k} + e^{i\phi_l}) \left(\frac{\pi_l}{\alpha_l} - \frac{\pi_k}{\alpha_k} \right) \right) + \frac{ip_\phi}{3} \left(\frac{e^{i\phi_k}}{a_k} - \frac{e^{i\phi_l}}{a_l} \right),$$

revealing structure that was previously hidden: the factors $(e^{i\phi_k} \pm e^{i\phi_l})$. The difference (when it is not zero) gives the direction of the internal angle bisectors at vertex X_j , while the sum gives the angle of the external angle bisector. That is $(e^{i\phi_k} - e^{i\phi_l}) \parallel \widetilde{X}$ and $(e^{i\phi_k} + e^{i\phi_l}) \parallel \widetilde{X} e^{i\frac{\pi}{2}}$. We see that the physical momenta are decomposed into orthogonal components with angles ψ_j and $\psi_j + \frac{\pi}{2}$.

Lemma A.10. *The argument of the difference of complex units $e^{i\phi_k} - e^{i\phi_l}$ is the same (up to sign) as the argument of \tilde{X}_j . That is, there exists some $\rho_j \in \mathbb{R}$ such that $\rho_j e^{i\psi_j} = e^{i\phi_k} - e^{i\phi_l}$.*

Proof. By geometry, illustrated in figure A.1: define $\tilde{\theta}_j = \frac{1}{2}(\pi - \theta_j)$. We now have $\psi_j = \phi_l - \theta_j - \tilde{\theta}_j = \phi_l - \frac{1}{2}(\theta_j + \pi) = \phi_k - \tilde{\theta}_j = \phi_k - \frac{1}{2}(\pi - \theta_j)$. Therefore we may rewrite each of ϕ_k, ϕ_l in terms of ψ_j, θ_j :

$$\begin{aligned}\phi_k &= \psi_j - \frac{\theta_j}{2} + \frac{\pi}{2} \\ \phi_l &= \psi_j + \frac{\theta_j}{2} + \frac{\pi}{2}.\end{aligned}$$

Now the expression $e^{i\phi_k} - e^{i\phi_l}$ may be rewritten

$$\begin{aligned}e^{i\phi_k} - e^{i\phi_l} &= e^{i(\psi_j - \frac{\theta_j}{2} + \frac{\pi}{2})} - e^{i(\psi_j + \frac{\theta_j}{2} + \frac{\pi}{2})} \\ &= e^{i(\psi_j + \frac{\pi}{2})} \left(e^{-i\frac{\theta_j}{2}} - e^{i\frac{\theta_j}{2}} \right) \\ &= 2 \sin \frac{\theta_j}{2} e^{i\psi_j} \\ &= 2 \frac{\alpha_j \alpha}{\sqrt{a_k a_l}} e^{i\psi_j} \\ &= \rho_j e^{i\psi_j}.\end{aligned}$$

□

Lemma A.11. *The argument of the sum of complex units $e^{i\phi_k} + e^{i\phi_l}$ is the same (up to sign) as the argument of $i\tilde{X}_j$. That is, there exists some $\rho \in \mathbb{R}$ such that $\rho e^{i(\psi_j + \frac{\pi}{2})} = e^{i\phi_k} + e^{i\phi_l}$.*

Proof. Similar to the proof of lemma A.10. Rewrite ϕ_k, ϕ_l to obtain

$$\begin{aligned}e^{i\phi_k} + e^{i\phi_l} &= e^{i(\psi_j - \frac{\theta_j}{2} + \frac{\pi}{2})} + e^{i(\psi_j + \frac{\theta_j}{2} + \frac{\pi}{2})} \\ &= e^{i(\psi_j + \frac{\pi}{2})} \left(e^{-i\frac{\theta_j}{2}} + e^{i\frac{\theta_j}{2}} \right) \\ &= 2 \cos \frac{\theta_j}{2} e^{i(\psi_j + \frac{\pi}{2})} \\ &= 2 \frac{\alpha_k \alpha_l}{\sqrt{a_k a_l}} e^{i(\psi_j + \frac{\pi}{2})} \\ &= \rho e^{i(\psi_j + \frac{\pi}{2})}.\end{aligned}$$

□

Using the results of lemmas A.10 and A.11, and applying the same technique to the terms corresponding to the angular momentum, we now obtain a reconstruction for the momenta that is only singular at triple collision:

$$P_j = \frac{e^{i\psi_j}}{2\sqrt{a_k a_l}} \left(\alpha \pi_j + i(\alpha_k \pi_l - \alpha_l \pi_k) + \frac{p_\phi}{3a_k a_l} ((a_k - a_l) \alpha_k \alpha_l + i(a_k + a_l) \alpha_j \alpha) \right). \quad (\text{A.12})$$

B Momenta and decomposed velocities near collision

A point near 23-collision is denoted by $z_\epsilon = (\alpha_1, \epsilon \cos \vartheta, \epsilon \sin \vartheta, \pi_1, \pi_2, \pi_3)^T$. We decompose the velocities $\dot{\alpha}_2, \dot{\alpha}_3$ into orthogonal components, v_{\parallel} in the radial direction and v_{\perp} perpendicular to the radial component. That is, we set $\dot{\alpha}_2 = v_{\parallel} \cos \vartheta - v_{\perp} \sin \vartheta$, $\dot{\alpha}_3 = v_{\parallel} \sin \vartheta + v_{\perp} \cos \vartheta$, where $v_{\parallel} = \dot{\epsilon}$ and $v_{\perp} = \epsilon \dot{\vartheta}$, and equate these velocities to the corresponding components of the vector field. Solving simultaneously for π_2, π_3 leads to the following expressions:

$$\pi_2 = \frac{8m_2}{A} (4m_3(V_1 v_{\parallel} \cos \vartheta - U_1 v_{\perp} \sin \vartheta) + W_1 \pi_1 \alpha_1 \epsilon \cos \vartheta) \quad (\text{B.1})$$

$$\pi_3 = \frac{8m_3}{A} (4m_2(V_2 v_{\parallel} \sin \vartheta + U_2 v_{\perp} \cos \vartheta) + W_2 \pi_1 \alpha_1 \epsilon \sin \vartheta), \quad (\text{B.2})$$

where

$$\begin{aligned} A &= B\alpha_1^8 + C\alpha_1^6\epsilon^2 + D\alpha_1^4\epsilon^4 + E\alpha_1^2\epsilon^6 + F\epsilon^8 \\ B &= 8m_1 n_1^2 \\ C &= 8m_1 n_1 (2n_1 + l_1) \cos 2\vartheta \\ D &= 2(5m_1 n_1^2 + 4m_2 m_3 m + m_1 l_1 (6n_1 + l_1 \cos 2\vartheta) \cos 2\vartheta) \\ E &= 2(m_1 n_1^2 + 4m_2 m_3 m + m_1 l_1 (2n_1 + l_1 \cos 2\vartheta) \cos 2\vartheta) \\ F &= m_2 m_3 m (1 - \cos 4\vartheta) \\ V_1 &= m_1 n_1 \alpha_1^4 + m_1 (n_1 + l_1 \cos^2 \vartheta) \alpha_1^2 \epsilon^2 + m_2 (m_1 \cos^2 \vartheta + m_3) \epsilon^4 \\ V_2 &= m_1 n_1 \alpha_1^4 + m_1 (n_1 - l_1 \sin^2 \vartheta) \alpha_1^2 \epsilon^2 + m_3 (m_1 \sin^2 \vartheta + m_2) \epsilon^4 \\ U_1 &= m_1 (n_1 \alpha_1^4 + (2m_2 - l_1 \sin^2 \vartheta) \alpha_1^2 \epsilon^2 + m_2 \cos^2 \vartheta \epsilon^4) \\ U_2 &= m_1 (n_1 \alpha_1^4 + (2m_3 + l_1 \cos^2 \vartheta) \alpha_1^2 \epsilon^2 + m_3 \sin^2 \vartheta \epsilon^4) \\ W_1 &= m_1 n_1 \alpha_1^6 + m_1 w_{1,3} \alpha_1^4 \epsilon^2 + w_{1,2} \alpha_1^2 \epsilon^4 + w_{1,1} \epsilon^6 \\ W_2 &= m_1 n_1 \alpha_1^6 + m_1 w_{2,3} \alpha_1^4 \epsilon^2 + w_{2,2} \alpha_1^2 \epsilon^4 + w_{2,1} \epsilon^6, \end{aligned}$$

and

$$w_{1,1} = m_3^2 \sin^4 \vartheta + m_2 n_2 \cos^4 \vartheta$$

$$\begin{aligned}
w_{2,1} &= m_2^2 \cos^4 \vartheta + m_3 n_3 \sin^4 \vartheta \\
w_{1,2} &= m_3^2 \sin^2 \vartheta + (m_1 n_1 + m_2 n_2) \cos^2 \vartheta + m_1 l_1 \cos^4 \vartheta \\
w_{2,2} &= m_2^2 \cos^2 \vartheta + (m_1 n_1 + m_3 n_3) \sin^2 \vartheta - m_1 l_1 \sin^4 \vartheta \\
w_{1,3} &= n_1 + 2m_2 \cos^2 \vartheta \\
w_{2,3} &= n_1 + 2m_3 \sin^2 \vartheta,
\end{aligned}$$

with

$$\begin{aligned}
m &= m_1 + m_2 + m_3 \\
n_j &= m_k + m_l \\
l_j &= m_k - m_l.
\end{aligned}$$

In terms of the momenta, ϵ , and ϑ , the decomposed velocities are

$$\begin{aligned}
v_{\parallel} = \dot{\epsilon} &= \frac{1}{4m_2 m_3} (G_1 \pi_2 \cos \vartheta + G_2 \pi_3 \sin \vartheta - G_3 \pi_1 \alpha_1 \epsilon) \\
v_{\perp} = \epsilon \dot{\vartheta} &= \frac{1}{4m_2 m_3} (H_1 \pi_3 \cos \vartheta - H_2 \pi_2 \sin \vartheta + H_3 \pi_1 \alpha_1 \epsilon \sin 2\vartheta),
\end{aligned}$$

where

$$\begin{aligned}
G_1 &= n_1 \alpha_1^4 + (m_3 + m_2 \cos^2 \vartheta + m_3 \sin^2 \vartheta) \alpha_1^2 \epsilon^2 + m_3 \sin^2 \vartheta \epsilon^4 \\
G_2 &= n_1 \alpha_1^4 + (m_2 + m_2 \cos^2 \vartheta + m_3 \sin^2 \vartheta) \alpha_1^2 \epsilon^2 + m_2 \cos^2 \vartheta \epsilon^4 \\
G_3 &= (m_2 \cos^2 \vartheta + m_3 \sin^2 \vartheta) \alpha_1^2 + (m_2 \cos^4 \vartheta + m_3 \sin^4 \vartheta) \epsilon^2 \\
H_1 &= n_1 \alpha_1^4 + (n_1 + l_1 \cos^2 \vartheta) \alpha_1^2 \epsilon^2 + m_2 \left(\frac{m_3}{m_1} + \cos^2 \vartheta \right) \epsilon^4 \\
H_2 &= n_1 \alpha_1^4 + (n_1 - l_1 \sin^2 \vartheta) \alpha_1^2 \epsilon^2 + m_3 \left(\frac{m_2}{m_1} + \sin^2 \vartheta \right) \epsilon^4 \\
H_3 &= \frac{1}{2} (l_1 \alpha_1^2 + (m_2 \cos^2 \vartheta - m_3 \sin^2 \vartheta) \epsilon^2).
\end{aligned}$$

In the limit, then, as $\epsilon \rightarrow 0$, we see that $\pi_2 \rightarrow \frac{4\mu_1}{\alpha_1^4} v_{\parallel} \cos \vartheta$ and $\pi_3 \rightarrow \frac{4\mu_1}{\alpha_1^4} v_{\parallel} \sin \vartheta$. Similarly, $v_{\parallel} \rightarrow \frac{1}{4\mu_1} (\pi_2 \cos \vartheta + \pi_3 \sin \vartheta) \alpha_1^4$ and $v_{\perp} \rightarrow \frac{1}{4\mu_1} (\pi_3 \cos \vartheta - \pi_2 \sin \vartheta) \alpha_1^4$.

C Stages of the explicit integrator

Section 5.2.2 described the construction of an explicit symplectic integrator of arbitrary even order for the fully reduced and regularised 3-body problem. This construction is based on a first order method obtained by splitting the Hamiltonian equation (1.36) into ten integrable parts and composing their exact flows. This appendix gives the formulæ for each flow for each integrable term in the splitting equation (5.7), followed by the choice of ordering for a second order, reversible generalised leapfrog integrator. In the following we continue to use $a_j = \alpha_k^2 + \alpha_l^2$, the pairwise reduced masses μ_j , and the pairwise products $M_j = m_k m_l$, and define their sum $N = \sum M_j$.

$$\varphi_{H_0}^\tau = \begin{pmatrix} \alpha_1 \\ \alpha_2 \\ \alpha_3 \\ \pi_1 + 2\alpha_1 ((h(\alpha_1^2 + \alpha^2) + N) a_1 + 2M_1 \alpha_1^2) \tau \\ \pi_2 + 2\alpha_2 ((h(\alpha_2^2 + \alpha^2) + N) a_2 + 2M_2 \alpha_2^2) \tau \\ \pi_3 + 2\alpha_3 ((h(\alpha_3^2 + \alpha^2) + N) a_3 + 2M_3 \alpha_3^2) \tau \end{pmatrix} \quad (\text{C.1})$$

$$\varphi_{H_1}^\tau = \begin{pmatrix} \alpha_1 \exp\left(\frac{1}{4}\left(\frac{\alpha_2^2}{\mu_2} + \frac{\alpha_3^2}{\mu_3}\right)\alpha_1 \pi_1 \tau\right) \\ \alpha_2 \\ \alpha_3 \\ \pi_1 \exp\left(-\frac{1}{4}\left(\frac{\alpha_2^2}{\mu_2} + \frac{\alpha_3^2}{\mu_3}\right)\alpha_1 \pi_1 \tau\right) \\ \pi_2 - \frac{\alpha_2}{4\mu_2} \alpha_1^2 \pi_1^2 \tau \\ \pi_3 - \frac{\alpha_3}{4\mu_3} \alpha_1^2 \pi_1^2 \tau \end{pmatrix} \quad (\text{C.2})$$

$$\varphi_{H_2}^\tau = \begin{pmatrix} \alpha_1 \\ \alpha_2 \exp\left(\frac{1}{4}\left(\frac{\alpha_3^2}{\mu_3} + \frac{\alpha_1^2}{\mu_1}\right)\alpha_2 \pi_2 \tau\right) \\ \alpha_3 \\ \pi_1 - \frac{\alpha_2}{4\mu_2} \alpha_2^2 \pi_2^2 \tau \\ \pi_2 \exp\left(-\frac{1}{4}\left(\frac{\alpha_3^2}{\mu_3} + \frac{\alpha_1^2}{\mu_1}\right)\alpha_2 \pi_2 \tau\right) \\ \pi_3 - \frac{\alpha_3}{4\mu_3} \alpha_2^2 \pi_2^2 \tau \end{pmatrix} \quad (\text{C.3})$$

$$\varphi_{H_3}^\tau = \begin{pmatrix} \alpha_1 \\ \alpha_2 \\ \alpha_3 \exp\left(\frac{1}{4}\left(\frac{\alpha_1^2}{\mu_1} + \frac{\alpha_2^2}{\mu_2}\right)\alpha_3\pi_3\tau\right) \\ \pi_1 - \frac{\alpha_1}{4\mu_2}\alpha_3^2\pi_3^2\tau \\ \pi_2 - \frac{\alpha_3}{4\mu_3}\alpha_3^2\pi_3^2\tau \\ \pi_3 \exp\left(-\frac{1}{4}\left(\frac{\alpha_1^2}{\mu_1} + \frac{\alpha_2^2}{\mu_2}\right)\alpha_3\pi_3\tau\right) \end{pmatrix} \quad (\text{C.4})$$

$$\varphi_{H_4}^\tau = \begin{pmatrix} \alpha_1 + \frac{1}{4}\left(\frac{\alpha_2^4}{\mu_2} \frac{2\alpha_2^2\alpha_3^2}{m_j} + \frac{\alpha_3^4}{\mu_3}\right)\pi_1\tau \\ \alpha_2 \\ \alpha_3 \\ \pi_1 \\ \pi_2 + \left(\frac{\alpha_2^2}{2\mu_2} + \frac{\alpha_3^2}{m_1}\right)\alpha_2\pi_1^2\tau \\ \pi_3 + \left(\frac{\alpha_3^2}{2\mu_3} + \frac{\alpha_2^2}{m_1}\right)\alpha_3\pi_1^2\tau \end{pmatrix} \quad (\text{C.5})$$

$$\varphi_{H_5}^\tau = \begin{pmatrix} \alpha_1 \\ \alpha_2 \\ \alpha_3 \\ \pi_1 + \left(\frac{\alpha_1^2}{2\mu_1} + \frac{\alpha_3^2}{m_2}\right)\alpha_1\pi_2^2\tau \\ \pi_2 \\ \pi_3 + \left(\frac{\alpha_3^2}{2\mu_3} + \frac{\alpha_1^2}{m_2}\right)\alpha_3\pi_1^2\tau \end{pmatrix} \quad (\text{C.6})$$

$$\varphi_{H_6}^\tau = \begin{pmatrix} \alpha_1 \\ \alpha_2 \\ \alpha_3 + \frac{1}{4}\left(\frac{\alpha_1^4}{\mu_1} + \frac{2\alpha_1^2\alpha_2^2}{m_3} + \frac{\alpha_2^4}{\mu_2}\right)\pi_3\tau \\ \pi_1 + \left(\frac{\alpha_1^2}{2\mu_1} + \frac{\alpha_2^2}{m_3}\right)\alpha_1\pi_3^2\tau \\ \pi_2 + \left(\frac{\alpha_2^2}{2\mu_2} + \frac{\alpha_1^2}{m_3}\right)\alpha_2\pi_3^2\tau \\ \pi_3 \end{pmatrix} \quad (\text{C.7})$$

$$\varphi_{H_7}^\tau = \begin{pmatrix} \alpha_1 \left(1 + \frac{1}{2}\left(\frac{1}{m_3}\alpha_2\pi_2 + \frac{1}{m_2}\alpha_3\pi_3\right)\alpha_1^2\tau\right)^{-\frac{1}{2}} \\ \alpha_2 \exp\left(-\frac{1}{4m_3}\alpha_1^3\pi_1\tau\right) \\ \alpha_3 \exp\left(-\frac{1}{4m_2}\alpha_1^3\pi_1\tau\right) \\ \pi_1 \left(1 + \frac{1}{2}\left(\frac{1}{m_3}\alpha_2\pi_2 + \frac{1}{m_2}\alpha_3\pi_3\right)\alpha_1^2\tau\right)^{\frac{3}{2}} \\ \pi_2 \exp\left(\frac{1}{4m_3}\alpha_1^3\pi_1\tau\right) \\ \pi_3 \exp\left(\frac{1}{4m_2}\alpha_1^3\pi_1\tau\right) \end{pmatrix} \quad (\text{C.8})$$

$$\varphi_{H_8}^\tau = \begin{pmatrix} \alpha_1 \exp\left(-\frac{1}{4m_3}\alpha_2^3\pi_2\tau\right) \\ \alpha_2 \left(1 + \frac{1}{2}\left(\frac{1}{m_1}\alpha_3\pi_3 + \frac{1}{m_3}\alpha_1\pi_1\right)\alpha_2^2\tau\right)^{-\frac{1}{2}} \\ \alpha_3 \exp\left(-\frac{1}{4m_1}\alpha_2^3\pi_2\tau\right) \\ \pi_1 \exp\left(\frac{1}{4m_3}\alpha_2^3\pi_2\tau\right) \\ \pi_2 \left(1 + \frac{1}{2}\left(\frac{1}{m_1}\alpha_3\pi_3 + \frac{1}{m_3}\alpha_1\pi_1\right)\alpha_2^2\tau\right)^{\frac{3}{2}} \\ \pi_3 \exp\left(\frac{1}{4m_1}\alpha_2^3\pi_2\tau\right) \end{pmatrix} \quad (\text{C.9})$$

$$\varphi_{H_9}^\tau = \begin{pmatrix} \alpha_1 \exp\left(-\frac{1}{4m_2}\alpha_3^3\pi_3\tau\right) \\ \alpha_2 \exp\left(-\frac{1}{4m_1}\alpha_3^3\pi_3\tau\right) \\ \alpha_3 \left(1 + \frac{1}{2}\left(\frac{1}{m_2}\alpha_1\pi_1 + \frac{1}{m_1}\alpha_2\pi_2\right)\alpha_3^2\tau\right)^{-\frac{1}{2}} \\ \pi_1 \exp\left(\frac{1}{4m_2}\alpha_3^3\pi_3\tau\right) \\ \pi_2 \exp\left(\frac{1}{4m_1}\alpha_3^3\pi_3\tau\right) \\ \pi_3 \left(1 + \frac{1}{2}\left(\frac{1}{m_2}\alpha_1\pi_1 + \frac{1}{m_1}\alpha_2\pi_2\right)\alpha_3^2\tau\right)^{\frac{3}{2}} \end{pmatrix} \quad (\text{C.10})$$

Additionally, several other (auxiliary) variables may be updated during this process: the rotation ϕ by $\dot{\phi}\tau$ for reconstruction, the physical time t by $t + a_1a_2a_3\tau$, and the geometric phase G by $G + \dot{G}\tau$.

In order to construct the generalised leapfrog integrator, we would use the uniqueness of H_0 and place this stage in the middle of the compositions, and during this stage update the auxiliary variables ϕ , t , G . Then the generalised leapfrog integrator looks like

$$\varphi_{K,2}^\tau = \varphi_{H_9}^{\frac{\tau}{2}} \circ \cdots \circ \varphi_{H_1}^{\frac{\tau}{2}} \circ \varphi_{H_0}^\tau \circ \varphi_{H_1}^{\frac{\tau}{2}} \circ \cdots \circ \varphi_{H_9}^{\frac{\tau}{2}}. \quad (\text{C.11})$$

D Coefficients for higher order methods

Section 5.2.2.1 discusses the construction of higher order numerical schemes. Given a basic symmetric method of order 2, we can construct integrators of the following orders with the following coefficients.

Order 6, 1:

$$\begin{aligned}\gamma_1 &= \gamma_7 = 0.78451361047755726381949763 \\ \gamma_2 &= \gamma_6 = 0.23557321335935813368479318 \\ \gamma_3 &= \gamma_3 = -1.17767998417887100694641568 \\ \gamma_4 &= 1.31518632068391121888434973\end{aligned}$$

Order 6, 2:

$$\begin{aligned}\gamma_1 &= \gamma_9 = 0.39216144400731413927925056 \\ \gamma_2 &= \gamma_8 = 0.33259913678935943859974864 \\ \gamma_3 &= \gamma_7 = -0.70624617255763935980996482 \\ \gamma_4 &= \gamma_6 = 0.08221359629355080023149045 \\ \gamma_5 &= 0.79854399093482996339895035\end{aligned}$$

Order 8, 1:

$$\begin{aligned}\gamma_1 &= \gamma_{15} = 0.74167036435061295344822780 \\ \gamma_2 &= \gamma_{14} = -0.40910082580003159399730010 \\ \gamma_3 &= \gamma_{13} = 0.19075471029623837995387626 \\ \gamma_4 &= \gamma_{12} = -0.57386247111608226665638773 \\ \gamma_5 &= \gamma_{11} = 0.29906418130365592384446354 \\ \gamma_6 &= \gamma_{10} = 0.33462491824529818378495798 \\ \gamma_7 &= \gamma_9 = 0.31529309239676659663205666 \\ \gamma_8 &= -0.79688793935291635401978884\end{aligned}$$

Order 8, 2:

$$\begin{aligned}
 \gamma_1 &= \gamma_{17} = 0.13020248308889008087881763 \\
 \gamma_2 &= \gamma_{16} = 0.56116298177510838456196441 \\
 \gamma_3 &= \gamma_{15} = -0.38947496264484728640807860 \\
 \gamma_4 &= \gamma_{14} = 0.15884190655515560089621075 \\
 \gamma_5 &= \gamma_{13} = -0.39590389413323757733623154 \\
 \gamma_6 &= \gamma_{12} = 0.18453964097831570709183254 \\
 \gamma_7 &= \gamma_{11} = 0.25837438768632204729397911 \\
 \gamma_8 &= \gamma_{10} = 0.29501172360931029887096624 \\
 \gamma_9 &= -0.60550853383003451169892108
 \end{aligned}$$

Order 10:

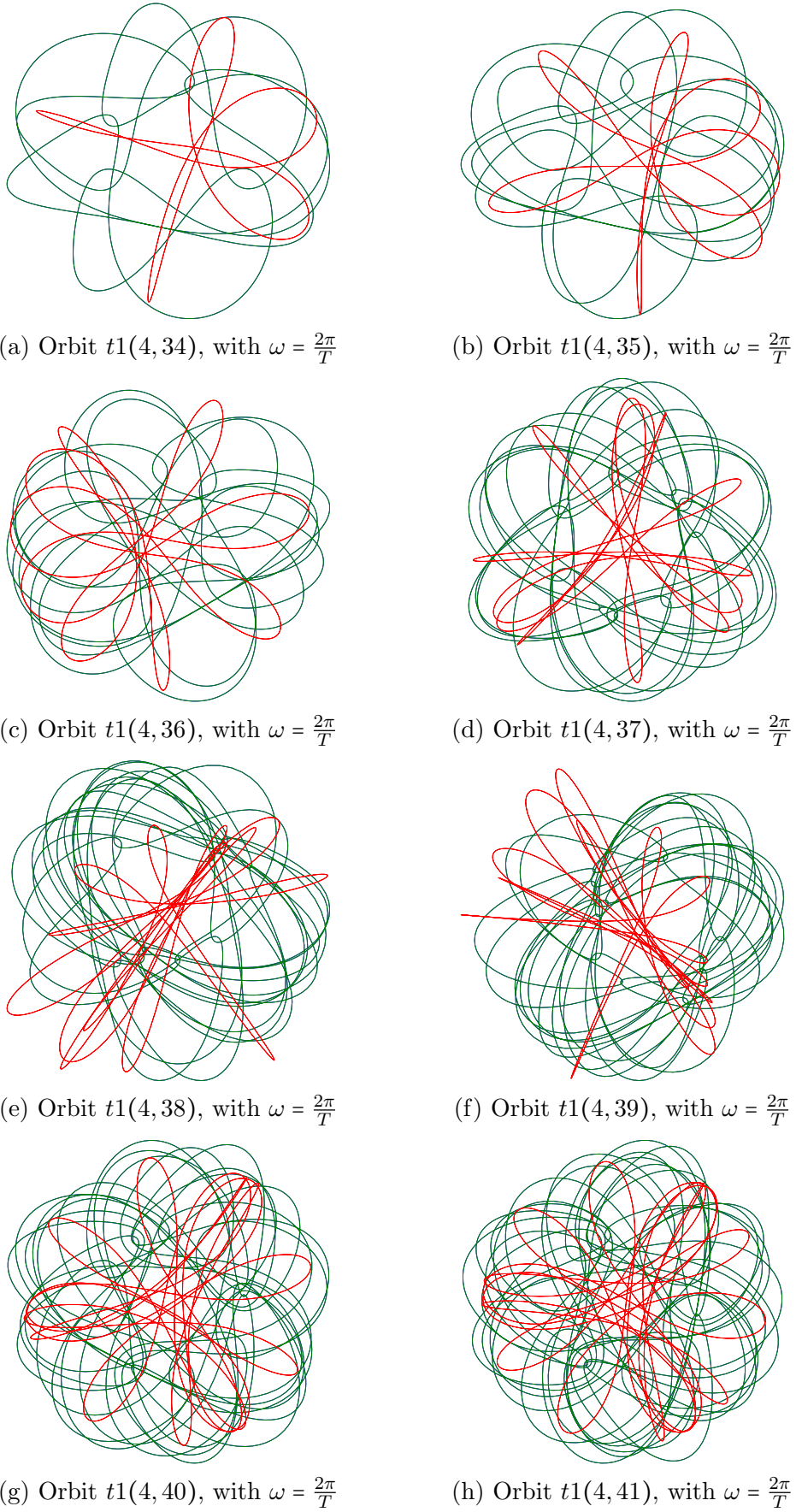
$$\begin{aligned}
 \gamma_1 &= \gamma_{35} = 0.07879572252168741926390768 \\
 \gamma_2 &= \gamma_{34} = 0.31309610341510852776481247 \\
 \gamma_3 &= \gamma_{33} = 0.02791838323507806610952027 \\
 \gamma_4 &= \gamma_{32} = -0.22959284159390709415121340 \\
 \gamma_5 &= \gamma_{31} = 0.13096206107716486317465686 \\
 \gamma_6 &= \gamma_{30} = -0.26973340565451071434460973 \\
 \gamma_7 &= \gamma_{29} = 0.07497334315589143566613711 \\
 \gamma_8 &= \gamma_{28} = 0.11199342399981020488957508 \\
 \gamma_9 &= \gamma_{27} = 0.36613344954622675119314812 \\
 \gamma_{10} &= \gamma_{26} = -0.39910563013603589787862981 \\
 \gamma_{11} &= \gamma_{25} = 0.10308739852747107731580277 \\
 \gamma_{12} &= \gamma_{24} = 0.41143087395589023782070412 \\
 \gamma_{13} &= \gamma_{23} = -0.00486636058313526176219566 \\
 \gamma_{14} &= \gamma_{22} = -0.39203335370863990644808194 \\
 \gamma_{15} &= \gamma_{21} = 0.05194250296244964703718290 \\
 \gamma_{16} &= \gamma_{20} = 0.05066509075992449633587434 \\
 \gamma_{17} &= \gamma_{19} = 0.04967437063972987905456880 \\
 \gamma_{18} &= 0.04931773575959453791768001
 \end{aligned}$$

E Absolutely periodic orbits as relative partial choreographies

Section 6.5.3 contains a list of orbits that are relative partial choreographies under extra rotation during one period. The isotropy subgroups of all such orbits have one or another of the cyclic subgroups $\{(I, 0), (\sigma_j, \frac{1}{2})\}$, $\{(I, 0), (\sigma_j s_j, \frac{1}{2})\}$, or $\{(I, 0), (\sigma_j s_l, \frac{1}{4}), (s_j, \frac{1}{2}), (\sigma_j s_k, \frac{3}{4})\}$, but are not partial choreographies in the frame rotating with $\omega = \frac{\Delta G}{T}$; some are indeed absolutely periodic, and in this appendix we depict as relative partial choreographies those which are absolutely periodic.

Collision orbits (type-1 and type-2) are absolutely periodic. Those with the necessary symmetries are shown in rotating frames such that they are relative partial choreographies in figures E.1 and E.2.

Isosceles and rectilinear orbits are also absolutely periodic. Those with the necessary symmetries can also be made into relative partial choreographies, shown in figures E.3 and E.4.

Figure E.1: Type-0 , sequence class $(B\Omega M\Omega')^2$.

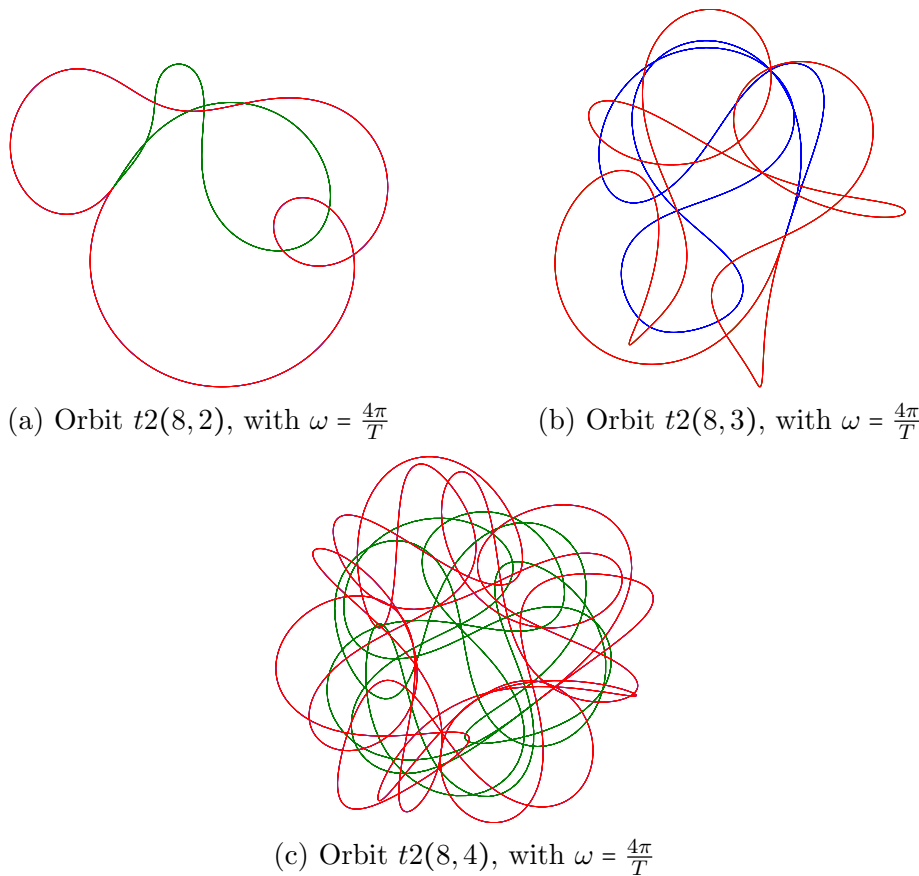
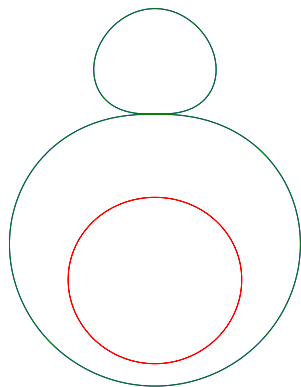
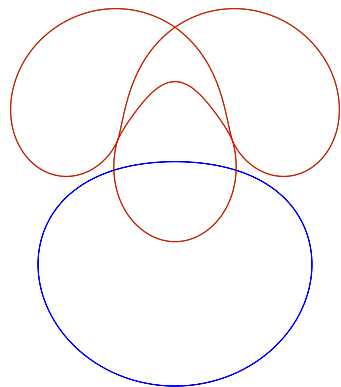
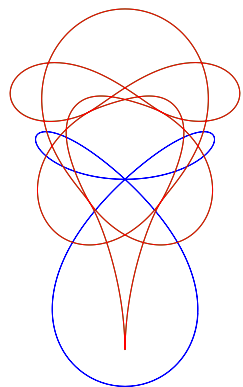
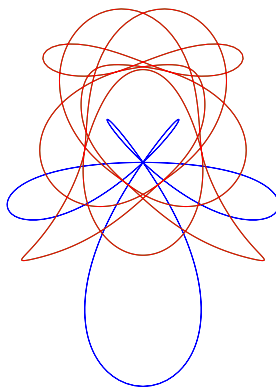


Figure E.2: Type-0 , sequence class $(B\Omega M\Omega')^4$.

(a) Orbit *isosceles*(8,1), with $\omega = \frac{2\pi}{T}$ (b) Orbit *isosceles*(8,2), with $\omega = \frac{2\pi}{T}$ (c) Orbit *isosceles*(8,3), with $\omega = \frac{2\pi}{T}$ (d) Orbit *isosceles*(8,4), with $\omega = \frac{2\pi}{T}$ Figure E.3: Isosceles, sequence classes $(B\Omega M\Omega')^2$ (a), $(F\Omega M\Omega')^2$ (b-d).

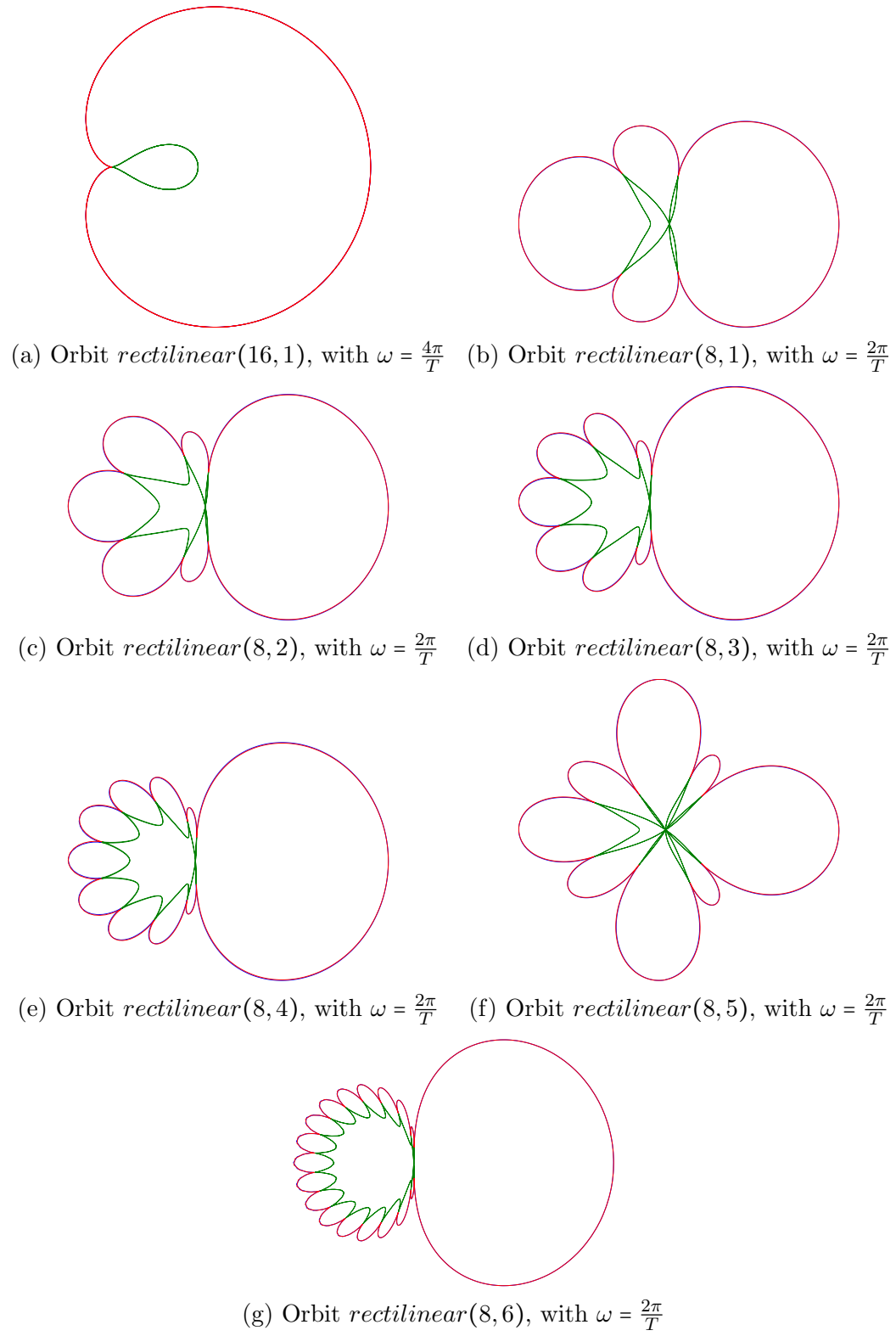


Figure E.4: Rectilinear, sequence classes $(B\Omega M\Omega')^4$ (a), $(F\Omega M\Omega')^2$ (b-g).

F Bestiary of periodic orbits

Please refer to the external appendix.